SOME APPLICATIONS OF MULTINUCLEAR NMR

A THESIS SUBMITTED TO THE

UNIVERSITY OF WAIKATO

FOR THE DEGREE OF

DOCTOR OF PHILOSOPHY

BY

RALPH ALEXANDER THOMSON

JULY 1990

Abstract

This work makes use of the rapidly expanding technique of Fourier Transform Nuclear Magnetic Resonance (FT-NMR) Spectroscopy to study a number of different areas of chemistry.

Work was carried out into the study of new pulse sequences, and composite pulses, to improve the observing conditions for low frequency nuclei. These techniques were applied to the study of ^{73}Ge NMR, a spin $^{9}/_{2}$ nucleus of low resonance frequency.

The polarisation transfer pulse sequence INEPT has found considerable use in ^{13}C NMR but is less widely used for other nuclei, despite its inherent advantages. This sequence was used in a ^{29}Si NMR study to determine the ^{2}J coupling constants of compounds in the series $Me_{(4-x)}Si(GeH_3)_x$ (x = 1,2,3). Inversion of peaks as a result of the INEPT sequence help clarify the couplings in this twelve spin system.

^{11}B NMR was used to study the adducts formed by the reaction of the boron trihalides BCl_3, BBr_3, and BI_3 with the donors PPh_3, NPh_3, and $AsPh_3$. Other techniques have not been able to provide a clear picture of what is happening in these reactions, but NMR has provided a much clearer picture. Unfortunately it has not provided a definite answer on the pathway of halogen exchange within the adducts formed.

Another system undergoing halogen exchange was also studied, this time using ^{119}Sn NMR. In the reactions of Et_4NSnX_3 with $Y_3SnCo(CO)_4$ (X,Y = Cl, Br) a crystal structure of the products could not be refined because of disorder in the halogen atoms. While other techniques were able to show that a number of different species existed in solution ^{119}Sn NMR was able to show what these species were and was able to indicate the amount of each existing in solution.

Acknowledgements

I would like to thank my supervisors Prof. K.M.Mackay and Dr. A.L.Wilkins for their assistance and encouragement throughout this work.

My thanks also to Dr. J.Coddington of Auckland University for her assistance in coming to terms with the Bruker AM400, and Dr. M.J.Taylor, also from Auckland University, for generously letting me get involved in the boron-adduct project.

Thank you also to Dr. B.K.Nicholson for helpful discussions, and to the Chemistry Dept. Technicians for their support.

My greatest thanks go to my sons, Matthew and Simon, for whom this work must of at times seemed like a selfish sibling taking far more of their father's time than they felt it might have deserved.

Table of Contents

List of Figures

List of Tables

Chapter 1 Introduction and Overview

This chapter provides a general introduction to this work and describes some of the less apparent difficulties encountered in the observation of nuclei other than ^{1}H or ^{13}C.

Fourier Transform Nuclear Magnetic Resonance Spectroscopy (FT-NMR) has seen rapid growth over the past decade, not only as a result of technical advances such as superconducting magnets that provide higher stable static magnetic fields, but also because of a better understanding of the spin systems and how they may be manipulated.

The rapid change has meant that it is often difficult to keep up with the hardware required for some of the newer experiments. The majority of the experimental work in this thesis was carried out on a JEOL FX90Q instrument. (It is common shorthand to define an instrument, and its field strength, by its proton frequency, thus this instrument has a proton resonance frequency of 90MHz.) When the University purchased this in 1981, it was the only instrument in New Zealand capable of being tuned through the full multinuclear range. The instrument is equipped with a pulse programmer that is by today's standard extremely limited. For any pulse sequence sixty-four lines of program are available, and within this space phasing commands as well as timing intervals must be included. At the time of purchase this was quite adequate for the sequences available but the growth of pulse sequences has been such that the pulse programmer has become a major limitation of the instrument. It was not until 1987 that a high-field instrument with good pulse programming capabilities became available. Installation of a Bruker AM400 instrument (proton resonance frequency 400MHz) at Auckland University provided access to an up-to-date instrument, and gave the opportunity to use a large range of experiments, e.g. the full range of 2-D experiments, for the first time. It also allowed

access to a pulse programmer that allowed for a better range of phase cycling and pulse programming.

A number of different terms have been used to describe the field of NMR for all nuclei other than ^{1}H and ^{13}C. These include "other nuclei", "less-sensitive nuclei", "X-nuclei", or "multinuclear". In this work the latter term will be used.

This work looks at a number of aspects of multinuclear NMR and will not attempt to explain in any detail the basic FT-NMR experiment. A number of extremely readable books are now available that provide clear descriptions of the single- and multi-pulse FT-NMR experiment. For example A.E.Derome's[1] "Modern NMR Techniques for Chemistry Research" gives a clear description of many of the new experiments and what may go wrong with them. Other useful books (but not an exhaustive listing) are listed in references 2-7.

Many of the new multi-pulse NMR experiments make use of a vector diagram to explain the effect of the pulse(s) on the spin systems (for example see the explanation in ref. 1,p63ff), and this technique provides a clear non-mathematical description although it should be noted that it cannot be used to describe all experiments. Unfortunately some confusion has arisen in the literature with some definitions, and while not critical the reader needs to be aware of their existence to avoid any confusion when comparing details from different authors. In a vector diagram description the residual spin is described by a vector aligned along the z axis, corresponding to the static magnetic field. Use of a rotating frame allows for a description of the effect of an applied r.f. field, or pulse, defined as lying along the x axis, on the magnetic vector. Pulses are defined by the angle they rotate the vector, with a subscript of the axis along which they are applied. Thus a 90°_{x}, or $\pi/2_{x}$, pulse would rotate the vector through 90° to lie along the y axis. Some authors (e.g. ref. 1) describe the effect of this pulse as being to turn the magnetic field onto the +y axis. Others (e.g. ref. 7, p4) assume the rotation

will be on to the -y axis. In fact the actual rotation is dependent on such things as the sign of the magnetogyric ratio, but it is important to be consistent with a particular convention when attempting to follow the effect of any particular pulse sequence.

Convention is also such that for any particular pulse sequence the receiver is in phase with an x pulse, i.e. a 90°_{x} pulse will generate a positive signal. While early instruments allowed for phase shifting such that pulses could be applied only along the two orthogonal x,y axes, the subscripts x, y, -x, -y were satisfactory. Defining the x axis as 0° the phase shifts of these pulses can also be defined as 0°, 90°, 180°, and 270° respectively. Modern instruments allow for phase shifting of the excitation pulse within 0.1° steps and thus the degree subscript has become more common. An example is seen in some of the recent composite pulses such as those described in Chapter 2.

Sensitivity, or the lack of it, has long been the major difficulty in obtaining good multinuclear NMR spectra. A look at a table of comparative sensitivities show many nuclei with sensitivities a factor of 10^{-2} or 10^{-3} that of carbon, itself possessing a sensitivity 1.7×10^{-4} that of hydrogen. While these figures provide a general guide to the ease, or difficulty, of observation other factors must be considered. Factors such as line broadening in non spin $^1/_2$ nuclei, long relaxation times, such as those in ^{29}Si NMR, or low observation frequencies can cause other difficulties when undertaking multinuclear NMR.

Higher static magnetic field instruments, currently up to 14.1Tesla, equivalent to 600MHz for ^{1}H, have assisted proton NMR with their higher dispersion of signals. The enhanced sensitivity of these higher fields has also assisted in multinuclear NMR observation, but along with the increase in field strength the development of new pulse sequences has been a major influence.

Development of the polarisation transfer pulse sequences, such as the INEPT[8] sequence resulted in improved sensitivity of X- nuclei in situations where there was a resolvable coupling to a more sensitive nucleus. The sensitivity improvement is determined by the ratio (γ_S/γ_I), where γ_s and γ_I are the gyromagnetic ratios of the sensitive and insensitive nuclei respectively. More recent pulse sequences, such as the family of inverse experiments[9], mean, that as instruments are updated with the appropriate hardware, the overall sensitivity of nuclei with resolvable coupling to sensitive nuclei such as ^{1}H and ^{31}P will increase by a factor of $(\gamma_S/\gamma_I)^{5/2}$.

The growth of multinuclear NMR can been seen by looking at the growth in the literature for any of the nuclei. ^{73}Ge, described in detail in Chapter 3, provides one such example, but a more illustrative case might be that of ^{33}S. In the 1978 book that has become a benchmark in multinuclear NMR[10] Harris was able to list 13 observations for sulphur, the earliest dating back to 1972. By 1983 a review of ^{33}S NMR[11] noted only two further references consisting of 22 further observations, but a review in 1987[12] was able to list 142 different compounds, and noted four further references since completion of the manuscript.

Signal to noise (S/N) ratios are regularly used to compare sensitivity of various instruments. The ratio is commonly defined[2] as 2.5H/h where H is the signal height, and h the height of the noise 'signal'. Martin et al (*ibid* p45 - 47) note that this definition is not as objective as other definitions for S/N, but regardless of the definition used Fourier Transform (FT) NMR is considered to be an ideal technique as repetitive scanning is capable of improving the S/N ratio in an experiment at a rate proportional to $\sqrt{n}$, where n is the number of scans. Unfortunately the technique has practical limits as is well illustrated in Table 1.1 which shows the time required to improve the S/N ratio in an experiment with a 1s recycle time, and where a S/N ratio of 2 is achieved after 30min.

Table 1.1 Experimental Time (Hours) for Improved S/N.

S/N	Expt. Time
2	0.5
4	2
8	8
16	32
32	128
64	512

This latter time is equivalent to 21.3 days, a totally impractical experimental time. It may be seen from the above list that a realistic experimental time of one day will improve the S/N by less than a factor of 8 compared to a signal showing after 30min.

S/N ratios normally quoted for any particular nucleus are on sharp line signals and are therefore of little use when considering whether a particular signal will be observable on a particular instrument. Line broadening, for whatever reason, is a major problem when trying to observe what is already an insensitive nucleus as signals quickly become unobservable. Consider a signal with a measured half-width of 4Hz, possessing a S/N ratio of 250:1. As a first approximation this may be drawn as an equilateral triangle of height 100 and base width 8 (see Fig 1.1(a)). Figs 1.1(b) and 1.1(c) represent triangles of equal area to that in Fig 1.1(a) but where the S/N is 25 and 5 respectively. The latter may be considered to be a signal of minimal observable intensity under equivalent conditions to that used to obtain the signal in Fig 1.1(a). The half-width of this signal is 100Hz and any signal wider than this would be unobserved.

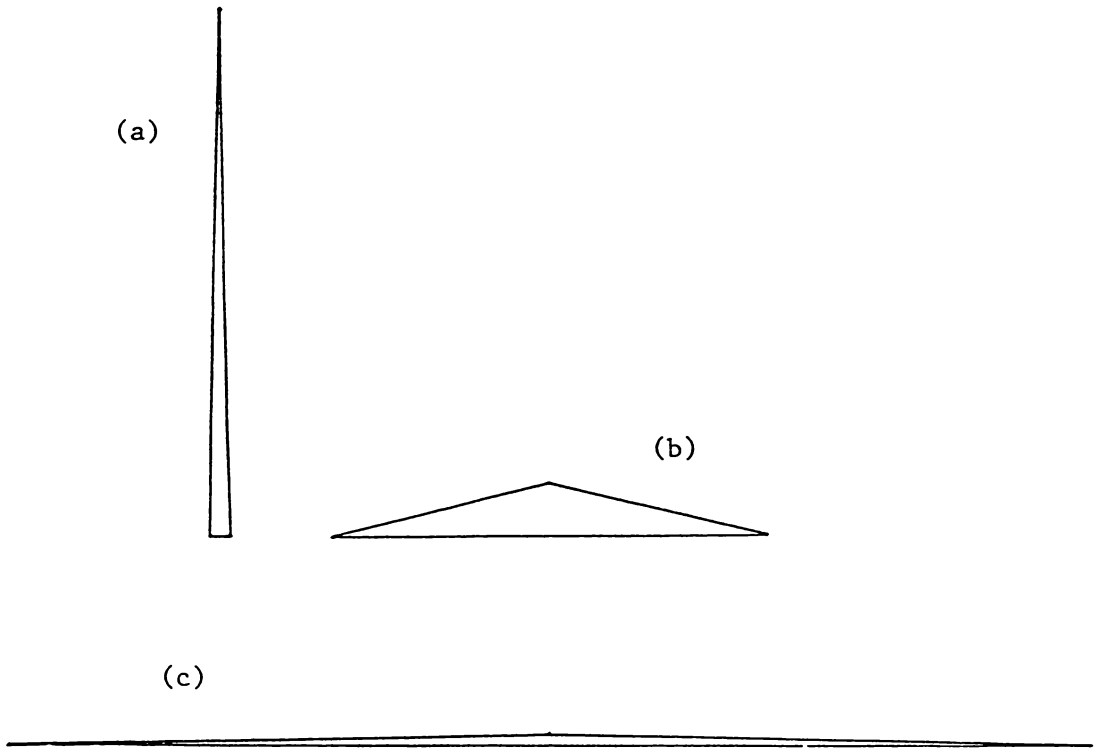

Fig. 1.1 The effect of linewidth on peak intensity in NMR; (a) an equilateral triangle approximating an NMR signal with a S/N ratio of 250 and a halfwidth of 4Hz., (b) an equilateral triangle of equal area to that in (a) but possessing a S/N ratio of 25. results in a halfwidth of 40Hz, (c) a triangle representing a signal of minimum observability (S/N 5). The halfwidth in this case is 100Hz.

Guide to Thesis Chapters

To be certain of seeing a broad line it is important to ensure a smooth baseline in the NMR experiment. The problem of uneven baseline and techniques for generating smooth baselines are discussed in detail in Chapter 2, along with results obtained when observing the low frequency nucleus ^{73}Ge.

The general difficulties of observability when studying a low frequency nucleus, with problems of acoustic ring and low inherent sensitivity, are considered in greater detail in Chapter 3 where work with ^{73}Ge is discussed.

As mentioned before the most common problem in obtaining spectra for X nuclei is the overall lack of sensitivity. ^{29}Si does not suffer from this difficulty, being 2.1 times more sensitive than ^{13}C, but here the long relaxation times cause problems, as the number of scans that may be collected in a reasonable time is considerably reduced. For example the measured T_1 times in the compound $Me_2Si(GeH_3)_2$, a compound studied in this work, were Si 65.3s, Ge 7.4ms, C**H** 11.9s, and Ge**H** 4.4s. The polarisation transfer sequences, such as INEPT are useful in the observation of ^{29}Si, not only because of the improved sensitivity they provide, but also because the relaxation time that is important in the experiment is that of the protons, which are normally considerably less than silicon. Description of this pulse sequence and application of the technique to obtain $^{29}Si—^{1}H$ coupling constants is detailed in Chapter 4.

Often the information obtained from multinuclear NMR cannot be obtained by any other technique. Chapter 5 details work with boron trihalide adducts where NMR has proved to be the only technique suitable for the study of the adduct-donor bond.

The final chapter looks at the use of multinuclear NMR in the study of exchanging systems. The use of ^{119}Sn NMR provides details of halide exchange that other techniques had failed to provide.

General Experimental Methods

While specific details are provided in the appropriate chapters general experimental details are noted here.

As mentioned above the two instruments used in this work were a JEOL FX90Q and a Bruker AM400. Details of the instruments are as follows:-

JEOL FX90Q 2.11T electromagnet, internal or external heteronuclear lock (either ^{7}Li or ^{2}D), TI 980B 16 bit 56K minicomputer, ADC: 12bit 2 channel, max. spectral width of ≤ 30KHz, twin floppy disc drive, PG200 pulse

programmer, foreground/background system, multinuclear observation using two probe inserts (a) 'Low frequency insert NM-IT10LF' covering the frequency range 2.76-6.5MHz and (b) 'Broadband insert NM-OBS1' covering nuclei from ^{103}Rh at the low frequency limit to ^{1}H with the exception of the region of ^{205}Tl.

Bruker AM400 9.4T superconducting magnet, internal 2D lock, ASPECT 3000 24bit computer with FT coprocessor installed, ADC: 12bit word, max. spectral width of 166kHz, mid-range 10mm multinuclear probe extended to cover the range ^{31}P to ^{73}Ge, temperature maintained at 295°K by a VT-1000 variable temperature unit,

Air or moisture sensitive samples were sealed in 5mm O.D. or 8mm O.D. tubes that were then placed concentrically in a 10mm O.D. NMR tube using two spacers. D_2O was placed in the 10mm tube to provide a lock signal. The sealed tubes were made from standard thin wall tubing, not NMR grade tubing. The resultant loss in homogeneity was not serious when observing X nuclei, with only marginal line broadening resulting. These tubes could not be used for ^{1}H NMR however, and in the cases where proton spectra were required sealable tubes made from the considerably more expensive Wilmad NMR grade tubing were used.

Chapter 1 References

1. A.E.Derome,*'Modern NMR Techniques for Chemistry Research'*, Pergamon Press, Oxford, 1987.
2. M.L.Martin, J.J.Delpuech, G.J.Martin, *'Practical NMR Spectroscopy'*, Hayden, London. 1980.
3. E.Fukushima, S.B.W.Roeder, *'Experimental Pulse NMR: A Nuts and Bolts Approach'*, Addison-Wesley, London. 1981.
4. P.Lazlo (Ed.), *'NMR of Newly Accessible Nuclei. Vol 1 and 2'*, Academic Press, New York, 1983.
5. J.B.Lambert, F.G.Riddell (Eds.), *'The Multinuclear Approach to NMR Spectroscopy'*, D.Reidel, Dordrecht, 1983.
6. J.Mason (Ed.), *'Multinuclear NMR'*, Plenum Press, New York, 1987.
7. W.S.Brey (Ed.), *'Pulse Methods in 1D and 2D Liquid-Phase NMR'*, Academic Press, San Diego, 1988.
8. G.A.Morris and R.Freeman, *J. Am. Chem. Soc.*, **101**, *760*, 1979.
9. G.Bodenhausen and D.J.Ruben, *Chem. Phys. Lett.*, **69**, *185*, 1980.
10. R.K.Harris and B.E.Mann (Eds.), *'NMR and the Periodic Table'*, Academic Press, London, 1978.
11. Ref. 5, p.390.
12. *'Annual Reports in NMR Spectroscopy'*, Vol. 19, 1987. G. A Webb (Ed)

Chapter 2 Acoustic Ring Suppression Sequences

2.1 Introduction

2.1.1 Baseline Distortions

In the Introductory Chapter mention was made of broad signals and how, even for samples with relatively high S/N ratios, only minor broadening lowers the S/N to the point where the signal becomes unobservable. It is especially important to have smooth spectral baselines when searching for broad signals.

A major source of baseline distortion in spectra observed at all frequencies results from 'ring' arising from the bandpass filter's response to the excitation pulse[1]. This filter, used between the receiver and the ADC, can be stimulated into oscillation by the NMR pulse and a reasonable delay is required between the end of the pulse and the start of acquisition to avoid this oscillation appearing in the signal. Techniques proposed[2] to overcome the problem include,

(i) increasing the delay between the end of the pulse and the start of acquisition.

(ii) zero-filling the start of the FID before the fourier transform.

(iii) applying a trapezoidal window to the FID.

The first technique creates difficulties as the increased delay creates a third order phase twist that often cannot be adjusted for by the spectrometer phasing routines. Care must also be taken to ensure that the delay is not so large as to lose most, or all, of the signal. This is a particular problem for broadline bands from fast-relaxing nuclei as the delay must be less than $(\pi\Delta\upsilon_{1/2})^{-1}$ to avoid serious loss of signal[3]. Zerofilling the FID, or application of a trapezoidal window, accentuates the sinx/x appearance of the peaks.

Roll in the baseline can be a problem when accurate integration is required, but can often be corrected, with varying degrees of success, by

software subroutines that may apply up to a fifth order polynomial smoothing.

Another cause of base-line problems arises from the use of long, low power, selective pulses to cancel strong signals[4], such as water in biological samples, to allow observation of the weak signals. Because of long time delay between the centre of the pulse, and the start of acquisition, there is a resultant phase twist in the spectrum[5] that is not easily removed by normal software routines.

2.1.2 Acoustic Ringing

A further form of 'ringing' known as 'acoustic ringing' is a more serious problem in spectra observed at lower frequencies[3] (i.e. from nuclei of lower gyromagnetic ratio). This spurious signal results from the electromagnetic generation of ultrasonic waves in metallic material[6]. The acoustic energy, in the presence of a static magnetic field B_0 is converted into a r.f. field detected by the coil. The r.f. phase of this acoustic response is coherent with the phase of the exciting pulse and the amplitude (A) of the spurious signal is given by[7]

$$A=kB_1B_0^2/mv_s(1+\beta^2) \qquad ...(2.1)$$

where m= material mass density, v_s= shear velocity of the material, and

$$\beta^2 = 2.5.10^{13}.(\rho^2/v_s^4)\nu^2$$

where ρ is the resistivity and ν is the frequency.

The body of the commercial probes ~~are~~ is generally made of aluminium, but the data in Table 2.1 shows that other metals provide a better choice.

Table 2.1 Values of m, v_s, ρ, and β^2 for Various Metals[a]

	m (10^3 kg/m^3)	v_s (m/sec)	ρ ($10^{-8}\Omega$–m)	mv_s mv_s(Al)	β^2 (at 5MHz)
Aluminium	2.7	3040	2.7	1.0	0.005
Brass (70% Cu)	8.5	2110	6.2	2.2	0.121
Copper	8.9	2270	1.7	2.5	0.007
Gold	19.7	1200	2.4	2.9	0.173
Lead	11.4	690	20.7	1.0	118
Platinum	21.4	1730	10.6	4.5	0.783
Silver	10.4	1610	1.6	2.0	0.024
Stainless (347)	8.0	3100	73	3.0	3.61
Tungsten	19.3	2640	5.7	6.2	0.042
Zinc	7.1	2440	5.9	2.1	0.061

(a) from ref. 7 and references therein.

Table 2.1 shows that aluminium is a poor choice because of its small β^2 and m. The situation is worse at low temperatures where, with all pure metals, β^2 decreases rapidly. Calculation of the denominator of eq. (2.1) shows that brass is about 2.4 times better than aluminium and stainless steel about 14 times better.

The resultant signal transforms to a broad envelope of frequencies centred around the carrier frequency and in phase with the exciting pulse[6]. It can been seen that the amplitude of the signal is proportional to B_1 (and therefore the inverse of the pulse width), the square of the static field B_0, and inversely proportional to the pulse frequency (via ω). Initial studies of this phenomenon were made at the time when iron core magnets were the norm in NMR spectroscopy, and it was suggested that at these fields acoustic ringing becomes a problem at somewhere between 15 to 20MHz and below[6]. The duration of the acoustic signal at very low frequencies can be as long as

2ms[6] thus obscuring any signal broader than 160Hz. The intensity of the signal is such that weak sample signals may not even trigger the ADC under normal sample conditions. For a signal such as this, the baseline roll removal techniques discussed above are even less useful. If the ring was reproducible a simple blank subtraction could be used to remove the acoustic signal from the sample signal, but it has been found that the acoustic ring signal varies[8] even if the same sample is removed from the probe and then replaced.

That the acoustic ring signal is in phase with the exciting pulse, while the phase of the NMR signal will depend on its 'pulse history', has been used to generate a number of pulse sequences using signal echoes to remove the unwanted acoustic signal. The first pulse sequence [A] proposed[9] to take advantage of this technique uses the simple spin echo sequence

$$90° - \Delta t - 180° - \Delta t - ACQ - T_d \qquad \text{..... [A]}$$

where Δt is the preaquisition delay, and T_d is the relaxation delay. (Note: No consistent symbol has emerged for defining interpulse delays, with Δ, Δt or τ being the most commonly used.)

Canet[10] and Patt[11] independently proposed the pulse sequence [B]

$$90^\circ_x - \Delta t - ACQ(+) - T_d - 180^\circ_x - \tau - 90^\circ_x - \Delta t - ACQ(-) - T_d \qquad \text{.....[B]}$$

where τ is the inversion recovery delay.

To avoid the acoustic response from the 180° pulse Patt [11] suggested that its phase should be alternated as $\pm x$. On the other hand Ellis[12] proposed that the 90° pulses should be alternated as $\pm x$ while the 180° pulse phase was kept constant. In fact with normal CYCLOPS receiver phase cycling these two sequences become identical after eight pulses. While this pulse sequence was never directly published it has been used in a number of experiments to

reduce baseline roll in ^{99}Ru[13], ^{43}Ca[14][15], and ^{33}S[8][16] NMR spectra. Harris in his work on ^{33}S NMR[8] gave pulse sequence [B] the acronym RIDE (for RIng Down Elimination), an acronym since used by others. At the time that the RIDE sequence [B] was proposed, Ellis[12] suggested a further sequence [C] that would address the non-linearity of the acoustic ring signal. In this sequence a spin echo is observed rather than observing the signal directly.

$$90^\circ_x - \Delta_1 - 180^\circ_x - \Delta_2 - ACQ(-) - T_d - 90^\circ_{-x} - \Delta_1 - 180^\circ_{-x} - \Delta_2 - ACQ(+) - T_d - 180^\circ - \tau - 90^\circ_x -$$

$$\Delta_1 - 180^\circ_x - \Delta_2 - ACQ(+) - T_d - 180^\circ - t - 90^\circ_{-x} - D1 - 180^\circ_{-x} - \Delta_2 - ACQ(-) - T_d \ldots\ldots [C]$$

This sequence was utilised by Gerothanassis[17] in his study of acoustic ring sequences when observing ^{17}O at 48.8MHz where he called it the extended spin-echo sequence. Ellis later[18] pointed out that Gerothanassis appeared to have the pulse phasing incorrect but he then, unfortunately, went on to call pulse sequence [C] RIDE even though it is quite different to the sequence [B] named RIDE by Harris. The sequence and phase cycles published by Ellis and also noted in ref. 13 is as follows

$$90^\circ_\alpha - \tau_1 - 180^\circ_\beta - \tau_2 - ACQ - T_d - 180^\circ_\gamma - 90^\circ_\delta - \tau_1 - 180^\circ_\beta - \tau_2 - ACQ - T_d \quad \ldots [D]$$

For a constant receiver phase the pulse phases are

α = x,x, -x, -x

β = y, -y, x, -x

γ = x,x,x,x

δ = -x, -x, x, x

In this work, which looks at the efficiency of both sequences at both 3.13MHz on a JEOL FX90Q spectrometer and 13.96MHz on a Bruker AM400 spectrometer, the earlier acronyms of RIDE for [B] and EXSPEC (EXtended SPin ECho) for [C] respectively will be used.

Gerothanassis and Lauterwein[17] considered the merits of the above pulse sequences for ^{17}O NMR at 48.8MHz, and Gerothanassis[19] later proposed a sequence [E] suitable for use on earlier spectrometers

$$90^{\circ}_{x} - \Delta t_1 - FID(+) - T_d - 90^{\circ}_{x} - (\tau + \tau_p + \Delta t_1) - FID(+)$$
$$- T_d - 90^{\circ}_{x} - \tau - 90^{\circ}_{x} - \Delta t_1 - FID(-) - T_d \quad \text{....[E]}$$

that did not have the facility of r.f. pulse phase shifting. He called this a "Simple Reference Baseline Subtraction-90° Pulse Sequence" and will be known in this work as the RFB-90 sequence. This sequence has $\pi/2$ pulses of constant phase, with every third transient including a $\pi/2$-τ-$\pi/2$ pulse ($\tau <$ 1ms), which is in effect a two component composite pulse, designed to leave the sample magnetisation along the -z axis. The first and second transients generate two sample FID's imposed on two ring FID's, while the third transient subtracts two ring FID's. Thus only two of the three FID's yield sample signals and the sequence may be considered as being 50% less efficient than the earlier mentioned sequences.

Goc and Fiat[20] proposed a sequence [F] that may also be used on

$$270° - FID(+) - T_d - 90° - FID(-) - T_d \quad \text{.....[F]}$$

earlier spectrometers. They tested this sequence on a similar sample to that used by Gerothanassis in his earlier survey[17], but accumulation conditions were different enough that direct comparisons could not be made.

Laue *et al*[21] evaluated the use of the maximum entropy method (MEM), a technique where trial FID's are compared with the 'experimental' FID to improve the overall S/N of the experiment, to correct for acoustic ringing. They suggest that while the technique does assist in recovery of data from FID's that include ring signals, other techniques should be used to ensure minimisation of the ring signal during data collection.

2.1.3 Composite Pulses

A number of authors have noted[16,17] that the major difficulty with all these pulse sequences is that the use of 180° pulses results in reduced excitation windows. Gerothanassis[22] noted that in a sample where two signals were separated by 40,000Hz (750ppm), two separate experiments were required to allow observation of the signals. Ellis[18] has considered the effect of a three component composite 90° pulse, along with a three component I_z inversion and a seven component echo 180° pulse and found that he was able to nearly double the effective window.

In a standard single pulse experiment two effects work against the achievement of perfect $\pi/2$ or π pulses[23]. Variations in the B_1 field may result from imperfect coil construction, or from imperfect setting of tip angles, while tilted effective fields result from offset effects. The latter lead to phase errors in the spectrum that can usually be corrected during data processing. Better probe design has become necessary as static fields increase, with stronger B_1 fields required at the higher static field to ensure that acceptable performance is maintained. These newer probes generally provide better B_1 homogeneity but difficulties still exist.

With the newer multi-pulse experiments it is more important to ensure that proper tip angles are achieved. For example the INEPT and DEPT sequences (see Chapter 4) rely upon magnetisation vectors being placed along specified axes to ensure magnetisation transfer. Over the last ten years much work has gone into the development of composite pulses in an effort to overcome these difficulties. Composite pulses are a sequence of pulses of varying time, phase and/or amplitude designed to give $\pi/2$ or π pulses of satisfactory performance.

Early work tended to consider the two problems of B_1 field and offset separately.[24,25] The first π composite pulse[24], $90^\circ_x\,180^\circ_y\,90^\circ_x$, designed for B_1 compensation, resulted in a less than 1% deviation in inversion for up to

±20% deviation in pulse duration. It was noted that for better resonance offset compensation the 180° pulse should be replaced by one greater than 180° with 240° recommended for moderate offsets,[25] while 270° gave inversion independent of small offsets[26,27]. Other sequences have been designed using either 90° phase shifts[27,28] or 180° phase shifts[28].

Dual compensation sequences designed by Shaka and Freeman[28] resulted in the efficient GROPE 16 sequence which provides compensation for a ±20% misset pulse and offsets up to $\pm 0.5B_1$, while similar results were achieved by Starcuk and Sklenár[29]. Shaka has used numerical non-linear optimization to generate a number of π pulses[30,31]. An eleven segment sequence with 180° phase shifts gives good frequency offset compensation over a bandwidth of $\pm 2B_1$, while a thirty-one segment pulse compensates over $\pm 3.2B_1$.

Sequences using other than 90° or 180° phase shifts have been designed[32,33] while more recently, stemming from earlier work with frequency selective pulses, amplitude modulated composite pulses[34,35] have been designed.

Levitt's review[36] of composite pulses published up until 1986 contained 127 references but he noted that little practical work had been carried out using composite pulses. The best known use is in WALTZ decoupling sequences[28] with WALTZ-16, or derivatives, now standard on most new spectrometers. Composite π/2 pulses have been applied to help suppression of SPT artifacts in nOe experiments[37], while Schenker and von Philipsborn[38] have tested Shaka's three component composite π pulses, designed to compensate for B_1 errors[28], in the INEPT and DEPT sequences and found improved polarisation transfer at large offsets. Levitt and Ernst[39] have used composite pulses in DEPT and INADEQUATE experiments as have Wimperis and Bodenhausen[40].

Despite the large variety of composite pulse sequences, considerable care must be taken with their implementation as the lack of practical

application has meant doubts still exist as to their suitability in particular pulse sequences. While a number of sequences have been designed for spin 1 systems [36][41][42][43][44][45][46] the majority have been designed for the spin 1/2 case[36], and their effectiveness for higher spin systems is untested. While most composite π pulses have been designed with spin inversion in mind some may be used for spin echoes. At first the original $90^\circ_x 180^\circ_y 90^\circ_x$ composite π pulse was thought to be useful only for inverting z axis magnetism[25], for example in the T_1 inversion recovery sequence [π-τ-π/2-acquire], but it was later shown[26] that it could be used for spin-echo work, [e.g the $\pi/2(-\tau-\pi)_n$-τ-acquire, sequence] as long as only alternate echoes were observed. Phase distortions generated by the sequence are present only in odd number echoes and if these are ignored no difficulty arises.

Limitations observed to date include the warning[47] that all composite pulses that exhibit low phase distortion in the presence of B_1 inhomogeneity are relatively sensitive to resonance offset effects, and that composite spin inversion pulses using only 180° phase shifts are insensitive to small phase errors but are less tolerant to errors in pulse flip angle[29]. When a network of coupled spins is under study composite pulses must be of short duration compared with the inverse of the coupling constant if compensation is to be effective[48], while to be equally effective at positive and negative offsets constant amplitude composite pulses must be symmetric with respect to time[48].

It has been recommended[49] that testing the offset effectiveness of composite pulse sequences should be carried out on a sample having a single line, and to use a sequence where the composite pulse is applied off frequency followed by a read pulse on resonance, thus avoiding any additional off resonance effects. Unfortunately this is of little use when trying to observe a multiline spectrum and all experiments in this work involve all pulses being applied at the same resonance frequency.

It may be seen from the above comments that the ideal composite pulse has not yet been devised and so each has to be tested for its effectiveness. Because hardware limitations did not allow for use of amplitude modulated pulses or those requiring 1° phase shifts the π composite pulse sequences tested in this work were limited to a five composite sequence of Levitt[27], Shaka's[30][31] three, four, five and six component pulses, and Shaka and Freeman's six component GROPE 16 sequence[50]. Pulse programming limitations meant that composite π/2 pulses could not be tested in the sequences at the same time.

Derome has noted[49] that pulse droop may be a problem with some of the longer sequences quoting the difficulty arising for a transmitter designed for 20μs pulses that has to cope with a 160μs GROPE 16 pulse. In the case of germanium NMR on the JEOL FX90Q instrument, the current π/2 pulse is 150μs so in this case pulse droop might be expected to be even more of a problem. Derome also notes that it is important to test composite pulses on a machine-by-machine basis for optimum results.

2.2 Experimental

The initial work was carried out on a JEOL FX90Q equipped with a Low Frequency insert NM-IT10LF. The observation frequency for germanium is 3.13MHz. Pulse widths at this frequency were 130μs for a 90° pulse and all offset comparisons are made with data obtained using this pulse width. After repairs had been carried out on the instrument the pulse time increased to 150μs. The applications spectra (Figs. 2.9, 2.10 and 2.11) were obtained using this longer pulse time. The pulse sequences studied are shown in Fig. 2.1 along with the phase cycling of the pulses assuming a receiver phase of 0°. Full CYCLOPS phase cycling was applied in all cases. The basic spin-echo sequence [A] is defined as PHASE 2 or PHASE 4 depending on the extent of phase cycling of the pulses. Typical Δ or τ values were in the range 20 - 30μs.

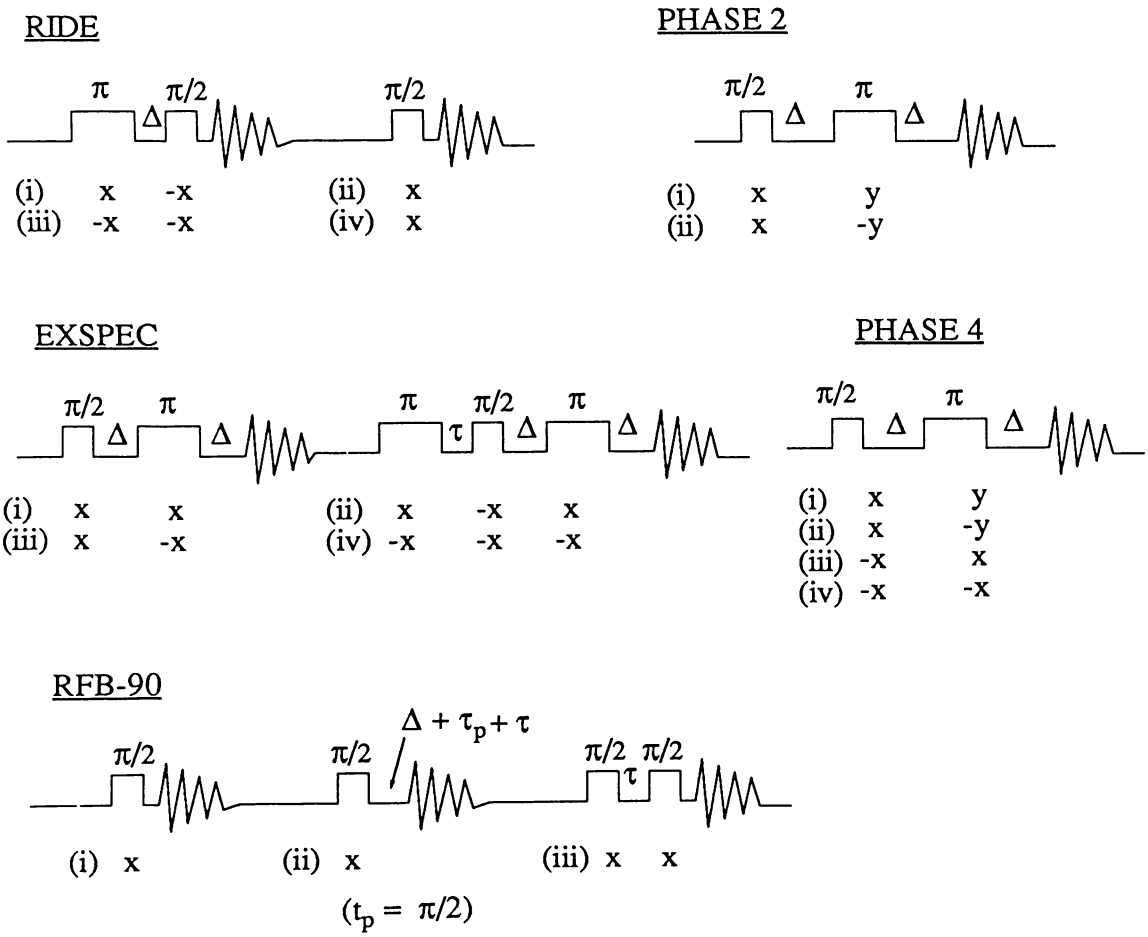

Fig. 2.1 Pulse sequences used during this work. The phase cycling is shown for a receiver phase of 0°.

Table 2.2 lists the composite pulses used in the course of this work.

Table 2.2 Composite Pulses Used in this Work.

Designation	π_x pulse train	total pulse time (ms)	relative time[a]
PHASE 4/3C	$90^\circ_x, 180^\circ_y, 90^\circ_x$	600	2.0
PHASE 4/3C(60)	$90^\circ_x, 60^\circ_y, 90^\circ_x$	400	1.33
PHASE 4/3C(240)	$90^\circ_x, 240^\circ_y, 90^\circ_x$	700	2.33
RIDE 3C	$90^\circ_x, 180^\circ_y, 90^\circ_x$	600	2.0
RIDE 3C(60)	$90^\circ_x, 60^\circ_y, 90^\circ_x$	400	1.33
RIDE 3C(240)	$90^\circ_x, 240^\circ_y, 90^\circ_x$	700	2.33
RIDE 4C	$34.2^\circ_{-x}, 123.0^\circ_x, 197.6^\circ_{-x}, 288.8^\circ_x$	1073	3.58
RIDE 5C	$90^\circ_x, 200^\circ_y, 80^\circ_{-y}, 200^\circ_y, 90^\circ_x$	1100	3.67
RIDE 6C	$158^\circ_x, 171.2^\circ_{-x}, 342.8^\circ_x, 145.5^\circ_{-x}, 81.2^\circ_x, 85.3^\circ_{-x}$	1640	5.47
RIDE G16	$270^\circ_{-x}, 360^\circ_x, 90^\circ_y, 270^\circ_{-y}, 90^\circ_x$	2400	8.0

(a) compared to a standard π pulse.

The JEOL PG200 pulse programmer combines the phase of the programmed pulse with the phase of the observation channel, shown as SCAN, and therefore care has to be taken when writing pulse programmes to ensure that the required phase of the observation pulse equals the sum of the programmed pulse and SCAN. Thus to obtain an x(0°) pulse when SCAN= -x(180°) the pulse phase must be set to -x, i.e. 180°(programmed pulse) + 180°(scan) = 0°(execution phase). Table 2.3 gives an example of the pulse and phase sequence required to obtain full phase cycling, in this case in the RIDE sequence. The first two lines show the pulse program as

written, followed by the effect of cycling of the full scan cycle to ensure all phase combinations are obtained. The underlined pulses generate the basic sequence [B].

Table 2.3 Pulse Sequence Phasing Used. Execution Phases are given in brackets.[a]

RIDE Sequence				
90°- D_t- ACQ	-T_d-	180°	-t-	90°-D_t-ACQ-T_d
0(0) 0		0 (0)		180(180) 0
0(0) 0		180(180)		180(180) 0
0(90) 90		0(90)		180(270) 90
0(90) 90		180(270)		180(270) 90
0(180) 180		0(180)		180(0) 180
0(180) 180		180(0)		180(0) 180
0(270) 270		0(270)		180(90) 270
0(180) 270		180(90)		180(90) 270

(a) The underlined sets of phases add up to the basic RIDE sequence of (signal + ring) - (-signal + ring). These are then cycled through the standard quadrature phase sequence.

The work was extended on the Bruker AM400 instrument at Auckland University when it was installed. Although this instrument did not have a low frequency probe the standard multi-nuclear probe had been 'stretched' to allow for observation of germanium which has a resonance frequency 13.96MHz at this field. The 90° pulse is 31μs which may at first glance appear to be considerably better than the 130μs of the 90MHz instrument, but the higher field (approx. x4) means that the overall excitation window (in p.p.m.) is virtually the same on both instruments. With the greater

programming capability of this instrument a composite 180° pulse version of the extended spin echo sequence could be studied and this was compared to the RIDE sequence, also with six-composite π pulses. As the only reported version of this sequence at the time of the study was that in ref. 17 this was the sequence used in the high field study. Ellis[18] points out the fact that the published sequence does not phase the 180° pulses correctly, and that this may account for some of the residual roll noted by Gerothanassis. This new phasing sequence has not yet been tried.

To avoid any difficulties resulting from overflow of the ADC the sequences were programmed to ensure alternate addition and subtraction of the ring signal.

Spectra were run on samples of $GeCl_4$ (on the JEOL FX90Q), and $GeBu_4$ (on the Bruker AM400), with increasing offsets from the centre of the spectrum. For any particular experiment all pulses were applied at the particular offset, so that conditions similar to those expected in a multi-line experiment were in effect. Intensity of the resulting signal was determined by calculating S/N values and normalising the figure to the on-resonance intensity. To avoid an inordinately long experimental time with the insensitive ^{73}Ge samples S/N ratios were often less than 20:1. As a result the error in calculated intensity may amount to 20%. Thus the relative intensity diagrams in the following sections should been seen as indicating trends rather than exact figures. On the Bruker AM400 instrument the AI command allows for a more accurate comparison of intensities between spectra. Most spectra were checked at both positive and negative offsets, and found to be symmetric within the experimental S/N error of 10%. Results are plotted for positive offset only.

2.3 Results and Discussion

2.3.1 Spectral Windows

Fig. 2.2 shows the excitation intensity and phase change, for varying offsets, using a standard 90° pulse (130μs) of the JEOL FX90Q at the resonance frequency of ^{73}Ge (3.13MHz).

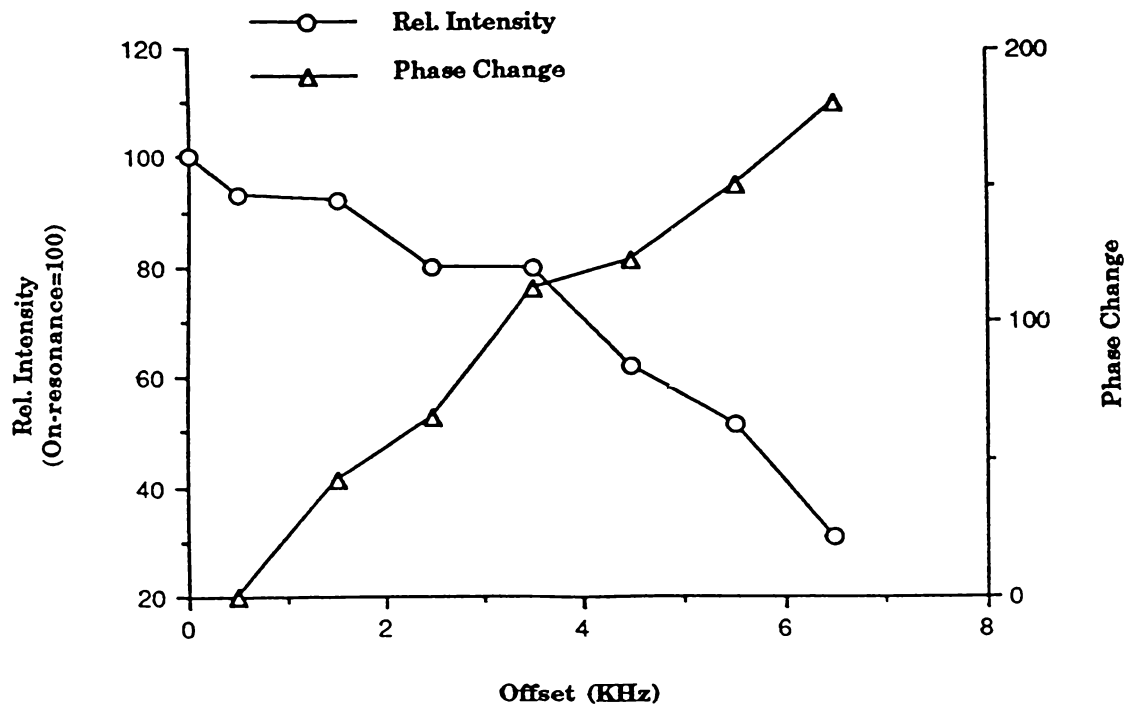

Fig. 2.2 Excitation window and phase change of a ^{73}Ge 90° pulse at varying offsets.

It should be noted that the phase change is not a serious problem as long as it is linear across the window. In such cases the normal software phasing routines will be able to correct for such changes, or use of the POWER display mode may be used as long as accurate line-widths are not important.

Fig. 2.3 shows the ^{73}Ge frequency spectrum resulting from a sample of $GeEt_4$ using the standard single pulse experiment on the JEOL FX90Q. A 5000Hz observation window was used and 1000 scans were acquired. The overall recycle time is 1.6s.

Fig. 2.3 Frequency spectrum of $GeEt_4$ obtained on the JEOL FX90Q using standard single pulse experiment. 1000 scans were collected over a 5000Hz window with a 1s relaxation delay.

Excitation windows for each of the pulse sequences investigated (Fig. 2.1) are shown in Fig. 2.4. PHASE 2 and PHASE 4 sequences gave virtually identical results and are plotted as one.

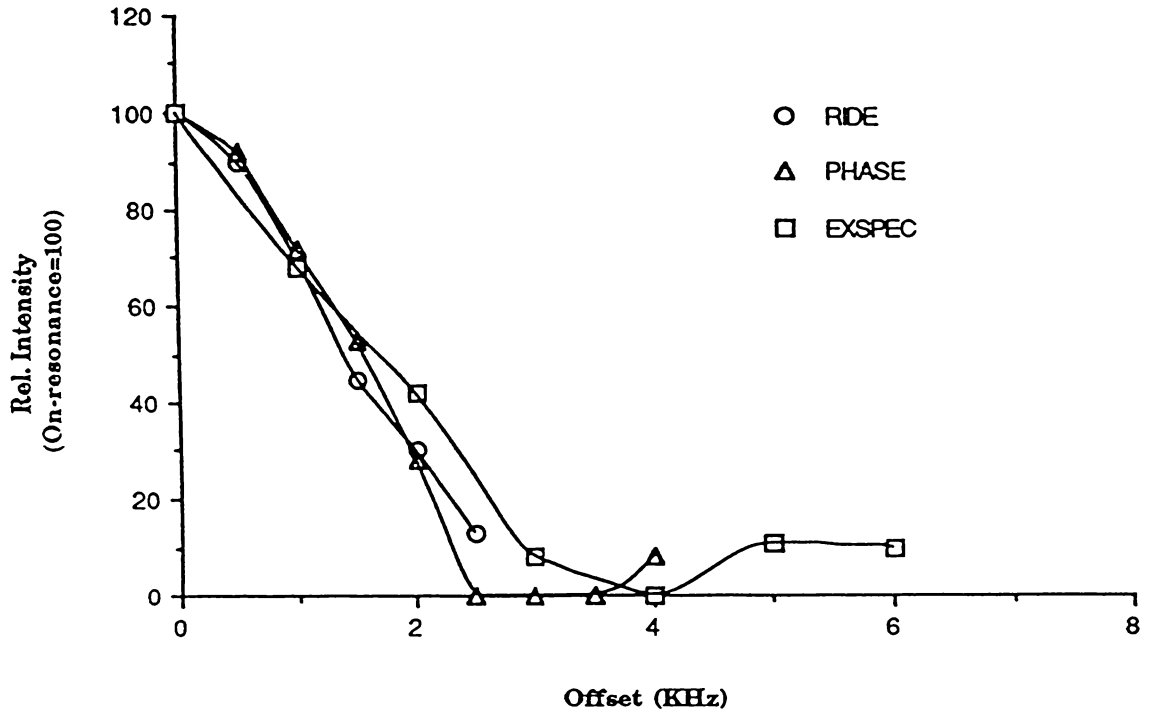

Fig. 2.4 Excitation windows on the JEOL FX90Q for each of the pulse sequences studied.

In each case the phase change across the window was no more than 80°, and linear, i.e. within limits that could be corrected by the software.

It is immediately apparent that these sequences have severely restricted excitation windows. The relative intensity has dropped to only 80% of the on-resonance value when the signal was shifted no more than ±1KHz off-resonance, and at 2KHz the intensity was below 50%. The PHASE 2 sequence resulted in incomplete cancellation of the ring signal. All other sequences provided complete cancellation. The extra phase cycling in the PHASE 4 sequence is apparently required to remove the residual ring signal from the spectrum. Ellis[18] indicated that a similar increased phase cycling might remove residual roll observed in ^{17}O NMR by Gerothanassis[17] when he used the EXSPEC sequence [C], rather than sequence [D].

In the PHASE sequence the delay time Δ (Fig. 2.1) should be set to a value that generates optimum echo signal. In a set of experiments the delay time was varied and the resultant spectrum intensity measured. It was found that signal intensity remained within ±10% as the delay was varied from 1μs through to 1ms delay, while still maintaining acceptable baseline. For a sample giving a wide line, this figure would need to be set as small as possible to obtain maximum signal.

A similar experiment was carried out using the RIDE sequence and delay times varying from 5μs through to 100μs were again found to give satisfactory results.

As noted in the Introduction a delay between the end of a pulse and the start of acquisition is necessary to avoid the effects of pulse breakthrough. For wide line signals this is of course a disadvantage as much of the signal may be lost during this delay time. With the read pulse in the RIDE sequence immediately prior to acquisition an experiment was run to determine how small this interval could be without seriously affecting the performance of the sequence. On the JEOL FX range of instruments the time between the end of a pulse and the start of acquisition is defined by the sum of two time intervals. One interval, denoted as DELAY, is normally set by the computer and is dependent on the observation window and the number of data points in the spectrum. For a spectral window of 10,000Hz and using 8000 data points this delay is 50μs. This delay can be altered by the operator but care must be taken to avoid difficulties with excessive phase roll. The second interval is defined as DEADT (DEAD Time) and is normally set at 50μs. In a series of experiments it was found that both these figures could be reduced to as low as 0.5μs (i.e. a total delay of 1μs) without any effect on the spectral base-line. This is obviously important when trying to observe broad-line signals.

To compare the RFB-90 pulse sequence with those described above an experiment was run where an equivalent number of scans were collected, at

varying offsets, for both the RFB-90 and the EXSPEC sequence. Results are plotted in Fig.2.5 and it may be seen that, as indicated earlier, the RFB-90 sequence is approximately 50% as efficient as the EXSPEC sequence on-resonance. The RFB-90 sequence retains some residual intensity out to 4KHz, while by this time the EXSPEC sequence is zero. Both sequences provide 50% of their original intensity out to ±2KHz off-resonance but the inherent overall sensitivity of the EXSPEC sequence must make it the one of choice.

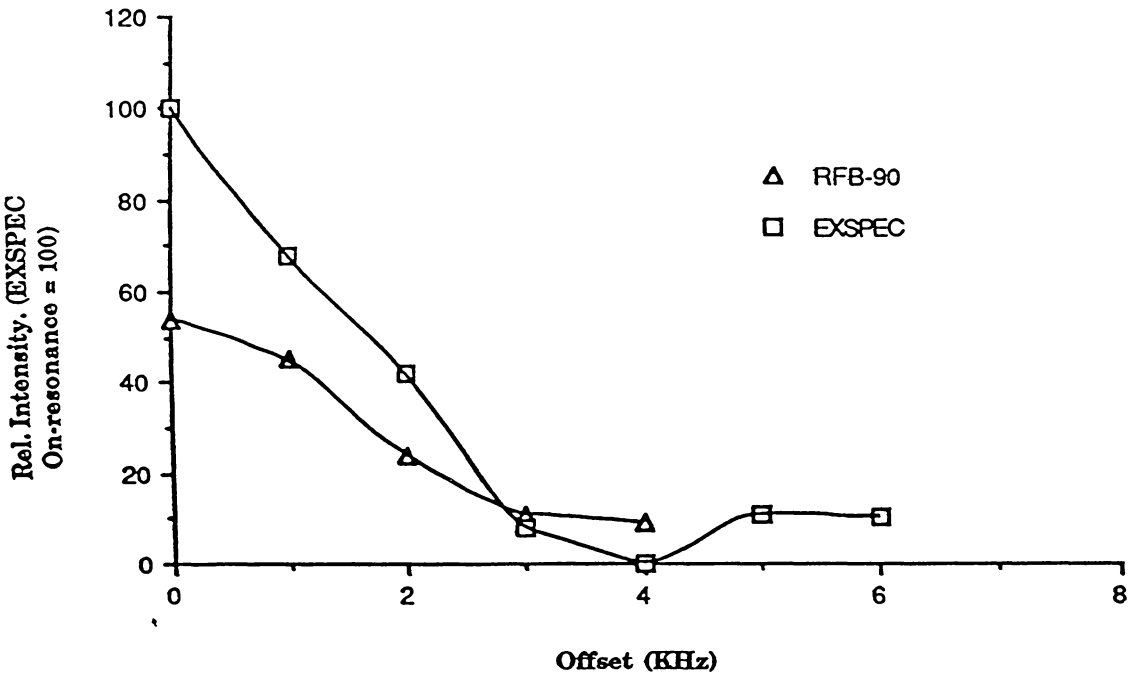

Fig. 2.5 Comparison of the signal intensities obtained from the RFB-90 and EXSPEC pulse sequences on the JEOL FX90Q.

2.3.2 Composite Pulses

In an effort to extend the useable excitation windows a number of composite π pulses were used. As the PHASE 2 sequence had not completely eliminated the ring signal no further work was carried out with this

sequence. The PG-200 pulse programmer limitations also meant that no composite pulses could be used in the EXSPEC sequence. Composite pulse sequences used are noted in Table 2.3 above, along with their lengths compared with a standard π pulse.

Figures 2.6, 2.7, and 2.8 show the excitation windows for the various composite pulses substituted in the PHASE 4 and RIDE sequences respectively.

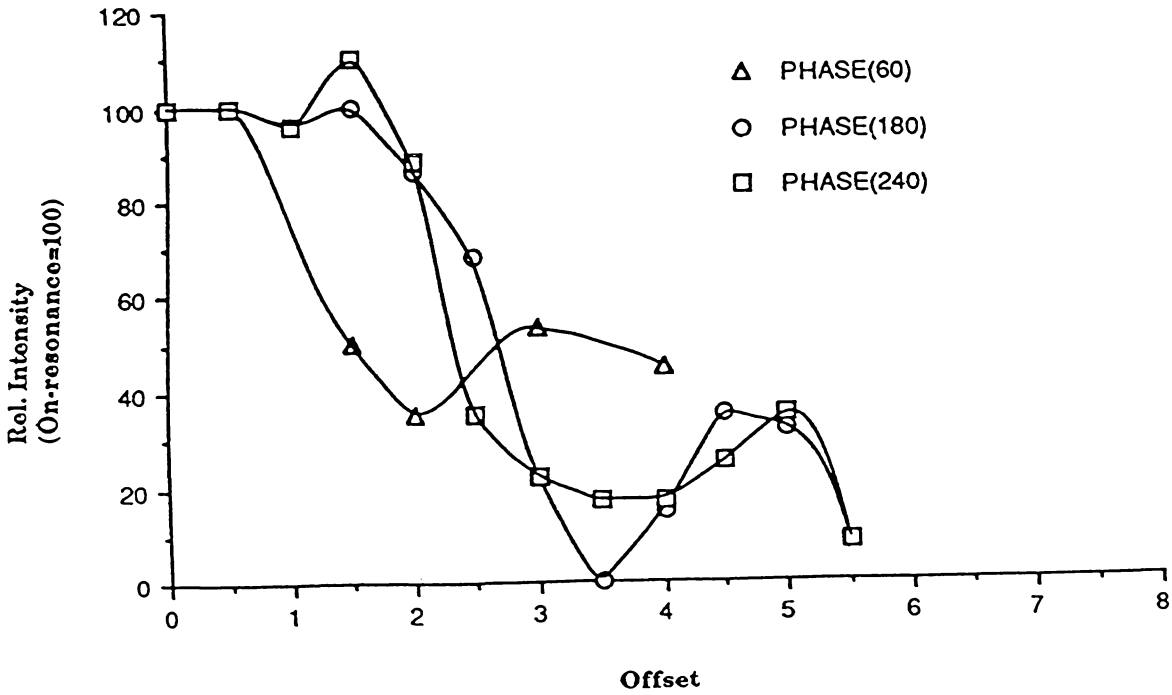

Fig. 2.6 Relative intensity of sample signal at varying offset for three θ values in the π composite pulse $90^\circ_x\ \theta^\circ_y\ 90^\circ_x$ substituted in the PHASE 4 sequence.

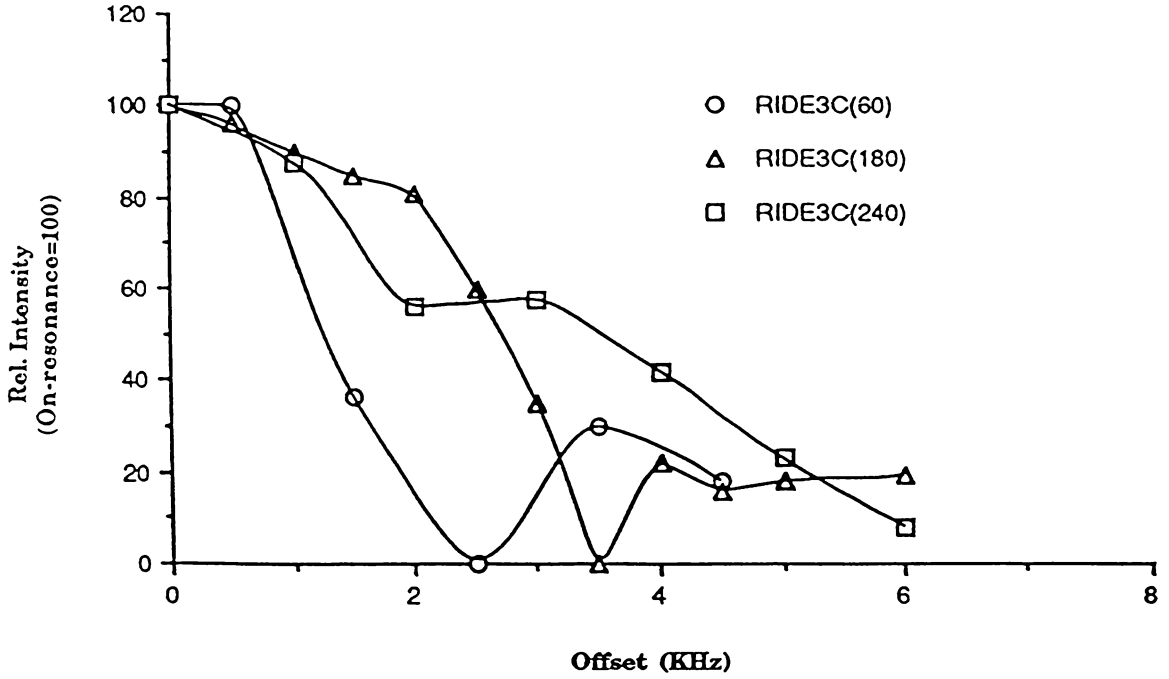

Fig. 2.7 Relative intensity of sample signal at varying offset for three θ values in the π composite pulse $90^\circ_x\ \theta^\circ_y\ 90^\circ_x$ substituted in the RIDE sequence.

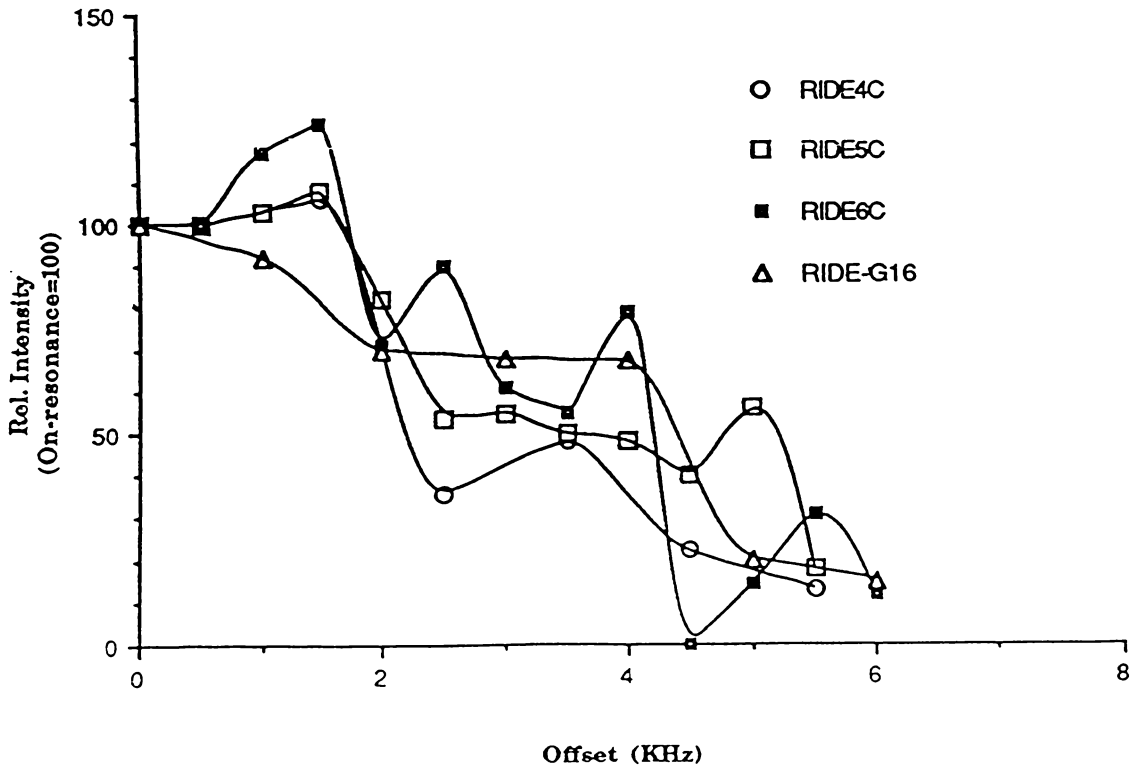

Fig. 2.8 Relative intensity of sample signal at varying offset for 4, 5, and 6 segment composite π pulses substituted into the RIDE sequence.

The composite pulses used have all improved the useable windows of the pulse sequences. In the PHASE sequence, despite using pulse sequences originally designed for z inversion as refocussing pulses, the point at which signal intensity remains at at least 80% of the on-resonance figure has increased to ±2KHz off-resonance.

In the RIDE sequence the 3C(60) composite pulse is not as successful as in the PHASE sequence while the 3C(180) composite pulse gives similar results to that of the PHASE sequence. The 3C(240) composite pulse has maintained a relative intensity of 60% out to ±3KHz off-resonance. The longer composite pulses show a more complicated off-set dependence than the relatively bell-shaped results of the 3C composite pulses, but in general provide broader windows while still maintaining 50% relative intensity. The 5C composite pulse pulse maintains this out to at least ±5KHz. The 6C composite pulse provides higher intensities than either the 4C or 5C composite pulse out to ±4KHz but then drops away rapidly. The G 16 pulse, in contrast, drops to a 75% relative intensity level at ±2KHz but maintains this level for a further 2KHz off resonance before dropping away.

Apart from the 3C(60) composite pulse all composite pulses tried have provided reasonable extension of usable window out to ±2KHz, with the longer composite pulses providing extension out to ±4KHz at the expense of up to 50% loss of signal intensity. This compares to a 50% signal loss at ±5KHz off-resonance in the case of the single pulse (see Fig. 2.2).

2.3.3 Applications

In this section three examples of applications of the sequences described above show their effectiveness. Two of the cases involve molecules with two different ^{73}Ge environments, while the third looks at a situation where signals from a halogen exchange reaction are spread over a large window.

Fig. 2.9 shows the standard single pulse ^{73}Ge spectrum of a dilute sample of GeH_3GeMe_2Cl. After 35,000 scans (16 hrs accumulation) no signal is distinguishable from the ring signal. Use of the RIDE 6C sequence located a signal *ca.* 2KHz off resonance. A proton-coupled RIDE 6C experiment (35,000 scans), with the signal on resonance, allowed confirmation of the signal as a GeH_3 group. The lower symmetry $GeMe_2Cl$ signal, broadened by quadrupolar effects, remains unobservable.

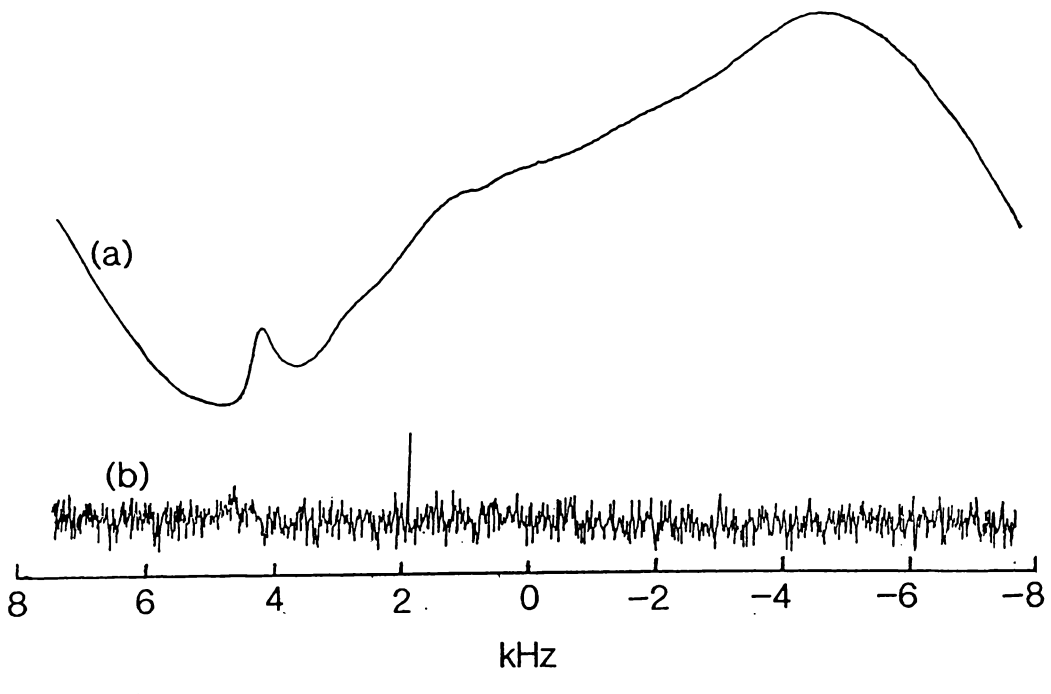

Fig. 2.9 ^{73}Ge NMR spectra of GeH_3GeMe_2Cl (dilute solution in C_6D_6); (a) standard $\pi/2$ single pulse experiment, (b) RIDE 6C experiment. Both spectra show a 15,000Hz spectral window with 4K data points zerofilled to 8K. 35,000 transients per f.i.d. were collected with an acquisition time of 136ms and relaxation delay of 1s.

The two signals in the ^{1}H decoupled ^{73}Ge spectra of GeH_3GeMe_3 are approximately 1KHz apart, with the broader $GeMe_3$ signal downfield from the sharp GeH_3 signal (Fig. 2.10). Use of the RIDE sequence, with standard pulses, resulted in better signal to noise for the on-resonance, $GeMe_3$, signal, but the intensity of the GeH_3 signal was diminished (Fig. 2.10). Such an effect could clearly complicate interpretation. However, this problem was overcome when composite pulses were used. The coupled and decoupled versions of the RIDE 6C sequence (Figs 2.10(b) and 2.10(c)) result in spectra that maintain an *ca.* 1:1 ratio of the two Ge signals.

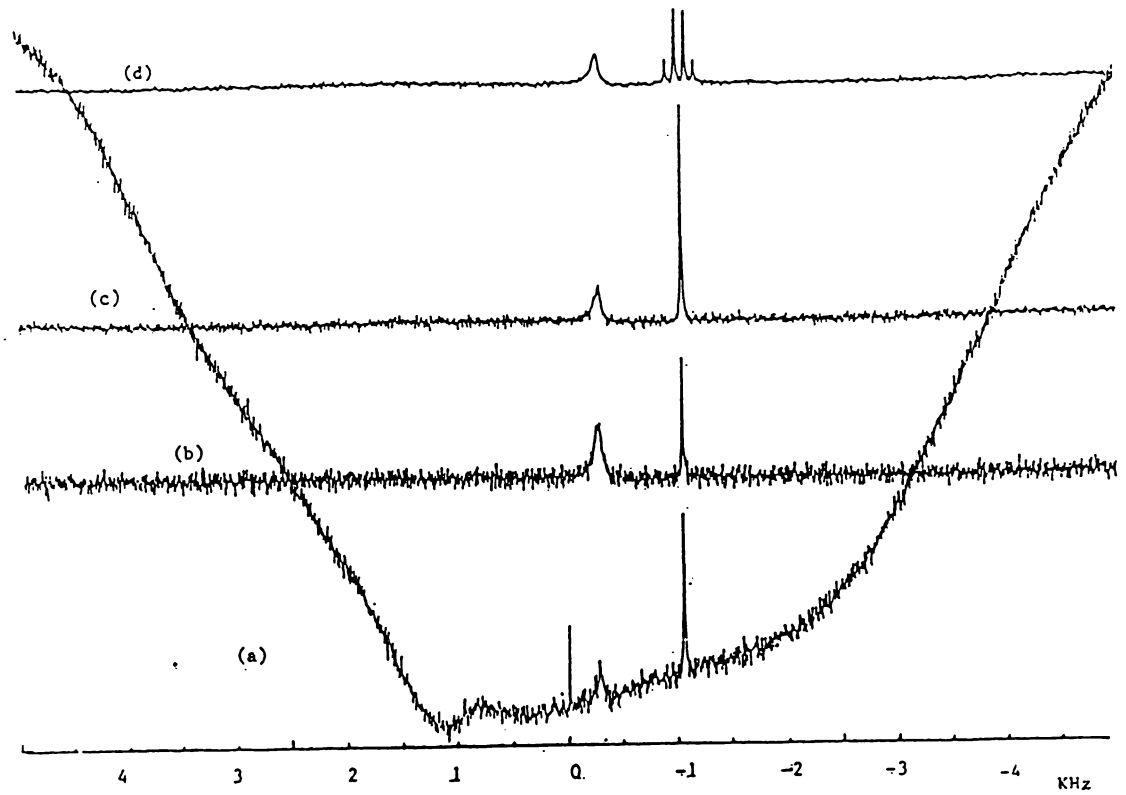

Fig. 2.10 ^{73}Ge NMR spectra of neat GeH_3GeMe_3; (a)standard $\pi/2$ pulse experiment, (b) RIDE experiment, (c) RIDE-6C experiment, and (d) ^{1}H coupled RIDE-6C experiment. All experiments were collected for 24,000 transients over an 8000Hz window with 4K data points, using a 1s relaxation delay.

In a study of halide redistribution in $GeI_4/GeBr_4$ mixtures, not only is chemical shift information important, the equilibrium populations need to be accurately measured. Figure 2.11 shows that the RIDE G 16 experiment provides a much closer approach to the actual equilibrium populations observed in the single pulse experiment than either the RFB-90 or the RIDE 5C experiment. It is clear than even in this best case care is still required in the interpretation of populations.

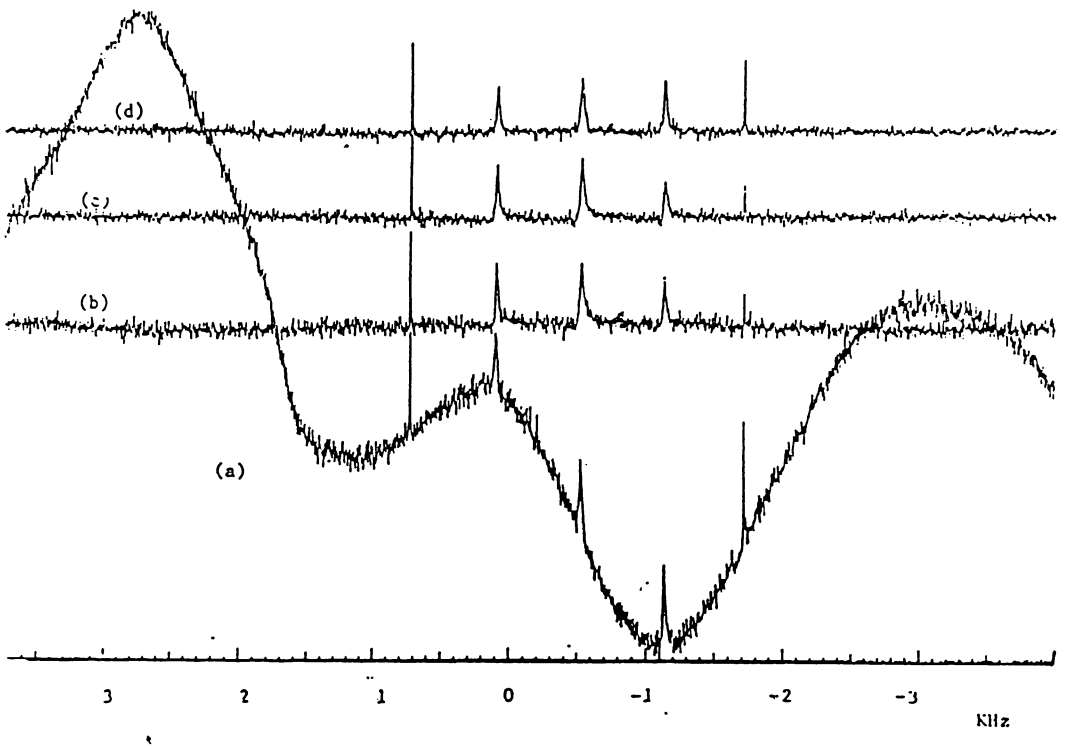

Fig. 2.11 ^{73}Ge NMR spectra of an equilibrated $GeI_4/GeBr_4$ sample (neat solution).; (a) standard $\pi/2$ single pulse experiment, (b) RFB-90 experiment, (c) RIDE-5C experiment, and (d) RIDE G 16 experiment. All spectra were determined over an 8000Hz window with 4K data points. 72,000 transients were collected per f.i.d. with a relaxation delay of 1s.

2.3.4 Experiments at 400MHz.

Initial experiments on the Bruker AM400 installed at Auckland University showed that for the standard single pulse experiment (Fig. 2.12(a)) the acoustic ring signal was, as expected, worse than that observed at 90MHz, because of the B_0^2 term in Eqn. 2.1, as well as the stronger B_1 field on this instrument. The PHASE sequence still left considerable residual baseline roll and no further work was carried out with this sequence. Both

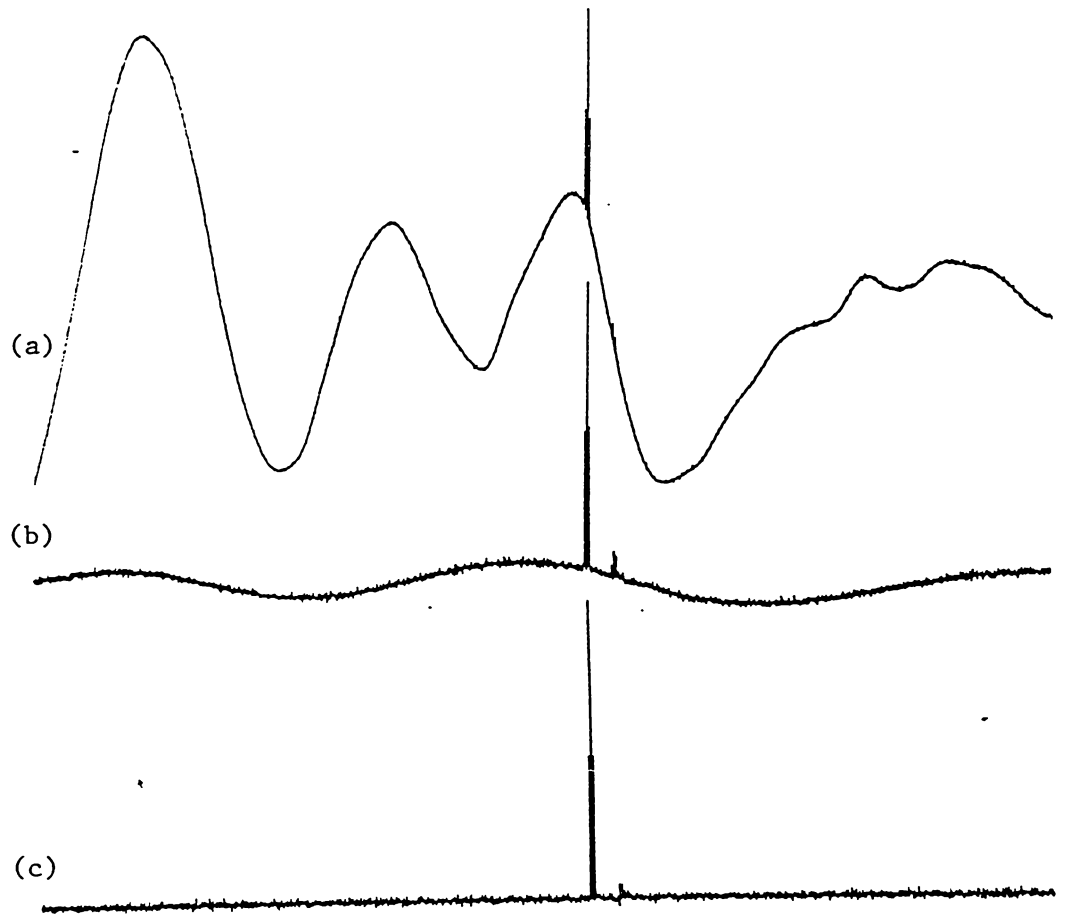

Fig. 2.12 Proton coupled ^{73}Ge NMR spectra of a mixed $GeMe_xH_{(4-x)}$ sample run on the Bruker AM400 spectrometer; (a) standard $\pi/2$ single pulse experiment, (b) RIDE experiment and, (c) EXSPEC experiment. All spectra were collected over a 42,000Hz window using 8K data points. 16 transients were collected with an acquisition time of 98ms and relaxation delay of 2s.

the RIDE and EXSPEC sequences gave considerable improvement over the standard experiment. Fig. 2.12. shows the result of a standard pulse experiment, at the ^{73}Ge resonance frequency, and those for the RIDE and EXSPEC sequences. It is apparent that the RIDE sequence has not completely removed the ring signal, a situation more strongly emphasised when weaker samples were run.

The offset dependence of the two sequences are shown in Fig.2.13.

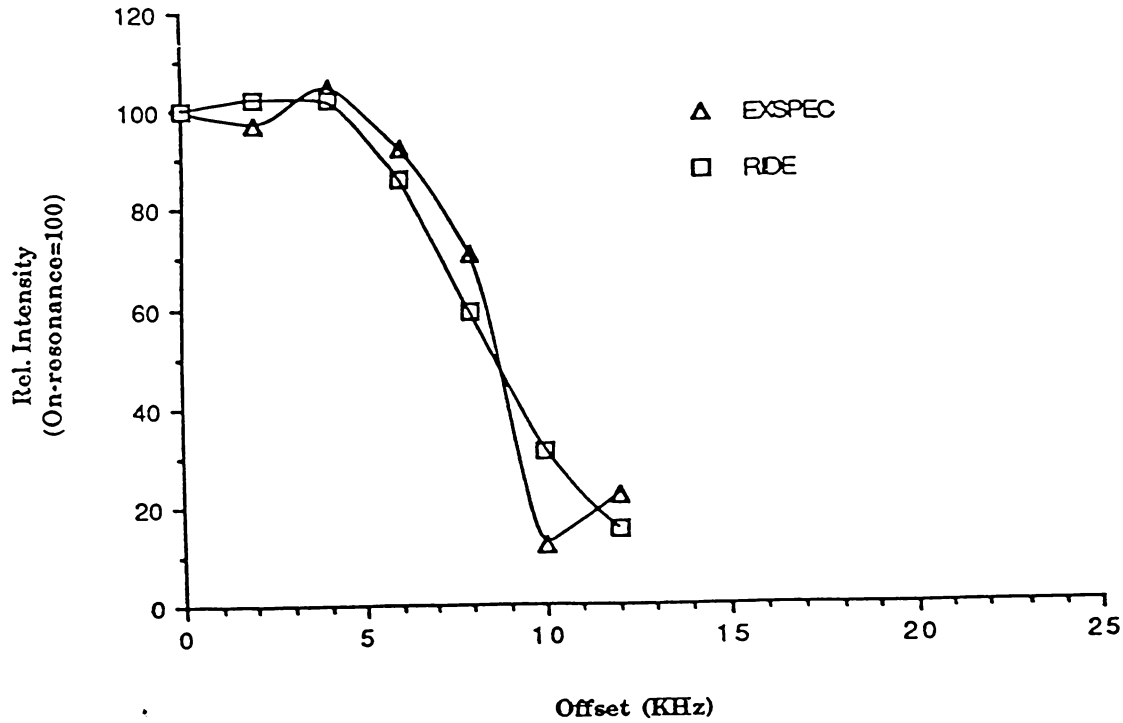

Fig. 2.13. Offset dependence of the RIDE and EXSPEC sequences on the Bruker AM400 instrument.

Remembering that the stronger B_0 field means that offsets need to be at least four times better than those of the 90MHz instrument to allow for equal window widths, in ppm, comparison of Figures 2.4 and 2.13 shows that on the high field instrument the windows are flatter, reflecting the short pulse

times, and extend 1.5 - 2 times further than the low field equivalent before dropping off.

Time limitations meant that a full trial of composite pulses could not be carried out, but based on experience at 90MHz the 6C versions of the two pulses were run. Fig. 2.14. shows the excitation windows achieved when this pulse was substituted into the two sequences.

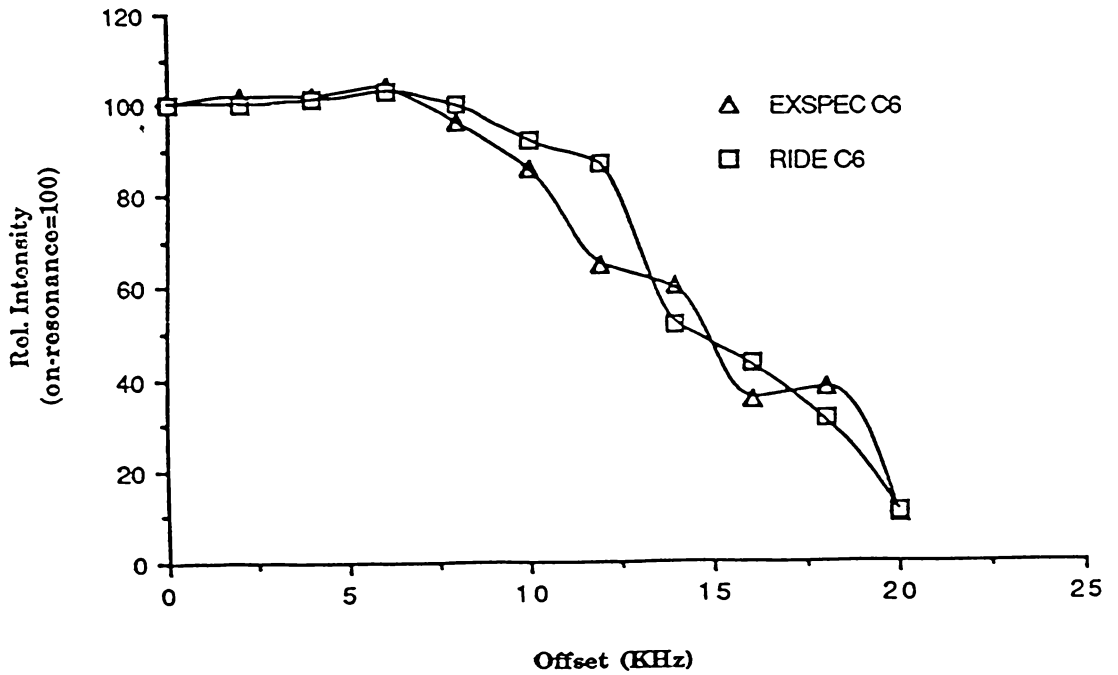

Fig. 2.14. Offset dependence of the C6 composite pulse versions of the RIDE and EXSPEC pulse sequences on the Bruker AM400.

The use of the composite π pulses has extended the windows out to ±15KHz, and generally provide consistent excitation across the window to this point. Again the EXSPEC sequence provided the smoother base-lines and thus would be better for a study of broad-line samples.

A more detailed study of other composite π pulses, and the effect of composite π/2 pulses within these sequences has not been possible because of an unfortunate instrument malfunction.

2.4 Conclusions

This work has shown that ring supression sequences do work, even when applied at the demanding low frequency of ^{73}Ge, although the use of composite pulses is necessary to overcome the window limitations imposed by the π pulses in the sequences. As better composite pulses, or perhaps shaped pulses, become available, especially refocussing pulses, it is hoped that these windows may be further extended. What they still do not allow is accurate integration across the full window, a difficulty at the edge of any window.

Ignoring all other factors, such as overall sensitivity, it now means that ^{73}Ge signals with half widths as much as 4KHz are theoretically observable, on a 90MHz instrument, assuming the signal is centered on the carrier. An equivalent figure for the 400MHz instrument would be *ca.* 15KHz. Similarly, two relatively sharp signals separated by up to 1300ppm (at 90MHz) and 1100ppm (at 400MHz), would be observable in the same experiment. (For a more detailed discussion on observability see Section 3.4.3 in the following Chapter.)

Fig. 2.15 shows the excitation profile obtained on the JEOL FX90Q from:

(a) a single pulse,

(b) the RIDE sequence,

(c) the RIDE sequence with the G 16 composite π pulse.

It is clear that even the standard single pulse does not give the ideal even excitation across a particularly wide window, but use of composite pulses within the RIDE sequence has resulted in this sequence providing a comparative excitation window.

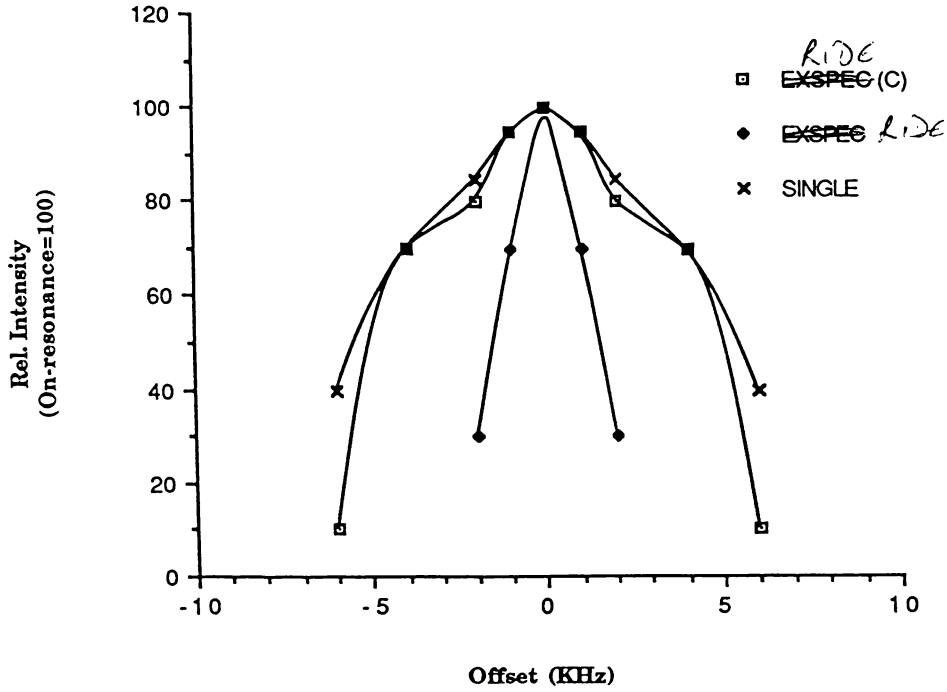

Fig. 2.15 Relative excitation levels, at varying offset, for; (a) a single pulse, (b) the RIDE sequence, and (c) the RIDE G 16 sequence on the JEOL FX90Q instrument.

Just as the water signal in biological sample ^{1}H spectra needs to be supressed, by one of the numerous water supression techniques, to ensure observation of weak signals, reduction in intensity of the ring FID signal by one of the ring supression sequences means that weaker signals are more likely to be observed. (A discussion on the limitations of observability of weak signals in the presence of strong signals may be found in reference 7.)

While this work was being carried out, and since experimental work was completed, a number of studies making use of the baseline suppression pulse sequences have been reported. Studies on ^{17}O[22], ^{33}S[8X16], and ^{99}Ru[13] report good cancellation of baseline, but comment is made on the narrow excitation windows. The low observation frequency, and use of composite pulses, make this work the most detailed attempt, so far, to apply baseline smoothing to the practical problem of trying to observe weak broad-line signals.

As more and more study is carried out on the 'difficult' nuclei it is to be hoped that better probes, made of more suitable materials, become available.

Regardless of the technique used to try and eliminate ring signal it is preferable not to generate such a signal in the first instance.

Chapter 2 References

1. A.E.Derome, *'Modern NMR Techniques for Chemistry Research'* Pergamon Press, Oxford, 1987, *p171.*
2. C.Brevard, P.Granger, *'Handbook of High Resolution Multinuclear NMR',* Wiley-Interscience, New York, 1981, *p50.*
3. C.Brevard in *'NMR of Newly Accessible Nuclei'*, (ed P.Laszlo), Academic Press, New York, 1983, *p17.*
4. A.G.Redfield, S.D.Kunz, and E.K.Ralph, *J. Magn. Reson.*,**19**, *114*, 1975.
5. P.Plateau, C.Dumas, and M. Gueron, *J. Magn. Reson.*, **54**, *46*, 1983.
6. Ref. 3, *p12.*
7. E.Fukushima and S.B.W.Roeder, *'Experimental Pulse NMR: A Nuts and Bolts Approach'*, Addison-Wesley , Mass. 1981, *p464.*
8. P.S.Belton, I.J.Cox, and R.K.Harris, *J.Chem. Soc., Faraday Trans. 2*, **81**, *63*, 1985.
9. D.I.Hoult. *'NMR-Specialist Periodical Reports'* (R.J.Abraham. Ed.), Vol.7, Chap. 5, Chemical Soc., London, 1978.
10. D.Canet, J.Brondeau, J.P.Marchal, and R.Robin-Lherbeir, *Org. Magn. Reson.*, **20**, *51*, 1982.
11. S.L.Patt, *J. Magn. Reson.*, **49**, *161*, 1982.
12. P.D.Ellis, Unpublished lecture notes.
13. Ref. 3, *p18.*
14. T.Drakenberg, T.Andersson, S.Forsen, and T.Wieloch, *Biochemistry*, **23**, *2387*, 1984.
15. H.J.Vogel, T.Drakenberg, S.Forsen, J.D.J.O'Neal, and T.Hofmann, *Biochemistry,* **24**, *3870*, 1985.
16. H.Ekert and J.P.Yesinowski, *J. Am. Chem. Soc.*, **108**, *2140,* 1986.
17. I.P.Gerothanassis and J.Lauterwein, *J. Magn. Reson.*, **66**, *32,* 1986.
18. A.J.Benesi and P.D.Ellis, *J. Magn. Reson.*, **78**, *511*, 1988.

19. I.P.Gerothanassis, *Magn. Reson. Chem.*, **24**, *428,* 1986.

20. R.Goc and D.Fiat, *J. Magn. Reson.*, **70**, *295,* 1986.

21. E.D.Laue, K.O.B.Pollard, J.Skilling, J.Staunton, and A.C.Sutkowski, *J. Magn. Reson.*, **72**, *493,* 1987.

22. I.P.Gerothanassis, M.Momenteau, and B.Loock, *J. Am. Chem. Soc.,* **111**, *7006,* 1989.

23. Ref. 1, *p159.*

24. M.H.Levitt and R.Freeman, *J. Magn. Reson.*, **33**, *473,* 1979.

25. R.Freeman, S.P.Kempsell and M.H.Levitt, *J. Magn. Reson.*, **38**, *453,* 1980.

26. M.H.Levitt and R.Freeman, *J. Magn. Reson.*, **43**, *65,* 198.

27. M.H.Levitt, *J. Magn. Reson.*, **50**, *95*, 1982.

28. A.J.Shaka, J.Keeler and R. Freeman, *J. Magn. Reson.*, **55**, *247*, 1983.

29. Z.Starcuk and V. Sklenár, *J. Magn. Reson.*, **62**, *113,* 1985.

30. A.J.Shaka, *Chem Phys. Letters*, **120**, *201,* 1985.

31. A.J.Shaka, P.B.Barker and R.Freeman, *J. Magn. Reson.*, **67**, *580*, 1986.

32. R.Tyko and A.Pines, *Chem. Phys. Letters*, **111,** *462*, 1984.

33. R.Tycko, H.M.Cho, E.Schreider and A.Pines, *J. Magn. Reson.*, **61**, *90,* 1983.

34. D.B.Zax, G.Cochman and S.Vega, *J. Magn. Reson.*, **80**, *375,* 1988.

35. Z.Starcuk, L.Pucek and Z.Starcuk Jr., *J. Magn. Reson.*, **80**, *352,* 1988.

36. M.H.Levitt, *Prog. in NMR Spectroscopy*, **18**, *61*, 1986.

37. A.J.Shaka, C.J.Bauer and R.Freeman, *J. Magn. Reson.*, **60**, *479* , 1984.

38. K.V.Schenker and W. von Philipsborn, *J. Magn. Reson.*, **66**, *219* , 1986.

39. M.H.Levitt and R.R.Ernst, *Mol. Phys.*, **50**, *1109*, 1983.

40. S.Wimperis and G.Bodenhausen, *J. Magn. Reson.*, **69**, *264*, 1986.

41. D.P.Raleigh, E.T.Olejniczak, and R.G.Griffin, *J. Magn. Reson.,* **81**, *453*, 1989.

42. R.Tyko, E.Schneider, and R.R.Ernst, *J. Chem. Phys.*, **81**, *680*, 1984.

43. M.H.Levitt, D.Suter, and R.R.Ernst, *J. Chem. Phys.*, **80**, *3064*, 1984.

44. D.J.Siminovitch, D.P.Raleigh, E.T.Olejniczak, and R.G.Griffin, *J. Chem. Phys.*, **84**, *2556*, 1986.

45. T.M.Barbara, *J. Magn. Reson.*, **67**, *491,* 1986.

46. T.M.Barbara, M.S.Greenfield, R.L.Vold, and R.R.Vold, *J. Magn. Reson.*, **69**, *311,* 1986.

47. A.J.Derome, *J. Magn. Reson.*, **78**, *123*, 1988.

48. A.J.Shaka and A.Pines, *J. Magn. Reson.*, **71**, *495* , 1987.

49. Ref. 1, *p161.*

50. A.J.Shaka and R.Freeman, *J. Magn. Reson.*, **55**, *487,* 1983.

Chapter 3 Germanium NMR

3.1 Introduction

While all other elements in Group 14 have a spin 1/2 isotope suitable for NMR observation the only NMR active isotope of germanium is high spin (9/2) and has a low resonance frequency. Table 3.1 lists the NMR properties of the magnetically active nuclides of Group 14.

Table 3.1 Magnetically Active Nuclides Of Group 14.[a]

	Spin	Nat. Abundance C/%	Gyromagnetic Ratio g/10^7 rad T^{-1} s^{-1}	Quad. Moment 10^{28} Q/m^2	Receptivity ($^{13}C = 1$)	Reson. Freq.[b] Ξ MHz.
^{13}C	1/2	1.108	6.7283	-	1	25.145
^{29}Si	1/2	4.70	-5.3146	-	2.09	19.867
^{73}Ge	9/2	7.76	-9.331	-0.18	0.617	3.488
^{115}Sn	1/2	0.35	-8.792	-	0.695	32.86
^{117}Sn	1/2	7.61	-9.5316	-	19.54	35.632
^{119}Sn	1/2	8.58	-9.9756	-	25.2	37.291
^{207}Pb	1/2	22.6	15.3078	-	11.8	57.224

(a) From ref. 1.

(b) Value in a magnetic field such that the protons in Me_4Si resonate at exactly 100MHz.

With the low resonance frequency creating the difficulties of acoustic ringing discussed in the previous chapter and the quadrupolar moment resulting in broad signals for anything other than a symmetric environment it is not surprising that ^{73}Ge NMR has been slow to gather momentum. As recently as 1983 Harris[1], in a review of NMR studies of Group 14 during the

1978-80 period, wrote "germanium-73 NMR is languishing and unlikely to become important".

The ^{73}Ge parameters were first measured[2] in the early 1950's but it was not until 1971 that Schwenk[3] first obtained direct high resolution measurements of germanium compounds. Coupling constants for GeH_4,[4][5] $GeMe_4$,[6][7] GeF_4 and GeF_6^{2-} [8] had been obtained by ^1H or ^{19}F NMR, but only from the direct observation of ^{73}Ge was it possible to measure accurate coupling constants. The first solid state NMR[9] was obtained for $GeCo_2O_4$ during this intervening period. By the time the invaluable 'NMR and the Periodic Table' was compiled by Harris and Mann[10] in 1977, 20 compounds had been observed in two high resolution studies.

At the commencement of this work Watkinson was just completing his major study of germanium compounds. His work included the extension of the INEPT[11] sequence to germanium[12], the highest spin to which the sequence has been applied. His work also included observations on a large range of germanium hydrides, with chemical shift, coupling constant, and relaxation data being obtained on nearly forty compounds[13]. While some of these, particularly the tetrahalides and tetraalkyls, had previously been studied the work was the first on a high resolution machine and helped to formalise the earlier work of Schwenk[2][3][14] and Spinney[15]. T_1 data were also obtained for twenty-one compounds. This work coincided with work concurrently being done by two other groups. In Latvia, Lukevics and others had made ^{73}Ge observations on germatranes[16][17], and carbo-functional tetra-alkyls[18]. Meanwhile a Japanese group headed by Takeuchi published observations on methylgermacyclohexanes[19] and has recently studied relaxation mechanisms in the tetraalkyl-[20] and tetrahalo- germanes[21][22] along with further studies of germa-, methylgerma- and dimethylgerma-cyclohexanes[23]. Publication of these findings has meant that by the time the two reviews of ^{73}Ge NMR, by ourselves[24] and Lukevics[25], appeared in 1987

we were able to list over 100 compounds (see Table 3.2) for which observations had been made.

Since the reviews, Takeuchi has published further work on relaxation in the tetrahalides[26] and Lukevics has published work on five[27,28] and six[29,30] coordinate species. This work by Lukevics is the first to be run on the new generation of high resolution spectrometers at frequencies higher than 3.13MHz.

The study reported here has added some 20 new ^{73}Ge observations which throw further light on a number of areas in the published literature. The background to these is reviewed here and the results under the same headings in Section 3.4.

3.1.1 Chemical Shifts and Coupling Constants

Table 3.2 lists the chemical shift and coupling constant data available at the time of the review (mid-1987). Mitchell's relationships between C/Si, Si/Sn, and Sn/Pb chemical shifts[31] were extended in 1984 to Ge/Si and Ge/Sn[32]. An alternative equation[33], having about half the gradient, was reported in 1986 to include new data on compounds with all four ligands were bonded to Ge through O. This confirmed anomalies noted earlier[18,32,34]. Any observations of other chemical shifts might be expected to assist in clarification of this anomaly.

While most solvents, except possibly for strong donors, appear to have little effect for the majority of compounds the ^{73}Ge shifts of the hydrides are somewhat more solvent sensitive[13], although even here the effects are no more than ±2ppm. Two significant exceptions have been noted: (a) an undiluted mixture of GeH_4, Ge_2H_6, and Ge_3H_8, and also neat Ge_3H_8, show shifts of 10-12ppm from the listed solution values[13], (b) GeI_4 has a chemical shift of -1106ppm as a dilute solution in C_6H_6 and -1139ppm when concentrated[3], compared to -1081ppm in mixtures of the germanium tetrahalides.

Table 3.2 ^{73}Ge Nuclear Magnetic Resonance Observations.

	δ(ppm)	$W_{\frac{1}{2}}$(Hz)	^nJ(Hz)		References and notes
A. Hydrides, Ge_nH_{2n+2}					
GeH_4	-299	1.1	97.6		12,13,32*(a)*
Ge_2H_6	-312	12.7	95.5		12,13,32*(a)*,*(i)*
Ge_3H_8	-298	25	94	(GeH_3)	13,*(i)*
	-310	40	90	(GeH_2)	
Ge_4H_{10}	-284	76		(GeH_3)	13,*(i)*
	-300	100		(GeH_2?)	
B. Alkylgermanes and alkylpolygermanes					
$GeMeH_3$	-209.2	1.5	94.5	(^1J)	12,13,*(i)*
			3.5	(^2J)	
$GeMe_2H_2$	-127.6	1.8	92.3	(^1J)	12,13,*(i)*
			3.4	(^2J)	
$GeMe_3H$	- 56.9	4.0	93		13,*(i)*
$GeEtH_3$	-186.4	3.4	92.4		13,
$GeEt_2H_2$	- 88	20	89		13,*(i)*
$GeEt_3H$	- 16	20	88		13,
GeH_3GeMeH_2	-306.2	2.0	90.0	(GeH_3,^1J)	12,13,*(i)*
			4.7	(GeH_3,^2J)	
	-210	13		($GeMeH_2$)	
$(GeMeH_2)_2$	-209	7			13
GeH_3GeMe_2H	-296	7	85	(GeH_3)	13
	-127	3		($GeMe_2H$?)	
GeH_3GeMe_3	-296	13	91	(GeH_3)	13,*(i)*
	- 48	63		($GeMe_3$)	

cont...

Table 3.2 (cont.) ^{73}Ge Nuclear Magnetic Resonance Observations.

$(GeMeH_2)_2GeMeH$	-206	2		$(GeMeH_2)$	13
	-125	8		(GeMeH)	
$C_5H_{10}GeH_2$	-131.2	16.4	92.8		19,*(b)*
$3\text{-}MeC_5H_9GeH_2$	-131.2				19,*(b)*
$4\text{-}MeC_5H_9GeH_2$	-134.3	21.0	94.0		19,*(b)*
$C_5H_{10}GeHMe$	- 65.3	22.3	90.8		19,*(b)*
$4\text{-}MeC_5H_9GeHMe$	- 61.5*(cis)*				19,*(b)*
	- 73.4*(trans)*				

C. Silicon-germanium hydrides and their alkyl derivatives

GeH_3SiH_3	-325	1.2	91.5	(^{1}J)	13
			2.7	(^{2}J)	
GeH_3SiMeH_2	-316	4			13
$GeMeH_2SiH_3$	-230	4.0			13
GeH_3SiMe_3	-315.5	65			*(i)*
$(GeH_3)_2SiMe_2$	-290.6	34	90.8		*(i)*
$(GeH_3)_3SiMe$	-277.0	4.4	90.5		*(i)*

D. Germanium tetraalkyls and related species

$GeMe_4$	0.0	1.0	2.95		3,18,34,35, 12,32
$GeEt_4$	17.8	0.9	3.0		3,12,13,34
$Ge(n\text{-}Pr)_4$	2.4	3.3			3,13
$Ge(n\text{-}Bu)_4$	6.0	5.1	2.7		3,13,18,34
$Ge(n\text{-}C_5H_{11})_4$	6.0	9.5			13
$Ge(n\text{-}C_6H_{13})_4$	5.6	18.0			13
$GeMe_3CH_2GeMe_3$	7.5	20.0			18
$GeMe_3(CH_2)_2GeMe_3$	6.6	25.0			18
$C_5H_{10}GeMe_2$	-13.7	15.6			19*(b)*
$3\text{-}MeC_5H_9GeMe_2$	-12.2				19*(b)*
$4\text{-}MeC_5H_9GeMe_2$	-17.2	18.3			19*(b)*
$C_4H_4GeMe_2$	39.8	75			18*(c)*

cont...

Table 3.2 (cont.) ^{73}Ge Nuclear Magnetic Resonance Observations.

$GeMe_3CMe_3$	20.7	10.3	18,35
$GeMe_3CH_2CH{=}CH_2$	1.7	30.0	18,35
$GeMe_3(CH)_2CH{=}CMe_2$	4.7	28	18
$GeMe_3R1$	11.2	20	18*(d)*
$GeMe_3CH_2Ph$	3.2	100	18
$GeMe_3R2$	6.6	20	18*(d)*
$GeMe_3R3$	5.8	22	18*(d)*
$GeMe_3R4$	8.1	22	18*(d)*
$GeMe_3R5$	5.4	26	18*(d)*
$GeMe(CH_2CH{=}CH_2)_3$	0.6	60	18*(d)*
$GeEt_3R2$	11.2	24	18*(d)*
$GePh_4$	-33.2	5.9	13,34,*(i)*
E. Carbofunctional alkyls			
$Ge(2\text{-furyi})_4$	-112.8	11	34
$Ge(2\text{-thienyl})_4$	- 95.5	8	34
$GeMe_3CH_2Cl$	6.9	152	18
$GeMe_3(CH_2)_2OH$	-2.6	36	18
$GeMe_3(CH_2)_2CO_2H$	6.3	54	34
$GeMe_2(CH_2Cl)_2$	17.5	315	18
$GeMe_2(CH_2SiFMe2)_2$	0.6	175	18
$GeEt_3(CH_2)_3COR'$	15.2	55	18*(e)*
$GeEt_3(CH_2)_3OH$	15.2	36	18
$GeEt_3(CH_2)_3OCOCH_3$	16.4	53	18
$GeEt_3(CH_2)_3OCOH$	17.5	36	18
$GeEt_3(CH_2)_3CO_2H$	15.2	30.0	18,35*(f)*
$GeEt_3(CH_2)_3Cl$	14.7	60	18

cont...

Table 3.2 (cont.) ^{73}Ge Nuclear Magnetic Resonance Observations.

F. Tetraalkoxides and Related Species				
$Ge(OMe)_4$	-37.8	10	1.9	3,33
$Ge(OEt)_4$	-43.9	30		33,35
$Ge(OPr)_4$	-45.6	40		33,35
$Ge(OBu)_4$	-45.6	40		33
$Ge(OPr^i)_4$	-49.7	25		33
$Ge(OBu^i)_4$	-45.5	30		33
$Ge(OBu^s)_4$	-47.5	45		33
$Ge(OCH_2CH{=}CH_2)_4$	-43.8	32		33
$Ge(OCH_2CF_3)_4$	-48.1	70		33
$N(CH_2CH_2O)_3GeOR$				
R = H	-55.2			16
R = Me	-60.6			16
R = Pr	-63.4			16
R = C_6H_5	-67.7	165		17
R = $SiMe_3$	n.o.			16,17*(g)*
R = $GeMe_3$	-73.8	13		16,17*(g)*
R = $SnMe_3$	-58.4	95		16,17*(g)*
$Ge(SMe)_4$	153.0		2.5	53
G. Tetrahalides				
$GeCl_4$	30.9	2.1		3,15,34,13
$GeBr_4$	-311.3	2.2		3,13,15
GeI_4	-1081.8	4.1		3,13,15
$GeCl_3Br$	-47.8	2.2		13,15*(h)*
$GeCl_2Br_2$	-131.3	2.2		13,15*(h)*
$GeClBr_3$	-219.4	2.2		13,15*(h)*

cont...

Table 3.2 (cont.) ^{73}Ge Nuclear Magnetic Resonance Observations.

$GeCl_3I$	-235.9	23	13,15*(h)*
$GeCl_2I_2$	-524	23	13,15*(h)*
$GeClI_3$	-810	22	13,15*(h)*
$GeBr_3I$	-509	22	13,15*(h)*
$GeBr_2I_2$	-707	29	13,15*(h)*
$GeBrI_3$	-900	20	13,15*(h)*
$GeCl_2BrI$	-326	7	13,15*(h)*
$GeClBr_2I$	-418	20	13,15*(h)*
$GeClBrI_2$	-611	27	13,15*(h)*

NOTES:

(*a*) Chemical shifts change by *ca* 12 ppm in a mixture of the hydrides[32] : δGeH_4 = -283.7; δGe_2H_6 = -300.5.

(*b*) germacyclohexanes

(*c*) germacyclopent-3-ene.

(*d*) From reference[18], R_1 = adamantyl, R_2 = cyclopent-2-ene, R_3 = cyclopent-2,4-diene (a signal at -21.9δ, $W_{\frac{1}{2}}$ = 18 was attributed to the dimer), R_4 = cyclopentyl, R_5 = cyclohexyl.

(*e*) R′ = - $N(CH_2CH_2)_2$ NMe

(*f*) These are the later values[35], the earlier report [18] gives δ = 12.8, $W_{\frac{1}{2}}$ = 40 Hz.

(*g*) These are the later values[17] in $CDCl_3$. The earlier measurements[16] in CH_3CN were reported as -73.8 (R = $SiMe_3$), -55.2 (R = $GeMe_3$), and -53.4 (R = $SnMe_3$).

(*h*) mixed halides measured in binary and ternary mixtures of $GeCl_4$, $GeBr_4$, GeI_4.

(*i*) This work.

3.1.2 Observability

The first ^{73}Ge study noted[3] that a resonance could not be found for $MeGeCl_3$. Since then, all workers in the field have made reference to compounds for which no signal was observed[12][13][16-21][32-34]. Work to date has shown that germanium is observable in a symmetric environment, but there are limits to the asymmetry tolerable in the electric field gradient. To date resonance has been observed for GeR_4 for R permutations of H, alkyl, silyl, alkylsilyl, germyl or alkylgermyl. Similarly all the mixed GeX_4 (X = Cl,Br,I) are seen, but no species with mixtures of X and R have been observed, even Me_3GeI where the electronegativies are similar. In the same way, carbofunctional germanes are observed if halogens or oxygen groups are remote from the Ge, but α substituents may not be tolerated. This is highlighted by the observation[18] of carbofunctional species containing halogen. Me_3GeCH_2Cl ($W_{1/2}$ = 152Hz) and $Me_2Ge(CH_2Cl)_2$ ($W_{1/2}$ =315Hz, the widest signal so far seen) were both observed but $Me_3GeCHCl_2$ was reported as "too wide to be resolved". Germanium species of the type $Ge(OR)_4$ have also been observed while $R_nGe(OR)_{4-n}$ species were not[33].

3.1.3 Relaxation Times

While a number of studies have been made of nuclear relaxation in germanium[3][13][20-22][26][34-36] compounds no two studies have used the same compounds under the same conditions. It has been impossible to be certain whether the differences in observations were a result of sample differences, or arose from systematic experimental errors. Relaxation times have a major impact on linewidth, and hence observability, and therefore the more data obtained the better will be our understanding of the factors affecting the broadening of the germanium signal.

In Section 3.4.3, a limited number of observations aimed at resolving these anomalies are reported. However, while this work was being done,

Takeuchi[20-22][26] has made major advances in germanium relaxation time studies. These are also reviewed in Section 3.4.3.

3.2 Experimental

NMR spectra were run on either a JEOL FX90Q or a Bruker AM400 instrument at 3.13MHz or 13.96MHz respectively. Early experiments were carried out using the standard single pulse sequence but development of the ring supression sequences meant that the later work was run using these.

The germanium-transition metal compounds were prepared by a coupling reaction between the halo-germane and a transition metal complex anion[37]. The fully deuterated germanes were made from the reaction of Mg_2Ge with a deuterated acid, while GeH_3D was produced by reacting GeH_3Br with lithium aluminium deuteride[38].

3.3 Results

NMR data from this work are listed in Table 3.3.

3.4 Discussion

3.4.1 Chemical Shifts and Coupling Constants

A number of observations in this work were made to clarify anomalies in results obtained by Watkinson. A Ge_2H_6 sample was run as a 1:1 mixture in $GeCl_4$. The observed chemical shift was midway in the range of chemical shifts observed by Watkinson for various mixtures containing Ge_2H_6. He observed Ge_2H_6 at -300.5 ppm in a sample containing GeH_4, Ge_2H_6, and Ge_3H_8 , a figure duplicated in this work at both 90MHz and 400MHz, and -316ppm for a 1:36 mixture of Ge_2H_6:Et_2O. A neat sample of Ge_3H_8 provided chemical shift figures similar to those observed by Watkinson in the aforementioned hydride mix. The sample of Ge_4H_{10}, which at 90MHz

Table 3.3 ^{73}Ge NMR Observations in this work.

A. On the JEOL FX90Q instrument.

	δ(ppm)	$W_{1/2}$(Hz)	^nJ(Hz)		
1.Hydrides					
Ge_2H_6	-308.6	31			in $GeCl_4$
Ge_2H_6	-300.7	20±2			Mixed Ge_2H_6,
Ge_3H_8	-287.84	30		(GeH_3)	Ge_3H_8 system
	-321.8	40		(GeH_2)	
Ge_3H_8	-286	32.3	96	(^1J)	neat
	-323.5	45.4	95	(^1J)	
Ge_4H_{10}	-287.1	70	91	(^1J GeH_3)	
	-310.5			(sh. GeH_2)	
2. Alkylgermanes and alkylpolygermanes					
$GeMeH_3$	-209.2	1.5	94.5	(^1J)	
			3.5	(^2J)	
$GeMe_2H_2$	-127.6	1.8	92.3	(^1J)	
			3.4	(^2J)	
$GeMe_3H$	-56.9	4.0	93	(^1J)	
$GeEt_2H_2$	-88.6	21.4			
$GeMe_3GeH_3$	-295.8	13.2	86.6	(^1J GeH_3)	
	-47.7	63			
$GeH_3Ge(Me)H_2$	-303.9	2.9	91.93	(^1J GeH_3)	
	-210.1	30	93	(^1J GeH_2)	
3. Silicon-germanium hydride derivatives					
GeH_3SiMe_3	-315.5	65			
$(GeH_3)_2SiMe_2$	-290.6	34	90.8		
$(GeH_3)_3SiMe$	-277.0	4.4	90.5		

cont....

Table 3.3 (cont.) ^{73}Ge NMR Observations in this work.

4. Other Germanium Compounds.				
GePh4	-33.2	7		in C_6H_6
GeH_3GeMe_2Cl	-280.5	39	90.3	only GeH_3 observed
$GeH_3GeH_2Mn(CO)_5$				
	-291.8	68	95.4	only GeH_3 observed
$GeH_3GeH(Me)Mn(CO)_5$				
	-277.9	17	88.5	only GeH_3 observed
5. Deuterated Compounds.				
GeH_3D	-293.3	1.95	97.4	($^1J_{Ge-H}$) c.f. δ -293.7 for GeH_4
			14.9	($^1J_{Ge-D}$) in same sample
GeD_4	-299.1	3.1	14.9	($^1J_{Ge-D}$))
Ge_2D_6	-318.0	63		
B. Observations On the Bruker AM400.				
Ge_2H_6	-299.6	42.5	94.6	
Ge_3H_8	-286.6	72	87	
	-321.9	83.3	89.5	
Ge_4H_{10}	-284.3	93		GeH_3
	-306.0	210		GeH_2

resulted in the GeH_2 signal showing as a shoulder on the GeH_3 peak, was resolved at 400MHz into a separate peak allowing accurate determination of chemical shift and linewidth data. The results on these samples highlight the medium effect on chemical shifts first noted by Watkinson. Neat and mixed hydride samples result in signals at lower field to those observed under other conditions. No explanation for this phenomenon is immediately apparent.

$GeEt_2H_2$ and $GeMe_3GeH_3$ spectra were run on neat clean samples to clarify variable data arising from the mixture of samples used by Watkinson. The reported observation[34] of a signal from $GePh_4$ in DMSO could not be repeated by Watkinson and it was not until the solvent was changed to C_6H_6 that a signal could be observed. It is assumed that the solvent was misreported in Takeuchi's original paper[34].

Work in this study allowed us[24] to redraw the Si/Ge chemical shift relationships. Fig 3.1 shows a plot of all ^{29}Si and ^{73}Ge chemical shifts known to date. The discrepancies between the lines proposed earlier[18][32-34] are best resolved by separating the data into two groups. Line B is the best fit line through all compounds containing oxygen ligands, while A is the best fit line for all other compounds. The equations match closely those reported - A[32] and B[33] - and are:

A $\quad \delta(^{73}Ge) = 3.4(\pm5.6) + 3.24(\pm0.05)\delta(^{29}Si)$ $(R = 0.994; n = 31)$

B $\quad \delta(^{73}Ge) = 55.9(\pm2.1) + 1.22(\pm0.03)\delta(^{29}Si)$ $(R = 0.996; n = 12)$

Line A falls into the series C/Si, Si/Ge, Ge/Sn, Sn/Pb (and related combinations like Si/Sn) where the shielding mechanisms are the same for all Group 14 elements. B represents those molecules where an additional effect is present for Si and absent, or greatly reduced, for Ge and this is readily identified[39] as additional π bonding of the $(p \rightarrow d)\pi$ type.

In a similar way the scatter in Mitchell's C/Si and Si/Sn plots[31] would be better rationalised by separating Si-O and Si-F values from the rest.

The silicon-germanium hydride derivatives combine with the observation by Watkinson of GeH_3SiH_3 to provide a full set of data for these compounds. These compounds also led to the silicon INEPT experiments discussed in Chapter 4.

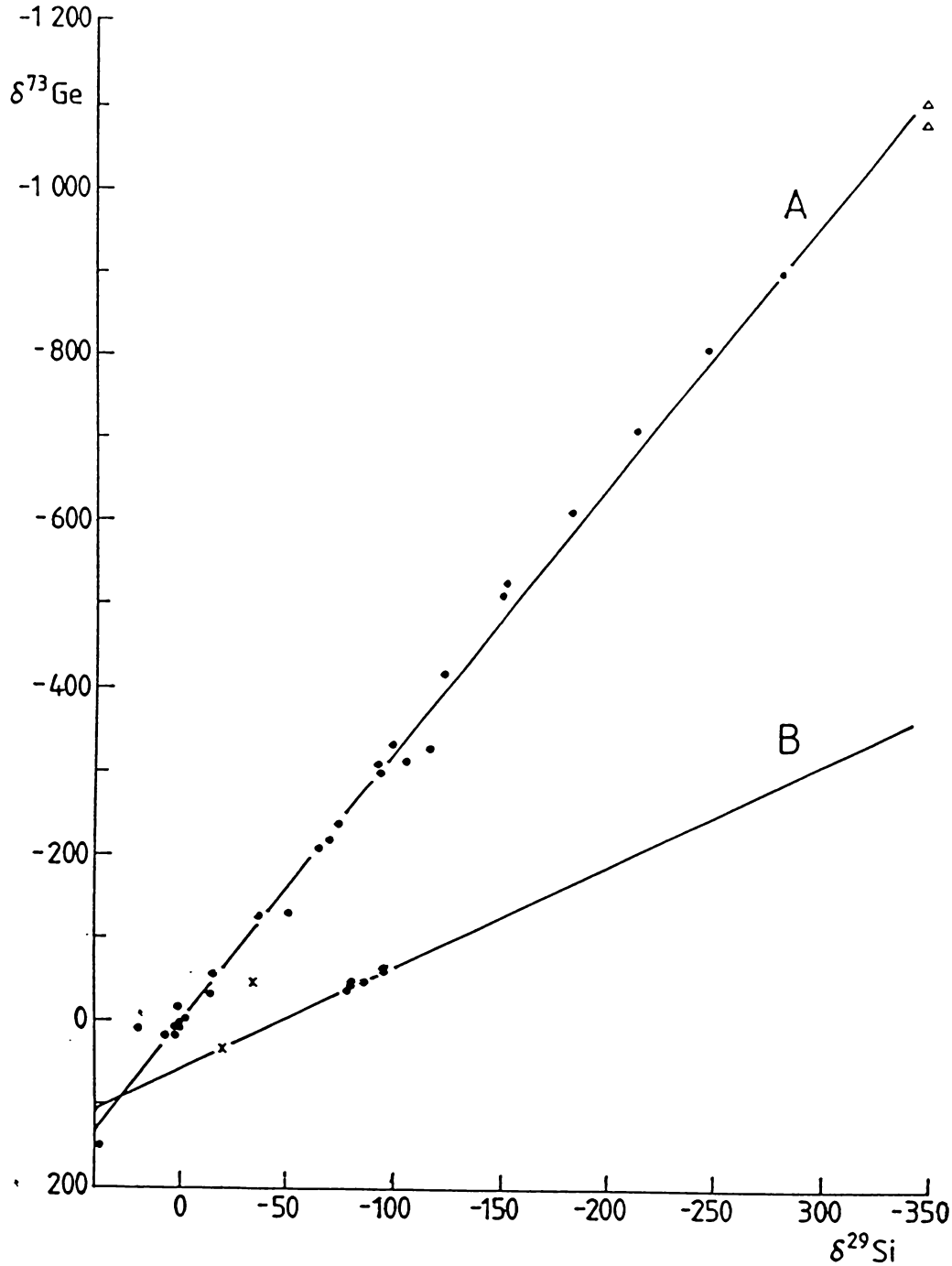

Fig. 3.1 Correlation of the ^{73}Ge chemical shifts in germanium compounds with the ^{29}Si chemical shifts of their silicon analogues. Line B is the best fit to all compounds with MO_4 coordination, while Line A is the best fit for all other compounds. Points X are MCl_4 which falls on B and MCl_3Br which lies midway between A and B. Line B probably reflects the greater degree of π bonding between Si and O compared with Ge and O. Points X suggest that such an effect persists with polychlorides. The two points marked Δ are the two literature values[3,13,15] for GeI_4, with the δ^{73}Ge figure of -1081.8ppm being a sample run in CS_2, and the figure of -1106ppm from a sample run in C_6H_6.

Fig 3.2 shows the standard proton coupled, and the INEPT proton coupled spectra of a mixed sample of GeH_4 and GeH_3D. Comparison of the two spectra, both requiring approximately twelve hours accumulation, shows the inherent advantage of the INEPT sequence when acquiring proton coupled spectra. The intensity of the outer lines of the GeH_4 pentet is clearly greater in the 1,2,0,-2,-1 INEPT signal compared to the normal binomial pentet (1,4,6,4,1) of the standard spectrum. While the INEPT sequence is helpful in the case of this sharp line signal the sequence is unfortunately limited in ^{73}Ge NMR because of the rapid relaxation of the more common wide line signals.

Chemical shifts and coupling constants obtained from these spectra are listed in Table 3.3, while data obtained from ^{2}D NMR of the deuterated germanes is listed in Table 3.4.

Table 3.4 ^{2}D NMR Parameters of the Deuterated Germanes.

	δ(ppm)[a]	$W_{1/2}$(Hz)	$J_{(D-H)}$(Hz)
GeH_3D	-1.17	2.1	1.22±0.02
Ge_2D_6	0.07	2.4	

(a) Referenced to external D_2O.

The deuterated germane chemical shifts show no anomalies but the GeH_3D sample again indicates the caution required when interpreting isotope effects in this type of sample. Watkinson reported ^{73}Ge chemical shifts for GeH_4 ranging from -283.7ppm in a mixture of GeH_4, Ge_2H_6, and Ge_3H_8 to -301.5ppm for GeH_4 very dilute in Et_2O. If a pure sample of GeH_3D had been used it would have be impossible to calculate the deuterium isotope effect on the ^{73}Ge signal. Fortunately the sample contained GeH_4 and by comparing the two it may be seen that the isotope shift effect is +0.4ppm, which is of the magnitude, but opposite in sign, to that measured for SnH_4.

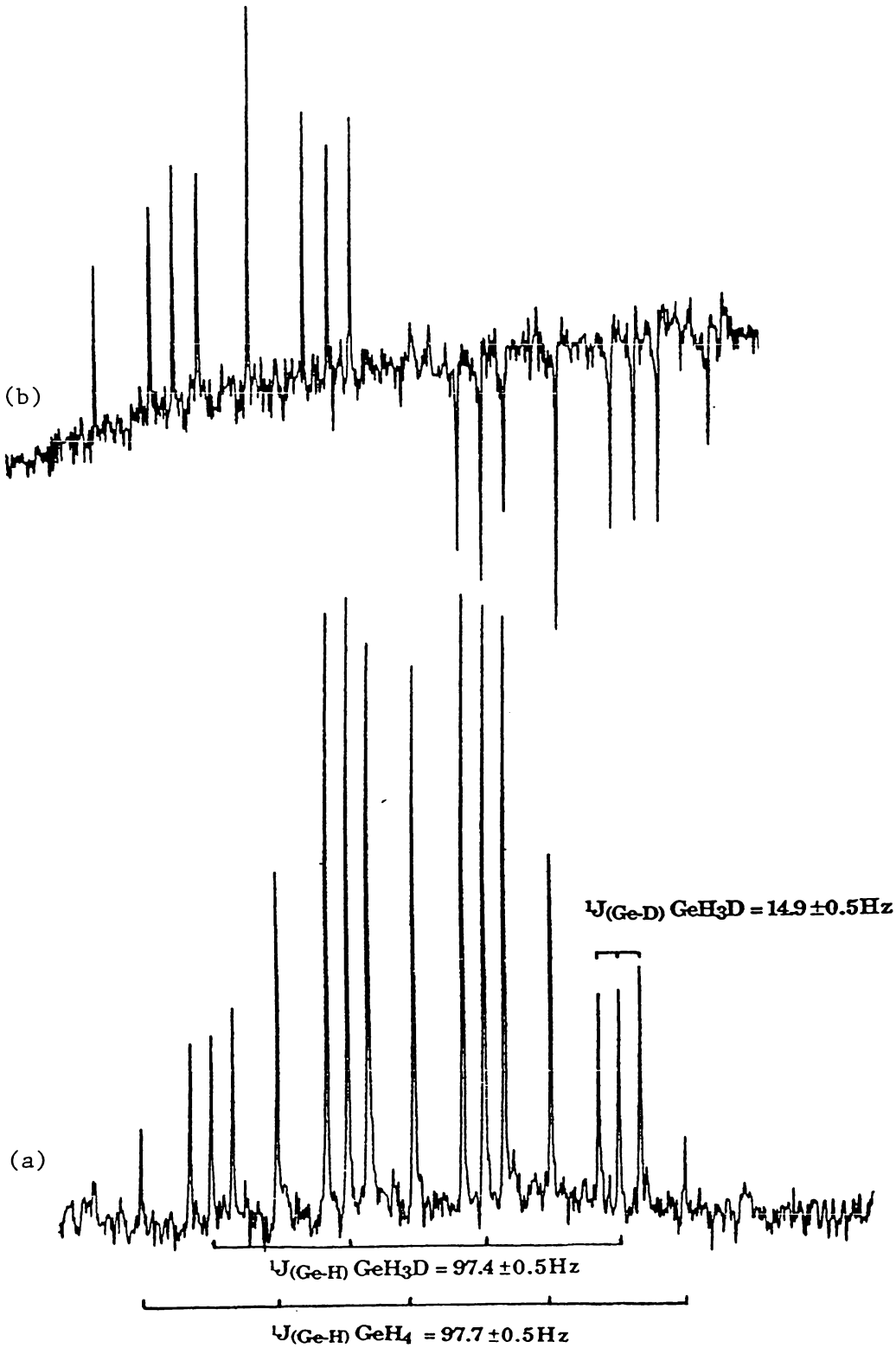

Fig. 3.2. ^{73}Ge {proton-coupled} spectrum of GeH_3D. (a) Standard experiment. (b) INEPT experiment. Spectral window in both cases was 2000Hz with 8K data points, acquisition time 1s. Relaxation delay for (a) was 10ms, and for (b) 30s. total acquisition time approximately equal.

The primary isotope effect on the ^{73}Ge, hydrogen spin-spin coupling constant of GeH_4 is measured by $(\gamma_H/\gamma_D).|J(^{73}Ge,D|-|J(^{73}Ge,H)|$. Using a figure of 6.514 for (γ_H/γ_D) the isotope effect is -0.36± 0.1Hz. Jameson and Osten[40] noted that primary isotope effects on J in hydrides are negative except where the central atom contains one or more lone pairs. The figure obtained is in accord with their observation.

The secondary isotope effect on J(Ge,H) is given by $|J(Ge,H)\ GeH_3D|-|J(Ge,H)\ GeH_4|$ and is calculated as -0.2Hz. Wasylishen and Burford[41] note that at present there appears to be no simple criterion for predicting the sign of Δ_sJ in a particular molecule. This data and that for other Group 14 hydrides are listed in Table 3.5.

Table 3.5 Deuterium Isotope Shifts in Group 14 Hydrides.[a]

	Chem Shift/D	Δ_pJ(Hz)	Δ_sJ(Hz)
CH_4	+0.187	no measurable effect	
GeH4	+0.4	-0.36	-0.2
SnH_4	-0.4	-2.8	-1.7

(a) CH_4 data from ref. 42, SnH_4 data from ref. 43.

Linewidths in the GeH_3D sample show no broadening as a result of the deuterium quadrupole but the sample of Ge_2D_6 gave a signal with a linewidth at least double that observed for Ge_2H_6. Although it is unlikely that 100% deuteration could be achieved the ^2D spectrum of Ge_2D_6 showed only a singlet in the proton coupled spectrum. While broadening of the Ge_2D_6 germanium signal by species such as Ge_2D_5H cannot be excluded they would have been present only in very small amounts.

This work has not extended the range of chemical shifts reported by other workers but has confirmed a few uncertain reports. The concentration

and/or medium effect for the smaller hydrides has again been highlighted and requires further work to determine the extent of the effect.

Before direct high resolution observation of ^{73}Ge, only fully symmetric molecules yielded coupling constants by ^{1}H or ^{19}F observation. For example ^{73}Ge satellites were not detected in the ^{1}H spectrum of Ge_2H_6 or of $GeEt_4$. While the number of J values determined is still relatively limited some useful patterns have emerged. Few signs have been determined[(2)] but those which have fit the general Group 14 pattern with $^{1}J(GeH)$ and $^{3}J(GeH)$ negative and $^{2}J(GeH)$ positive. This may be assumed for the rest. Only for GeF_6^{2-} has a coupling constant (^{1}J = 98Hz)[(8)] been determined for other than four-coordination.

Reduced coupling constants increase in absolute value from Si to Ge to Sn, as might be expected from the equivalent rise in *s* electron density: $^{1}K(M,H)^{(4X44)}$ = 8.5 (SiH_4), 23.3 (GeH_4), and 43.1 (SnH_4); $^{1}K(M,C)^{(3X45)}$ = -8.4 ($SiMe_4$), -17.8 ($GeMe_4$), and -30.2 ($SnMe_4$).

Those $^{1}J(GeH)$ values, which are accurately known, fall in the range 90 - 98 Hz (± 0.5 Hz or better). The highest, J = 97.6 Hz, is that for GeH_4 and the remainder decrease in the general sense expected for the decrease in *s* character of the GeH bond - e.g. on replacement of H by R or GeH_3. When less accurate determinations from broader bands are included, values down to 85Hz are found, but with uncertainties rising to ±2Hz, and again generally reflect expected changes in angles with bulky substituents. With the class of observable hydrides limited to those with H, C, Si, or Ge ligand atoms, more extreme effects on bond angles are not observed and the range is limited. The limited number of reliable $^{2}J(GeH)$ values fall in a range around 4Hz while the two $^{3}J(GeH)$ values are -1.9 and -2.5Hz. There are no clearly anomalous values, but not enough data to allow generalisation.

3.4.2 Observability

(i) Sample Limitations.

As mentioned in the introduction the major emphasis in this work has been in attempting to ascertain the limits of observability in ^{73}Ge NMR. A number of compounds were studied where no ^{73}Ge signal was observed. These include Me_3GeCl, Me_3GeBr, $MeGeI_3$, GeF_4 (gas), $GeH_3GeMe(H)(Cl)$, $GeCo_4(CO)_{14}$, $GeH_3Mn(CO)_5$, and $Me_2Ge(Cl)Co(CO)_4$.

When no ^{73}Ge signal is observed in a particular sample a lingering doubt remains that there is a problem with the sample. Sample preparation is often difficult with low solubilities and air sensitivity in many cases. Because of the poor sensitivity of ^{73}Ge, especially where wide lines would decrease the S/N, as much sample as possible is required. This means use of 10mm tubes, or 8mm tubes run concentrically within a 10mm tube, which do not allow for running of high resolution ^{1}H NMR. In circumstances where structure or sampling did not allow for ^{1}H NMR to confirm structure other multinuclear experiments were run to confirm sample integrity. Data obtained on samples used in this work are listed in Table 3.6.

With workers reporting that no signal had been observed for a number of compounds, experiments were run that tried to control line broadening. A series of digermane compounds with mixed ligands were studied.

(a) GeH_3GeMe_2Cl and Me_3GeCl were run under the same experimental conditions. No ^{73}Ge signal was seen from Me_3GeCl, confirming earlier reports[13]. For GeH_3GeMe_2Cl, the GeH_3 signal was readily detected with a linewidth similar to the polygermanes. There was no sign of a signal from the $GeMe_2Cl$ group, confirming the unobservability of Ge with mixed X and R groups (see Section 3.1.3) is intrinsic and not due to some experimental deficiency.

(b) A similar experiment on $GeH_3GeH_2Mn(CO)_5$ again showed a clear GeH_3 signal - surprisingly sharp in this case. The unobserved α Ge resonances strongly reinforce the earlier observations from $GeH_3Mn(CO)_5$

and $Me_2Ge(Cl)Co(CO)_4$ that the signal from a Ge bonded to a $M(CO)_x$ group is unobserved.

Table 3.6 Other NMR Observations of Samples Studied in this Work.

Sample[a]	$\delta(^1H)$	$\delta(^{13}C)$	Other[b]
$MeGe^*Cl_3$	1.25	6.33	
$Me_2Ge^*Cl_2$	1.75	12.14	
Me_3Ge^*Cl	2.22	17.38	
$MeGe^*I_3$	2.8	24.8	
$GeH_3Ge^*Me_2Cl$		6.9	
$Ge^*H_3Mn(CO)_5$		213	-2482 (^{55}Mn), 378, 370 (^{17}O)
$GeH_3Ge^*H_2Mn(CO)_5$		213.4	381, 371 (^{17}O), -2435(^{55}Mn)
$GeH_3Ge^*H(Me)Mn(CO)_5$		-2.8(Me), 211.3(CO)	379, 368 (^{17}O), -2450 (^{55}Mn)

(a). No ^{73}Ge signal observed for germanium marked with an asterisk.

(b). ^{17}O referenced to external H_2O, ^{55}Mn to external $KMnO_4$ (Satd.)

It is interesting to note that in the germanium-manganese compounds the carbonyl carbon signals are broadened (60Hz) into one signal while the oxygen signals are far enough away from the quadrupolar manganese to give separate signals. The manganese signals were very broad, with half-widths of 2000Hz and require further work to confirm the signals, although they agree well with an observation[46] of -2430 for $GePh_3Mn(CO)_5$.

The work on the deuterated species was an attempt to see the effect that a nucleus of moderate quadrupole bonded to germanium would have on linewidth. The doubling of linewidth in digermane, even with the modest deuterium quadrupole indicates that it will not require much asymmetry to broaden the ^{73}Ge signal beyond observability.

(ii) Effect of Field.

It is apparent from the observations on the Bruker AM400 that there is a price to pay for the extra field with the near doubling of linewidths. The increased acoustic ring signal may create difficulties with weak samples until better composite refocussing pulses improve the efficiency of the pulse techniques discussed in the previous chapter. The probe used in this work was not a dedicated, or even a low frequency probe, but an extended range multinuclear probe. Work with a dedicated or optimised multinuclear probe may well reduce some of these difficulties.

Apart from some recent results from a 360MHz instrument[27-30] all other germanium work to date has been carried out on 90MHz instruments. The 360MHz work, and our experiments at 400MHz, show advantages over 90MHz but further work is still required to determine the optimum field for ^{73}Ge observation. At present the limitation on observable window is the pulse times available on current technology probes.

(iii) Sensitivity Limitations.

When observing a nucleus for the first time it is easy, but naive, to imagine that the broadest signal that may be observed is that which will fit into the widest window allowable by the AD convertor. In the case of the JEOL FX90Q instrument this is 30,000Hz. Akitt[47] notes that any signal wider than this would be impossible to distinguish from noise. Ideally therefore one might say that the widest signal to be observed would have a half-width of approx. 14,000Hz. However the work in Chapter 2 notes that, of course, excitation windows have finite limits. For any given instrument pulse times increase as the observation frequency decreases, and as pulse times increase excitation windows decrease. As the previous chapter notes, the excitation window for the 90MHz instrument is 10,000Hz limiting the broadest observable signal to a half-width of 5000Hz. With the lower frequencies comes the difficulty of base-line roll and to ensure that this is

flattened, to allow for observation of broad lines, the 180° pulses needed limit the excitation window to 4000Hz, and therefore a linewidth of 2000Hz. On top of these limitations is the over-riding one of sensitivity. In a typical experiment, the ^{73}Ge study of $GeH_3GeH_2Mn(CO)_5$ resulted in the observation, after 20,000 scans, of one signal, that for GeH_3. The S/N for this peak, with a half-width of 64Hz, was 12:1 and as such the widest peak that could have been observed would have had a halfwidth of no more than 160Hz. (Calculated by use of the triangle method used in the thesis introduction.) Using the achieved S/N ratio for the narrow line signal of neat $GeCl_4$ (8.6M.) on the JEOL FX90Q calculation of the best S/N ratio likely to be achieved for ^{73}Ge over a 24hr experiment would be 1000:1. This translates into a possible broadline maximum of 1000Hz. As most of the samples do not attain anything like this concentration it may be seen that sensitivity is the main limitation to the observation of broad line signals in ^{73}Ge NMR.

Recent work by other workers highlights the difficulty of observing broad-line signals in conditions more favourable than those experienced with ^{73}Ge NMR. ^{99}Tc has a spin of 9/2 and may perhaps be considered as a useful comparison with ^{73}Ge. Its big advantages however are;

(a) it is the fifth most sensitive nucleus for NMR detection, and

(b) its high resonance frequency. (20.58MHz w.r.t 3.13MHz for ^{73}Ge).

Despite these advantages Clark *et al* [48] in a study of $Tc(CO)_9(PF_3)$ found signals whose width was very temperature dependent (see Fig 3.3). It is apparent that the chances of finding the broad peak, in the 257°K spectrum, would be small if overlaid on a rolling baseline. It is also clear that even a small change in electronic environment around the ^{99}Tc nucleus (as noted in the paper PF_3 has similar bonding characteristics to CO) lead to a large broadening of signal. This effect would also be expected in ^{73}Ge NMR.

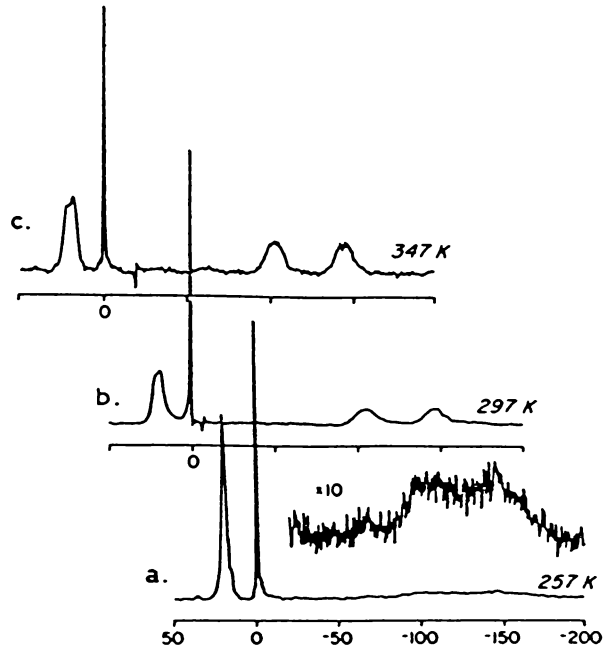

Fig. 3.3 ^{99}Tc NMR spectrum of ax-$Tc_2(CO)_9(PF_3)$ in $CFCl_3$ at: (a) 257K, (b) 297K, (c) 337K. Taken from Fig. 2 ref. 48. The peaks in (a) are unlikely to be observed without either (i) a smooth baseline, or (ii) indication from other temperatures of their existence.

Fig. 3.4, reproduced from Fig. 1 of ref. 47, indicates the amount of detail obtainable when one can be certain of smooth baselines. Note especially the expanded signals in the lower spectra of series (a). In this ^{27}Al NMR study of the hydrolysis products of aluminium, concentrations were calculated from such data. It would be impossible to obtain similar data from ^{73}Ge NMR with its inherent lack of sensitivity.

A very recent highlight of the observability difficulties in ^{73}Ge NMR is given in a 1990 paper published by Takeuchi[52] extending his earlier work with substituted germacyclohexanes[19]. In the new work (see Table 3.6) where he used ^{t}Bu as a substituent, on either the germanium atom or on the ring, he found that a sample of 4-^{t}Bu$C_5H_{10}GeH_2$ showed a similar ^{73}Ge chemical shift to the methyl substituted species (see Table 3.2) observed previously. ^{t}Bu substitution on the germanium atom shifted the resonances 100ppm downfield while additional ^{t}butyl substitution on the ring resulted in

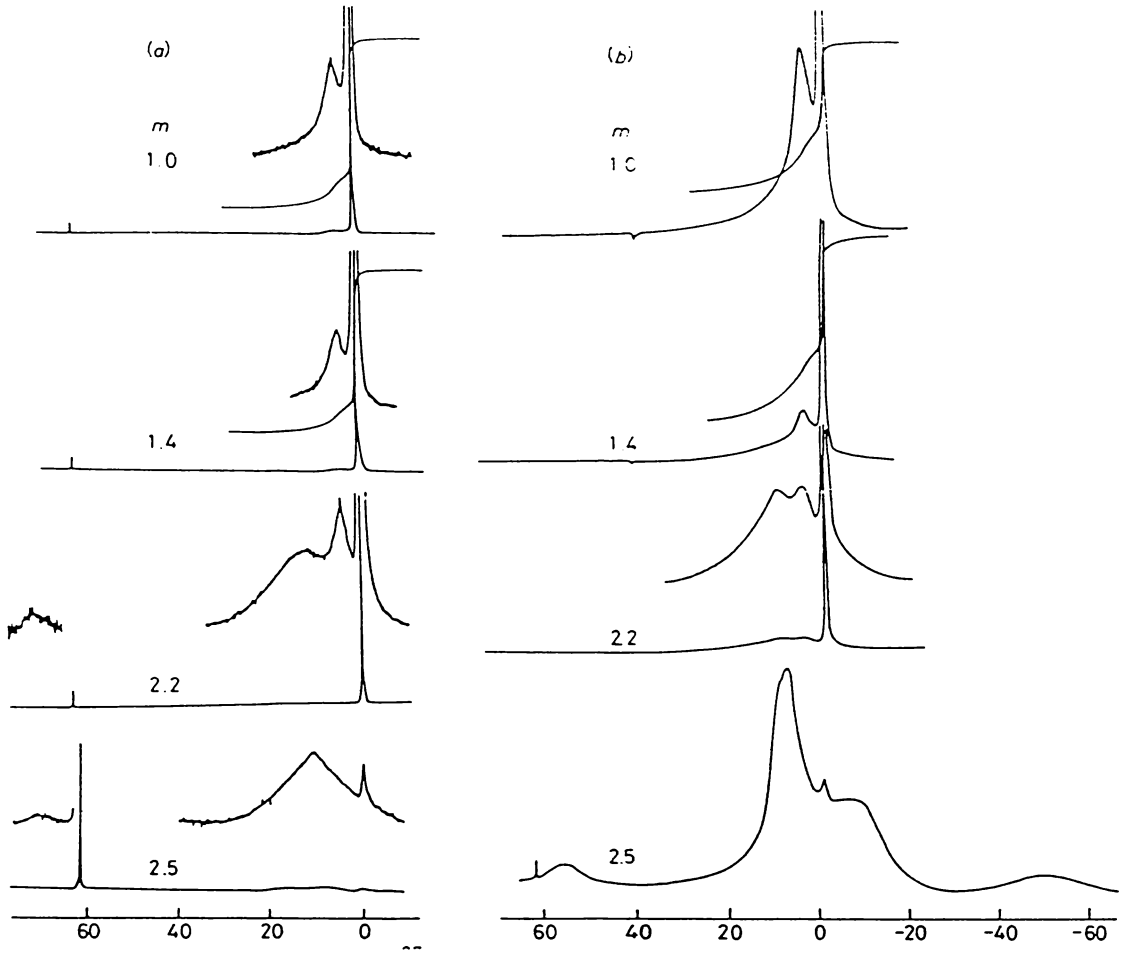

Fig. 3.4 ^{27}Al NMR spectrum of metal hydrolysed aluminium salt solutions. Taken from Fig. 1 of ref. 47. Concentration details obtained from expanded signals such as those in column (a), when m = 2.2 and 2.5 require the sort of S/N ratios not normally obtained in ^{73}Ge NMR.

germanium resonances with halfwidths of *ca.* 150Hz. No germanium resonance was observed for the species 4-^{t}BuC$_5$H$_{10}$GeH^{t}Bu. Likewise no germanium signal is reported where, for any of the compounds listed in Table 3.7, the hydrogen bonded to germanium is replaced by chlorine.

This again highlights the point made in Section 3.1.2 that no observation of mixed X and R ligands have so far been made in ^{73}Ge NMR.

Table 3.7 ^{73}Ge Chemical Shifts of ^{t}Bu Substituted Germacyclohexanes[a].

Compound	δ ^{73}Ge	Notes
4-^{t}BuC$_5$H$_9$GeH$_2$	-131.6	
C$_5$H$_{10}$GeH(^{t}Bu)	-27.8	
3-MeC$_5$H$_9$GeH(^{t}Bu)	-37.5	*cis* and *trans* forms unresolved
4-MeC$_5$H$_9$GeH(^{t}Bu)	-41.2	*cis* and *trans* forms unresolved
4-^{t}BuC$_5$H$_9$GeH(^{t}Bu)		not observed

(a) From ref. 52.

3.4.3 ^{73}Ge Relaxation Studies

Recent work by Takeuchi and co-workers[20-22,26] has done much to clarify conflicting data from earlier work. Table 3.8, taken from our review article, shows a wide variety of results for any particular compound, and some of the T_2 data was obtained before high resolution spectrometers were available.

For any nucleus the spin relaxation time (T_1) may be approximated by

$$1/T_1 = 1/T_1^{DD} + 1/T_1^{SR} + 1/T_1^{CSA} + 1/T_1^{QR} \qquad .....(3.1)$$

where T_1 contains contributions from separate spin-lattice relaxation mechanisms: DD = dipole - dipole, SR = spin - rotational, CSA = chemical shift anisotropy, and QR = quadrupolar.

Dipole - dipole relaxation results from fluctuation of local magnetic fields caused by dipolar interaction of the relaxing nucleus with neighbouring nuclei, either intramolecular or intermolecular. It is a function of r^{-6}, where r is the distance between the nuclei involved.

Spin - rotation effects arise because coherent molecular rotation generates a magnetic field which can couple with the nuclear spin. This

Table 3.8 Relaxation Data for Germanium Compounds.

Compound	Solvent(concn) (%)	T_1(ms)	T_2(ms)	T_2^*(ms)	Notes
$GeMe_4$	neat	1.110[35]	740[3]	550[3]	Linear temperature
	Bu_2O (75)	595		320	variation for
	C_6H_{12} (50)	1,100[35]		400[35]	T_1, neat[35] and in
	CD_3OD (50)	410[35]		245	$CDCl_3$[34,35]
	$CDCl_3$ (50)	350[35]		200[35]	
		295[34]		245[34]	
$GeEt_4$	neat	510	140[3]	350	Linear temperature
	Bu_2O (75)	365		290	variation for
	(25)	300		240	T_1, neat and
	$CDCl_3$ (50)	250[34]		190[34]	in $CDCl_3$[34]
	C_6H_{12} (6)	905		370	
$GePr_4$	neat	113	100[3]	95	
$GeBu_4$	neat	72	65[3]	62	Linear temperature
	$CDCl_3$ (50)	69[35]		55[35]	variation for T_1[35]
$Ge(C_5H_{11})_4$	neat	31		27	
$Ge(C_6H_{13})_4$	neat	19		19	
$GeMe_3CMe_3$	$CDCl_3$ (50)	42[35]		30[35]	
$Ge(OMe)_4$	neat		30[3]	29[3]	By curve fitting
$GeMeH_3$	Bu_2O (b)	375		250	
$GeMeH_3$		575		220	
$GeMe_2H_2$		295		180	As a mixture
$GeMe_3H$		340		190	
$GeEtH_3$	neat	95		94	
$GeEt_3H$	neat	12.5		12	Linear temperature
					variation for T_1[13]
GeH_4	Bu_2O (c)	1.300		12	Linear temperature
	$CDCl_3$ (50)	570[21]	320[21]		variation for
					T_2[21,13]
Ge_2H_6	Bu_2O (d)	22		20	
GeH_3GeMeH_2	(e)	265		160	GeH_3
		50		45	$GeMeH_2$
GeH_3SiH_3	Bu_2O (b)	575		270	

Table 3.8(cont.) Relaxation Data for Germanium Compounds.

$GeCl_4$	neat	1.020	165[3]	150[3,13]	
	$CDCl_3$ (50)	280 [21]	120[21]		Non-linear temperature variation for T_1[21]
		240			
$GeBr_4$	neat	205	195[3]	140,180	
	$CDCl_3$ (50)	160[21]	130[21]		
$GeCl_4$		520		140	
$GeCl_3Br$		235		140	
$GeCl_2Br_2$		215		140	In 1 : 1
$GeCl_3Br$		280		140	$GeCl_4/GeBr_4$
$GeBr_4$		335		140	

NOTES:

(a) All values from reference[13] unless otherwise indicated. Precision indicated by rounding.

(b) 0.7 atm (c) 1.2 atm (d) 0.2 atm

(e) In a mixture of methylgermanes

coupling involves a magnetic field at the nucleus which may be interrupted, e.g. by collisions, providing a relaxation mechanism.

The chemical shielding anisotropy term arises from the fact that the shielding at the nucleus, and therefore the magnetic field acting on it, varies with the molecular orientation in the static field B_0, except for sites of high symmetry. Relaxation arising from CSA is proportional to the square of the applied magnetic field, and may result in unacceptable line broadening for some nuclei at high field.

It is generally assumed that for quadrupolar nuclei (spin > 1/2) that the quadrupolar mechanism of relaxation dominates. It arises from the interaction of the electric quadrupole moment (eQ) with a time dependent electric field gradient (eq) induced by molecular motion.

For ^{73}Ge $1/T_1^{QR}$ may be approximated by

$$\chi' = \left(\frac{e^2qQ}{h}\right)\left(1 + \frac{\eta^2}{3}\right)^{0.5} \qquad .....(3.2)$$

where q is the electric field gradient and η the asymmetry parameter which describes deviation from cylindrical symmetry.

If relaxation occurs via the quadrupolar mechanism the spin-lattice (T_1) and spin-spin (T_2) relaxation times should essentially be equal. Early work, see Table 3.8, did not suggest that this was so, but Takeuchi's recent work found good correlation between T_1, T_2 measured by the CPMG (Carr-Purcell-Meiboom-Gill) technique, and T_2^* measured from linewidths, in a number of small molecule trialkylgermanes (see Table 3.9). In the case of the tetraalkylgermanes other mechanisms were excluded on the basis of;

(a) no measured n.O.e effect within experimental error, thus precluding any dipole-dipole interaction. (It should however be noted that a n.O.e of 0.3 was measured for $GeMe_4$ by Watkinson.[13])

(b) spin rotation shows a reverse temperature dependency to that of quadrupolar relaxation, and no such indication was found.

(c) chemical shielding anisotropy is excluded because of the tetrahedral environment in GeR_4.

With the tetrahedral symmetry of GeR_4 it might be expected that the electric field gradient was zero, and therefore the relaxation of the germanium nucleus would be extremely long.

A number of explanations of the non-ideality of quadrupolar relaxation in highly symmetric nuclei have been proposed. Brown and Colpa[49] related the results of molecular spectroscopy to those of nuclear spin relaxation and showed that the vibrational distortion of the very symmetric molecules corresponding to certain normal modes can generate an electric field

Table 3.9 Relaxation Times of Tetraalkyl- and Tetrahalo- Germanes[a]

Compound	T_1 (ms)	T_2 (CPMG)	T_2^*
Tetralkylgermanes			
$GeMe_4$	290	270	280
$GeEt_4$	220	200	240
$GePr_4$	100	100	90
$GeBu_4$	80	80	80
113MGC[b]	16	14	14
114MGC[c]	16	15	15
1135MGC[d]	24	24	24
Tetrahalogermanes[e]			
$GeCl_4$	280	120	120
$GeBr_4$	160	130	130
GeI_4	80	80	80

Notes: (a) From references (20) and (22).

(b) 1,1,3-trimethyl-1-germacyclohexane

(c) 1,1,4-trimethyl-1-germacyclohexane

(d) 1,1,3,5-tetramethyl-1-germacyclohexane

(e) At 303°K.

gradient at the centre that does not average to zero over the vibrational motion. Osten and Jameson[50] suggest that collisions generate an instant field gradient which average to zero but have a nonvanishing mean square, i.e. $(e^2Qq/h)^2 \neq 0$

In the tetrahalogermanes Takeuchi[22] noted that a plot of $\ln(1/T_2)$ against $1/T$ for $GeCl_4$ was concave, indicating that at least two mechanisms, with different temperature dependence, were involved. Scalar coupling via

chlorine would account for the observed temperature dependence, and a value for J(^{73}Ge-^{35}Cl) of 24Hz was estimated. Indications of similar mechanism were apparent in $GeBr_4$, but not in GeI_4, where the quadrupolar term dominates.

In more recent work [26] at higher temperature, scalar coupling was found to occur even in GeI_4. From the data obtained, estimated coupling constants of 64 and 220Hz were calculated for J(Ge-Br) and J(Ge-I) respectively.

The work by Takeuchi, described above, meant that little work was carried out here with relaxation experiments. The limited number of T_1 relaxation times obtained during the course of this work are listed in Table 3.10.

When Takeuchi published T_1 data for the tetrahalogermanes (in $CDCl_3$) his result for $GeCl_4$ of 287ms was markedly different to that obtained by Watkinson for a neat sample (1020ms). To check whether systematic experimental errors might be the cause of the discrepency in T_1 values a sample similar to Takeuchi's, i.e. 1:1 $GeCl_4$:$CDCl_3$, was used to obtain a T_1 value. The result of 250ms was within experimental error indicating no major differences in technique between the two groups.

Table 3.10 Relaxation Times Obtained During this Work.

Compound	T_1(msec)	Temp. (°C)
GeH_3D	1460	25
$GeMeH_3$	728	25
$GeCl_4$ (neat)	880	10
	1030	41
(at 400MHz)	880	25
$GeCl_4$ (1:1 in $CDCl_3$)	250	27
	290	42

Variable temperature experiments showed that the change with temperature was in the same direction for both the neat and dilute solutions.

The value obtained for GeH_3D compares with that obtained for GeH_4 [13] (1.2atm in Bu_2O), and is considerably longer than the figure obtained for a 50% solution of GeH_4 in $CDCl_3$. The effect of the deuterium quadrupole is obviously minimal as far as the quadrupolar relaxation term is concerned.

The determination of T_1 using a clean, neat sample of $GeMeH_3$ resulted in relaxation times longer than those found earlier on less pure samples (see Table 3.8). The T_1 observation for $GeCl_4$ made at high field cannot be considered significant without further work ensuring compatible samples are used at both fields.

In summary the greatest contribution to our understanding of germanium relaxation times over recent time has been provided by Takeuchi's group. From other data obtained we can see that the relatively symmetric compounds give sharp lines, e.g. $W_{1/2}$ = 1Hz for GeH_4, $GeEt_4$ or $GeMeH_3$, while polygermanes, non-functional tetralkyls, tetrahalides and simple tetra-alkoxides fall in a readily observable range up to ca $W_{1/2}$ = 50Hz. In general the pattern of linewidths is consistent with the changes expected from the effects of symmetry, concentration or viscosity, and temperature, on relaxation processes, together with the effects of unresolved coupling.

A further test for quadrupolar relaxation, suggested by Marks and Shimp[51], is based on the usual observation that $t_c \sim \eta^1/T$, where η^1 is the macroscopic viscocity of the solution and T is the absolute temperature. Since T_1 and t_c are the only variables in equation 3.2, for a given compound changes in t_c arising through dilution or temperature changes will affect the T_1 values such that dilution in an inert solvent, or increase in sample temperature should increase T_1. Little work has been done to correlate observed T_1 values with sample viscocity. Much work is still to be done in this field before we understand the mechanisms involved in germanium relaxation.

3.5 Overview of ^{73}Ge NMR

Although the observational difficulties, and the dominance of single environment samples might suggest that ^{73}Ge measurements would be of little general value, there are cases where a ^{73}Ge study is revealing. The classical example appears in the earliest work where mixed halide species like $GeCl_3Br$ were observed only through their ^{73}Ge signal in solution.

Studies of the mixed halide systems GeX_4/MX_4 (X = Si, Sn) found[13] that ^{73}Ge NMR allowed observation of all mixed halide signals, whereas ^{29}Si or ^{119}Sn NMR resulted in single line spectra. Here much more information was obtainable from ^{73}Ge NMR.

The recent observations by Lukevics[28,30] of six coordinate compounds, and their interaction in solution, have shown that, despite our earlier[24] predictions, ^{73}Ge NMR has a future in determining interactions in solutions.

As an example of the usefulness of ^{73}Ge NMR. Fig. 3.5 shows a spectrum of a reaction that attempted to make tetraalkylgermanes. This work was carried out as part of an undergraduate student course. While other simple spectroscopic techniques showed only a mixture of species, the ^{73}Ge data indicated the presence of, not only the major product of $GeEt_4$ at 17.8ppm, but also two other signals assigned as the mixed alkyl species (n-Bu)$GeEt_3$ (14.4ppm) and (n-Bu)$_2GeEt_2$ (*ca.* 12ppm) on the basis of stepwise difference between the chemical shifts of $GeEt_4$ and $GeBu_4$. In contrast, the ^{13}C spectra were strongly overlapping, the ^{1}H spectra are second order, and vibrational spectra cannot give detailed identification. While further work is required to confirm these assignments, the ^{73}Ge spectra were a readily obtained indication of the new mixed alkyl species.

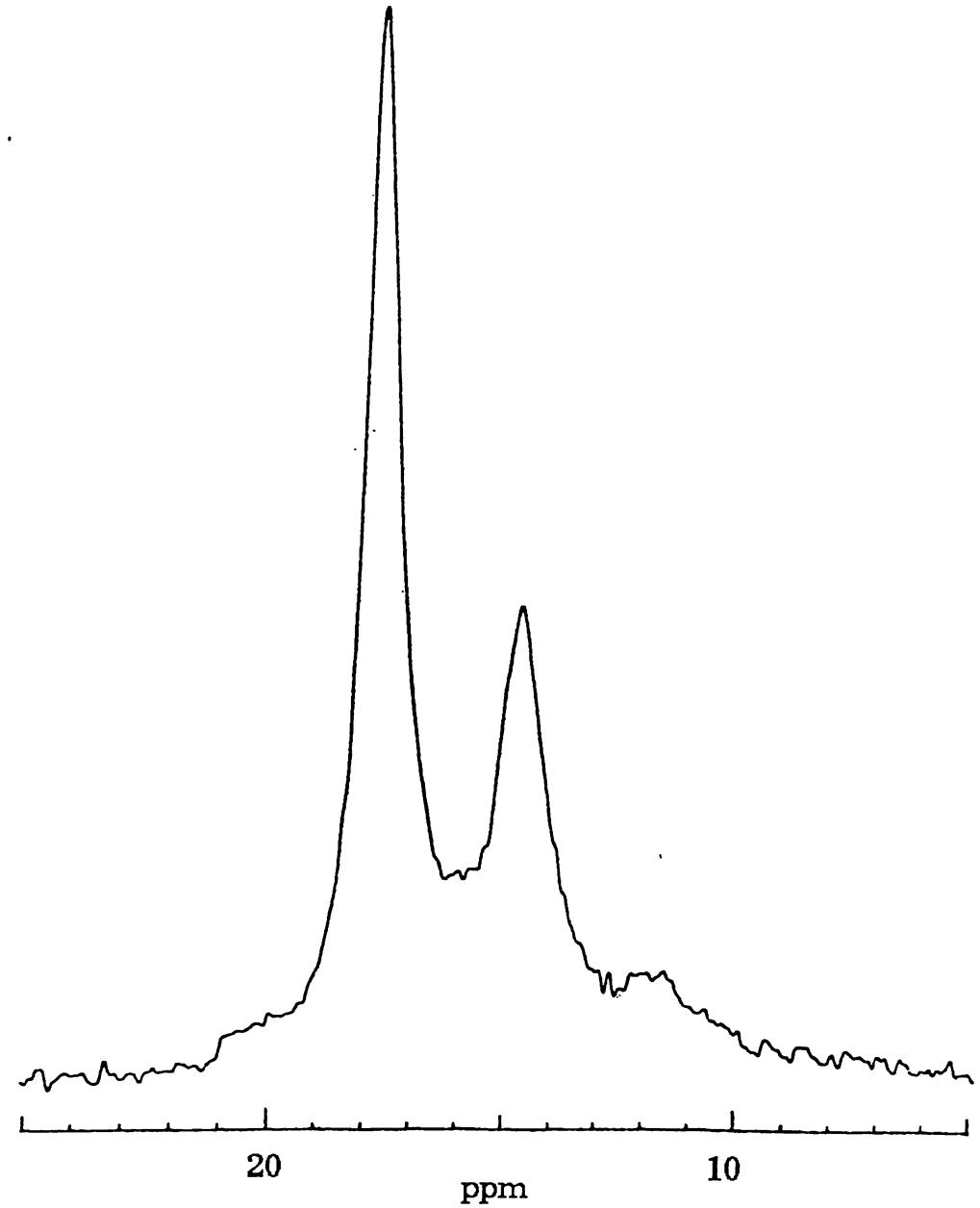

Fig. 3.5 ^{73}Ge NMR spectrum of mixed tetraalkylgermanes. The major peak at 17.8ppm is assigned as $GeEt_4$ while the other signals indicate the presence of mixed ethyl, butyl species.

Chapter 3 References

1. R.K.Harris in J.B.Lambert and F.G.Riddell (Eds) *'The Multinuclear Approach to NMR Spectroscopy'*, D.Reidel, Dordrecht, 1983, Chap.16.
2. C.D.Jeffries, *Phys. Rev.*, **92** *1262* 1953; S.I.Aksenov and K.V.Vladmirskii, *Dokl. Akad. Nauk. SSSR*, **96**, *37*, 1954; O.Lutz, A. Schwenk, and G.Z.Zimmerman, *Phys. Letters*, **25A**, *653,* 1967.
3. J.Kaufmann, W.Sahm, and A.Schwenk, *Z. Naturforsch., Teil A*, **26**, *1384*, 1971.
4. H.Dreeskamp, *Z. Naturforsch., Teil A,* **19**, *139*, 1964.
5. E.A.V.Ebsworth, S.G.Frankiss, and A.G.Robiette, *J. Mol. Spect.*, **12,** *299*, 1964.
6. G.W.Smith, *J. Chem. Phys.*, **39,** *2031*, 1963.
7. A.Tzalmona, *Molec. Phys.*, **7,** *497*, 1963.
8. (a) P.T.Inglefield and L.W.Reeves, *J. Chem. Phys.*, **40**, *2425*, 1964, (b) P.A.Dean and D.F.Evans, *J Chem. Soc.*, (a), *698*, 1967.
9. H.Saji, *Phys. Letters*, 45A, *469*, 1973.
10. R.K.Harris and B.E.Mann (Eds.) *'NMR and the Periodic Table'*, Academic Press, New York, 1978.
11. G.A.Morris and R.Freeman, *J.Am. Chem. Soc.*, **101**, *760*, 1979.
12. K.M.Mackay, P.J.Watkinson, and A.L.Wilkins, *J. Chem. Soc., Dalton Trans.*, *133*, 1984.
13. A.L.Wilkins, P.J.Watkinson, and K.M.Mackay, *J. Chem. Soc., Dalton Trans.*, *2365*, 1987.
14. J.Banck and A.Schwenk, *Z. Phys.*, **265**, *165*, 1973.
15. R.G.Kidd and H.G.Spinney, *J. Am. Chem. Soc.*, **95**, *88*, 1973.
16. W.A.Pestunovich, S.N.Tandura, B.Z.Shterenberg, N.Yu. Khromova, T.K.Gar, V.F.Mironov, and M.G.Voronkov, *Izv. Akad. Nauk SSSR, Ser. Khim.*, *959*, 1980.

17. G.Zelcans, A.Lapsina, I.I.Solomennikova, E.Lukevics, E.Liepins, and E.Kupce, *Zh. Obshch. Khim.*, **53**, *1069*, 1983.

18. I.Zicmane, E.Liepins, E.Lukevics, andT.K.Gar, *Zh. Obshch. Khim.*, **52**, *896,* 1982.

19. Y.Takeuchi, T.Harazono, and S.Tomoda, *Magnetic Resonance in Chemistry*, **23**, *580*, 1985.

20. T. Harazono, K.Tanaka, and Y.Takeuchi, *Inorg. Chem.*, **26**, *894*, 1987.

21. T.Harazono, K.Tanaka, Y.Takeuchi, and N.Kakimoto, *Chem. Lett.*,**11**, *1841*, 1986.

22. T.Harazono, K.Tanaka, Y.Takeuchi, and H.Fukutomi, *Inorg. Chem.*, **26**, *3851*, 1987.

23. Y.Takeuchi, M.Shimoda, K.Tanaka, S.Tomoda, K.Ogawa, and H.Suzuki, *J. Chem. Soc. Perkin Trans. II, 7*, 1988.

24. K.M.Mackay and R.A.Thomson, *Main Group Metal Chem.*, **1**, *83*, 1987.

25. E.Liepins, I.Zicmane and E.Lukevics, *J. Organomet. Chem.*, **341**, *315*, 1988

26. T.Harazono, K.Tananka, and Y.Takeuchi, *Inorg. Chem.*, **28**, *1813*, 1989.

27. E.Kupce, E.Lukevics, O.D.Flid, N.A.Viktorov and T.K.Gar, *J. Organomet. Chem.*, **372**, *187*, 1989.

28. E.Kupce, E.Upona, M.Trusule and E.Lukevics, *Polyhedron*, in press.

29. E. Kupce and E.Lukevics, *J. Mag. Reson.*, **79**, *325*, 1988.

30. E.Kupce, L.M.Ignatovich and E.Lukevics, *J. Organomet. Chem.*, **372**, *189,* 1989.

31. T.N.Mitchell, *J. Organomet. Chem.*, **255**, *279*, 1983.

32. P.J.Watkinson and K.M.Mackay, *J. Organomet. Chem.*, **275**, *39*, 1984.

33. E.Liepins, I.Zicmane and E.Lukevics, *J. Organomet. Chem.*, **306**, *327,* 1986.

34. Y.Takeuchi, T.Harazono, and N. Kakimoto, *Inorg. Chem.*, **23**, *3835*, 1984.

35. I.Sekacis, E.Liepins, I.Zicmane and E.Lukevics, *Zh. Obshch. Khim.*, **53**, *2064*, 1983.

36. P.Geerlings and C. van Alsenoy, *J. Organomet. Chem.*, **117**, *13*, 1976.

37. F.S.Wong and K.M.Mackay, *J. Chem. Research (S), 109*, 1980.

38. The deuterated compounds were made as part of an undergraduate laboratory course.

39. For example, N.Janes and E.Oldfield, *J. Amer. Chem. Soc.*, **108**, *5743*, 1984.

40. C.J.Jameson and H.T.Osten, *J. Am. Chem. Soc.*, **108**, *2497*, 1986.

41. R.E.Wasylishen and N.Burford, *J. Chem. Soc. Chem. Comm., 1414*, 1987.

42. M.Alei and W.E.Wageman, *J. Chem. Phys.*, **68**, *783*, 1978.

43. K.L.Leighton and R.E.Wasylishen, *Can. J. Chem.*, **65**, *2707*, 1987.

44. C.Schumann and H.Dreeskamp, *J. Mag. Reson.*, **3**, *204*, 1972.

45. G.C.Levy, D.M.White and J.D.Cargioli, *J. Mag. Reson.*, **8**, *280*, 1972.

46. G.M.Bancroft, H.C.Clark, R.G.Kidd, A.T.Rake, and H.G.Spinney, *Inorg. Chem.*, **12**, *728*, 1973.

47. J.W.Akitt, J.M.Elders, X.L.R.Fontaine, and A.K.Kundu, *J. Chem. Soc. Dalton Trans., 1889*, 1989.

48. C.S.Grimm, R.J.Clark, and R.Rosanske, *Inorg. Chimica. Acta*, **159**, *137*, 1989.

49. R.J.C.Brown and J.P.Copla, *J. Chem. Phys.*, **77**, *1501*, 1982.

50. H.J.Osten and C.Jameson, *J. Mol. Phys.*, **57**, *553*, 1986.

51. T.J.Marks and L.A.Shimp, *J. Am. Chem. Soc.*, **94**, *1542*, 1972.

52. Y.Takeuchi, K.Tanaka, T.Harazono and S.Yoshimura, *Bull. Chem. Soc. Jpn.*, **63**, *708*, 1990.

53. J. D Kennedy and J. Nekrolane, unpublished result in ref. 10.

Chapter 4 Silicon NMR

4.1 Introduction

Earlier reports[1,2] had suggested that syntheses in the series $Me_xSi(GeH_3)_{4-x}$ (x=0,1,2,3) became progressively more difficult from x=3 to x=0. Kin-Fai Leung[3] attempted the synthesis of these compounds and multinuclear NMR (^1H, ^{29}Si, ^{13}C and ^{73}Ge) was used to establish the structure of the prepared compounds [$Si(GeH_3)_4$ could not be synthesised]. Although the chemical shifts observed (see Table 4.1), along with the known case where x=4 i.e. T.M.S., showed trends in chemical shift in line with those expected in this type of series it was important to unequivocally establish the structures, as other techniques such as I.R. and Raman were unable to distinguish each individual compound. To do this a coupled spectrum was needed and the main technical interest in these spectra was the evaluation of the $^2J_{Si-H}$. Since J_{Si-C-H} and $J_{Si-Ge-H}$ are likely to be of similar value an interesting problem in analysis of the twelve proton interactions arises.

Table 4.1. NMR parameters of $Me_xSi(GeH_3)_{4-x}$ (x=0,1,2,3)

x	$\delta^1H_{(CH)}$	$\delta^1H_{(GeH)}$	$\delta^{13}C$	$\delta^{29}Si$	$\delta^{73}Ge$	$^1J_{GeH}$
4	0.00	-	0.00	0.00	-	-
3	0.10	2.44	-0.14	-9.45	-315.5	n.o.
2	0.82	3.17	-0.38	-31.0	-290.6	90.8
1	1.06	3.80	-1.46	-71.7	-277.0	90.5

Although silicon has an inherent sensitivity advantage of 2.09 with respect to ^{13}C (see Table 3.1) observation of this nucleus is hampered by its negative gyromagnetic ratio and long relaxation times. Care is required in setting up the experiment to ensure that the null signal state does not result[4]. Any technique that enhances the sensitivity is obviously of great

assistance, and selective population inversion (SPI) has been used successfully in the observation of ^{29}Si signals in a variety of compounds[5-11]. This technique involves the application of a selective pulse, i.e. one of low power and long duration, at the frequency of one of the ^{29}Si satellites in the ^{1}H spectrum. This results in complete population inversion of the corresponding energy levels. An observe pulse immediately after saturation by the selective pulse results in a signal enhancement of $|\gamma_{(H)}/\gamma_{(Si)}| = |26.7519/-5.3188| \approx 5$.

The reason for this signal enhancement is more easily understood by consideration of the energy levels and their populations in a particular system. Fig. 4.1 shows the energy level diagram for an AX spin system. For A=H, X=Si Boltzmann's law indicates that proton transitions will have five

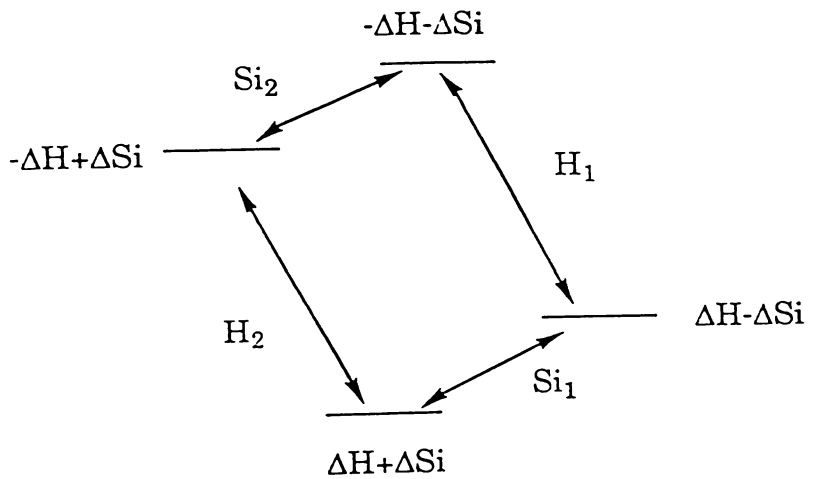

Fig. 4.1 Energy levels and populations of a heteronuclear AX system.

times the population difference of the silicon transitions i.e. $\Delta H = 5\Delta Si$. The actual population of each level is dependent on the total number N of nuclei present but the deviation of each level from a population N/4 is noted for each energy level in Fig. 4.1. If the H_1 transition is subjected to a selective pulse the proton populations are inverted and the resultant population inversions are shown in Fig. 4.2. The two proton transitions remain the same as before but one now has inverted sign. Transition Si_1 which previously had a population

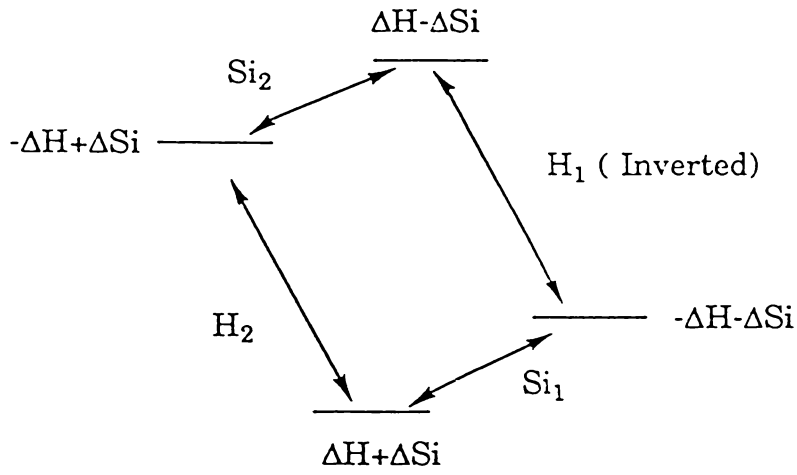

Fig. 4.2 Energy levels and populations of a heteronuclear AX system after inversion of one of the H transitions by a selective pulse.

difference of 2ΔSi now has a difference of (ΔH+ΔSi) - (-ΔH-ΔSi) i.e. 2ΔH+2ΔSi. For transition Si_2 the result is -2ΔH + 2ΔSi. The proton population difference has been transferred onto the silicon transitions and been added to the existing differences. With ΔH = 5ΔSi the resultant ^{29}Si doublet components have relative intensities of +6 and -4 with respect to the direct observation. While a number of useful results have been obtained using the SPI experiment the technique has some limitations. As a selective pulse is required, only one resonance at a time is observed. Thus in a multi-line spectrum a number of separate experiments would be required. In cases of closely overlapping signals this may be of some use in separating data[11], but in the majority of cases the selectivity leads only to longer experimental time. The selective pulse has to be applied to an often unobservable satellite so considerable care has to be taken in setting up the experiment to ensure maximum gain is achieved.

More recently, techniques such as INEPT and DEPT have been developed and these have the advantage of being relatively nonselective and providing quite substantial enhancements. A review by Blinka *et al* [4] has described the use of these techniques in ^{29}Si NMR. The aim of these

experiments is to place pairs of proton transitions anti-phase, as in the SPI experiment, but with non-selective pulses independent of chemical shift. The first sequence published was INEPT[12].

INEPT

^{1}H	90°_{x} - τ -	180°_{x} - τ -	$90^{\circ}_{\pm y}$	
^{29}S		180°_{x}	90°_{x}	acquire

Fig. 4.3 shows a vector diagram description of this sequence for an AX system. The proton 90° pulse tips magnetisation into the x-y plane where it is allowed to precess for time τ. As the doublet components precess in the rotating frame at $\pm$J/2Hz, τ is set to 1/4J to achieve one-eighth of a cycle before application of the 180° pulses. The ^{1}H 180° pulse rotates the components into the second half of the x-y plane while the ^{29}Si 180° pulse reverses the sense of precession. By the end of the second τ interval, chemical shift and inhomogeneity are refocused while the two components of the ^{1}H doublet are aligned along the $\pm$x axis. Application of the final two 90° pulses;

(a) rotates the proton components on to the z- axis, one up and one down as required, so that

(b) the ^{29}Si read pulse occurs while the proton components are anti-phase as required for SPI enhancement.

As in the case of the SPI experiment the enhancement is unequal at +6 and -4 for a ^{29}Si doublet. To average this enhancement out the final ^{1}H 90° pulse is cycled $\pm$y so that the sense of polarisation is reversed.

The DEPT[13][14] pulse sequence also provides enhancement but retains

DEPT

^{1}H	90°_{y} - τ -	180°_{x} - τ -	$\theta_{\pm x}$ - τ -	decouple	
^{29}Si		90°_{x}	180°_{x}	acquire	

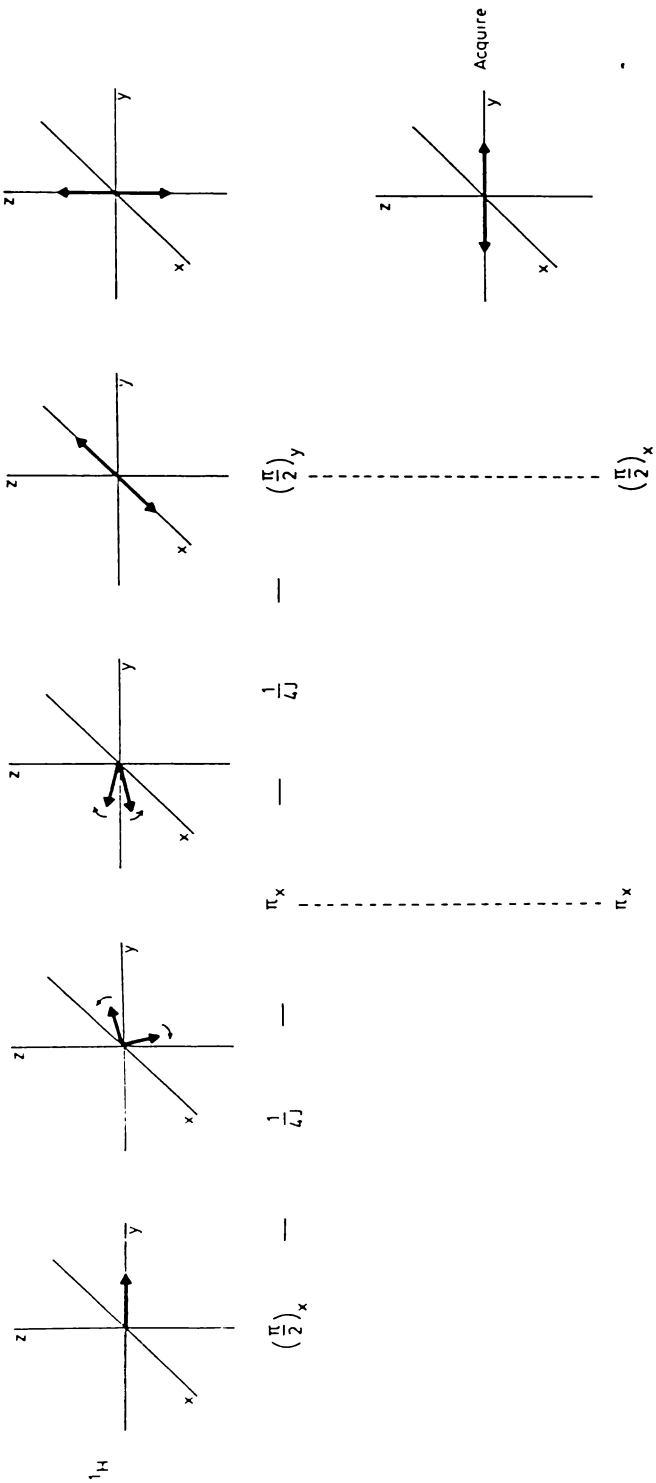

Fig. 4.3 Vector diagram description of the INEPT sequence for an AX system.

the normal binomial splittings in the coupled spectrum. This may sometimes be considered an advantage, but with overlapping signals the inverted INEPT signals often make for easier interpretation. The interpulse times, τ, are 1/2J in the DEPT sequence so that the overall time of this sequence is approximately three times greater than for INEPT. This may count against the former when T_2 relaxation time is short, but the DEPT sequence has the advantage that it is less sensitive to variations of J within the sample. All sequences have the advantage of the shorter relaxation times of the protons assisting in energy removal so that the proton relaxation time is the limiting time not the longer ^{29}Si time. A further advantage of the INEPT sequence is the enhancement provided to the outer lines of the coupled experiment. For example in the standard proton coupled experiment the binomial intensities for a thirteen line spectrum, i.e. the limiting case when x=0 or 4, are 1:12:66:220:495:792:924:792:495:220:66:12:1 while the intensities for the proton coupled INEPT experiment are 1:10:44:110:165:132:0:-132:-165:-110:-44:-10:-1. To see all the lines in the multiplet a S/N ratio of better than 924:1 is required in the normal experiment while a S/N ratio of better than 165:1 is required for the INEPT experiment. This five-fold reduction in the S/N ratio means a saving of twenty-five times the number of scans required in the FT experiment.

These last two factors together reduce the experimental time required to achieve comparable spectra by a factor of about 200 providing a substantial advantage in using the INEPT experiment.

While a number of authors[15][16][17] have presented analytical expressions for attainable enhancements in IS_n spin systems containing a single coupling constant *J(I,S)*, little work has been carried out on systems containing more than one coupling constant.

In earlier work in this Department Watkinson[18] had shown that quite different INEPT spectra are obtained for a sample of $MeGeH_3$ ($^1J_{GeH}$ = 94.3Hz, $^2J_{GeH}$ = 3.5Hz) depending on the timing intervals chosen (see Fig. 4.4). Both spectra gave enhancement but with timing intervals set for the $^1J_{(Ge\text{-}H)}$ coupling an INEPT quartet resulted, with each peak split binomally by the weaker ^2J coupling. With the timings set for the smaller ^2J value the resultant spectra consisted of INEPT splittings from the ^2J coupling with binomial splitting from the ^1J coupling. The latter spectrum had distorted

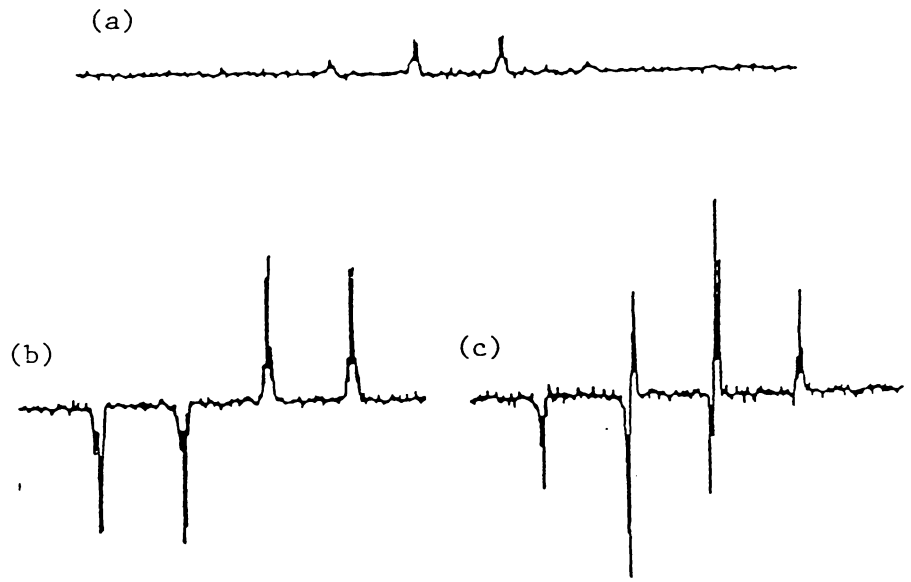

Fig. 4.4 Proton coupled ^{73}Ge NMR spectra of $GeMeH_3$: (a) Standard single pulse experiment, (b) INEPT spectrum with interpulse timing set for the ^1J (GeH) coupling, (c) INEPT spectrum optimised to the ^2J(GeH) coupling. The INEPT spectra collected over 482 scans, 1000Hz windows using 8K data points for (b) and 4K for (c).

peak shapes that might result from a number of causes. A similar experiment was run[19] on a sample of $GeMe_2H_2$. The results are shown in Fig. 4.5. Again the resultant spectra are dependent on the timing intervals. The original authors of the INEPT sequence[12] warn of phase problems when

using long range couplings. The likelihood of misset timing intervals, combined with inaccurate pulses can account for phase distortion within

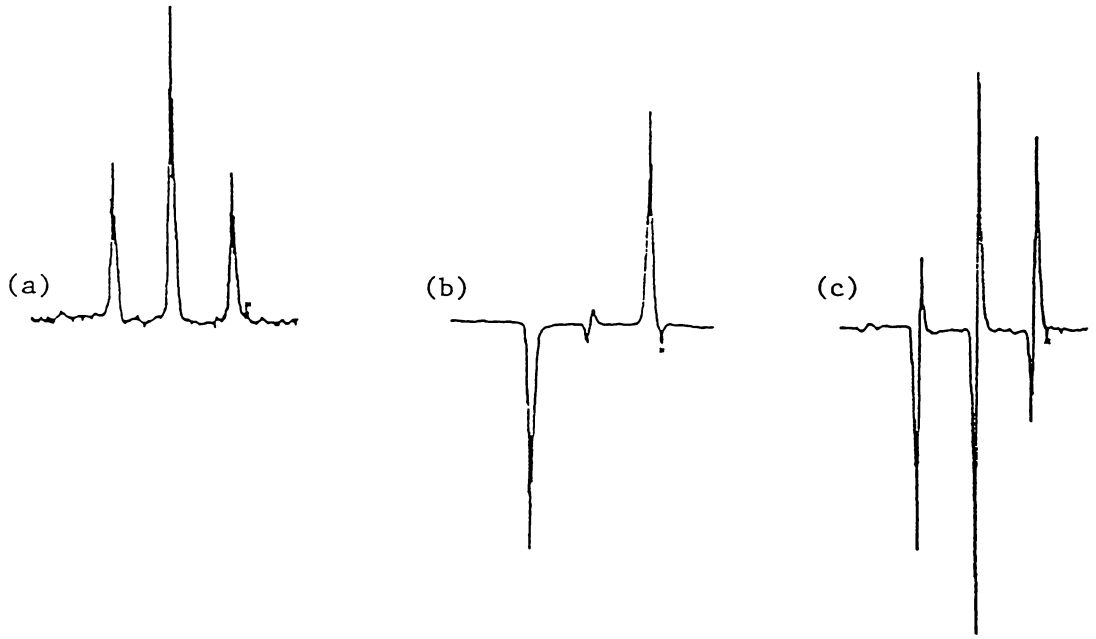

Fig. 4.5 Proton coupled ^{73}Ge NMR spectra of $GeMe_2H_2$: (a) Standard single pulse experiment, (b) INEPT spectrum with interpulse timing set for the ^1J (GeH) coupling, (c) INEPT spectrum optimised to the ^2J(GeH) coupling. All spectra collected over 300 scans using 8K data points over a 3000Hz window.

these spectra. It has also been noted[20] that coupling between the *S* spins can also create difficulties.

While INEPT/binomial combinations were understandable when there was a large difference in J values no obvious answer was apparent in the situation where two couplings of similar value were present within the molecule. In this circumstance the timing intervals would be within the acceptable limits of both couplings. In this situation could we expect a similar spectrum from both an A_3B_9 and an A_9B_3 system, or would they both appear as A_{12} systems?

4.2 Experimental and Results

Relaxation time experiments were run on a sample of $Me_2Si(GeH_3)_2$ using the standard spin echo pulse sequence, to ensure that acceptable interpulse relaxation delays were used when running the INEPT experiments. The resultant observations are listed in Table 4.2. along with other T_1 measurements made on compounds in the series.

Table 4.2. Observed Relaxation Times (in seconds except for Ge that are ms).

	^{29}Si	^{1}H	^{73}Ge
T.M.S.	16.3		
$Me_2Si(GeH_3)_2$	65.3	11.9 (C**H**) 4.4 (Ge**H**)	7.4
$MeSi(GeH_3)_3$	64.7		77.2

These results clearly show the problems that may arise when observing ^{29}Si using the normal single pulse experiment. To avoid signal saturation the long relaxation delays mean a very slow experiment to obtain a reasonable number of scans. The ^{1}H relaxation times mean that scan recycling can occur five to six times faster in the INEPT experiment compared to the single pulse experiment.

With the $^{2}J_{Si\text{-}C\text{-}H}$ known to be 6.59Hz in TMS[21] a coupled INEPT spectrum of T.M.S. was run, on a neat solution, to ensure that the experimental conditions for the INEPT experiment were satisfactory. This spectrum is shown in Fig. 4.6, and shows the expected INEPT thirteen line multiplet.

As a result of this spectrum the conditions used for all further INEPT spectra were set so that 8K data points were collected over a 500Hz window. The resultant acquisition time of 1.92s combined with a relaxation delay of 15s provided a total recycle time of 16.92s. A series of spectra was then run on the compound $Me_2Si(GeH_3)_2$ using J values varying from 9Hz through to 5Hz.

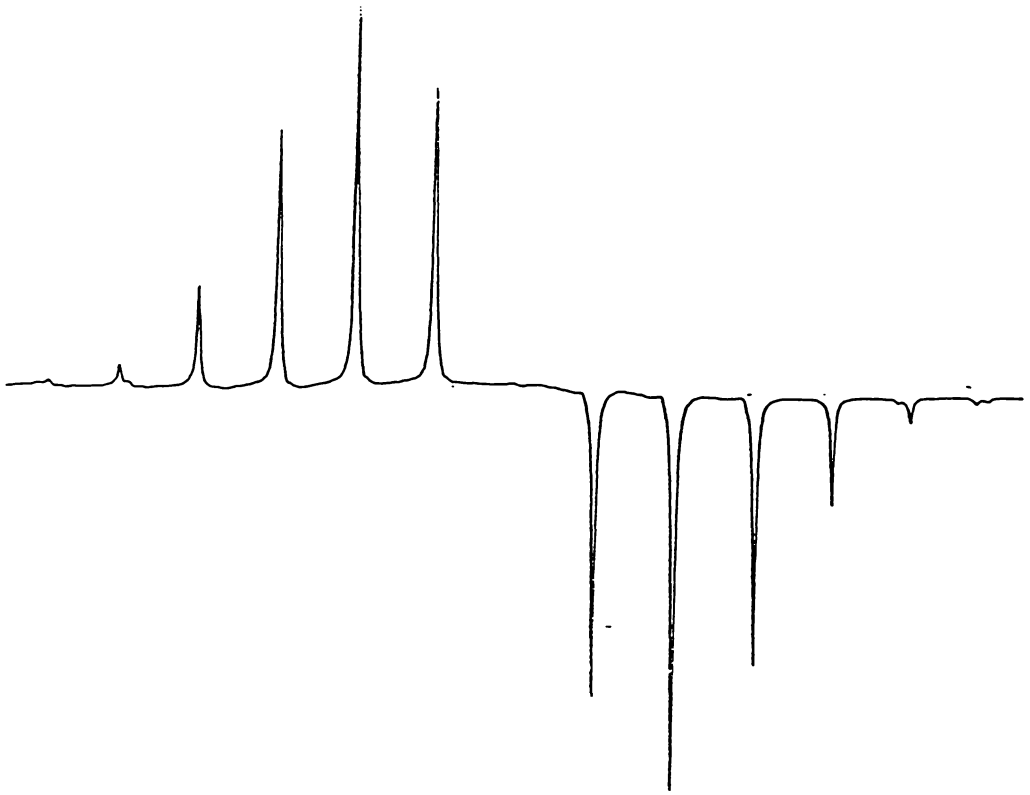

Fig. 4.6 Proton coupled ^{29}Si INEPT spectrum of T.M.S. showing the expected inversion around the centre, and cancellation of the centre line.

(Fig.4.7). 4000 scans were collected on these, and all further, samples resulting in a total experiment time of approximately 20hrs. No difference is apparent in these spectra despite timings covering the expected range of the two ^2J values.

Fig. 4.8 shows the observed spectra for (a) Me_3SiGeH_3 and (b) $MeSi(GeH_3)_3$. Again the spectra remained unchanged over the J value range of 5 to 9Hz. These two spectra indicate a clear difference between the A_3B_9 and A_9B_3 cases.

All spectra show the inversion through the centre expected from an INEPT spectrum, but some peaks of opposite sign are found near the centre.

The two possible ways of deriving these spectra, which are multiplets of multiplets, are

(a) an INEPT splitting from one of the ^2J couplings followed by an INEPT splitting from the second ^2J coupling, and

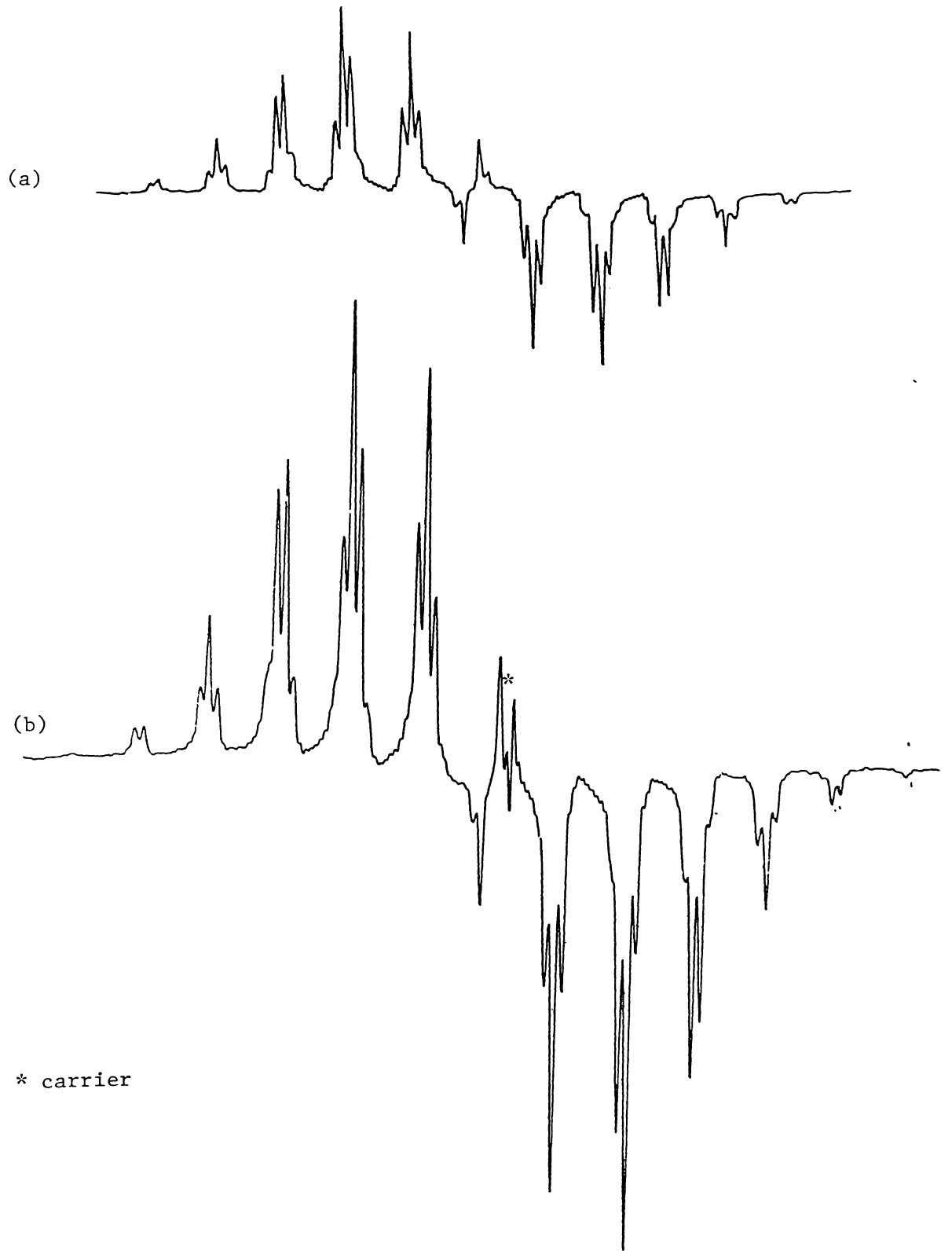

Fig. 4.7 Proton coupled ^{29}Si INEPT spectra of $Me_2Si(GeH_3)_2$ with the interpulse delays set for (a) 9Hz and (b) 5Hz.

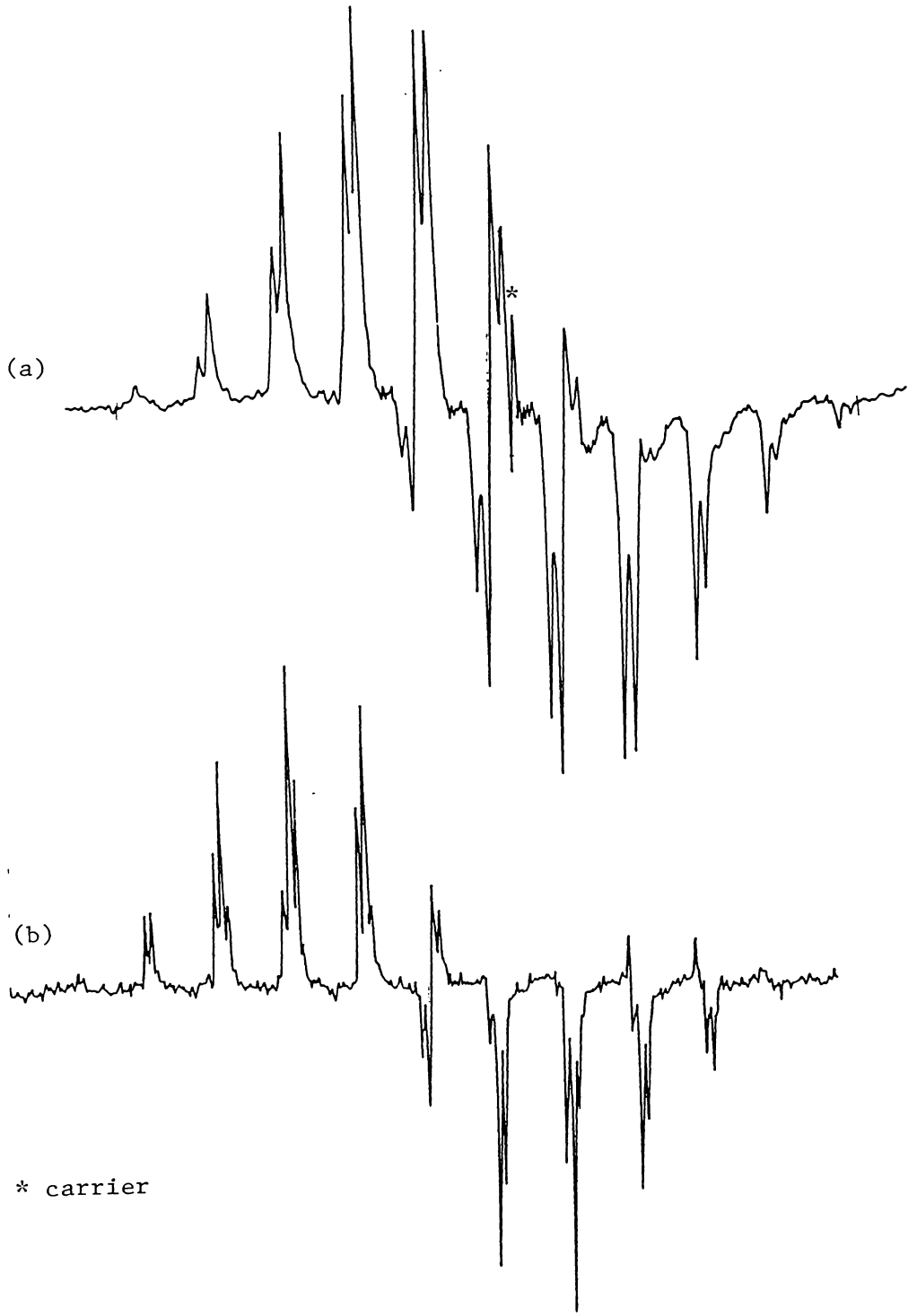

Fig. 4.8 Proton coupled ^{29}Si INEPT spectra of (a) $MeSi(GeH_3)_3$ and (b) $Me_3Si(GeH_3)$.

(b) an INEPT splitting from one ^2J coupling followed by a binomial splitting from the second coupling.

With clusters of peaks occurring approximately 7Hz apart in the spectrum of $MeSi(GeH_3)_3$, and with peaks within the cluster approximately 1Hz apart theoretical spectra were calculated for the A_3B_9 case. The values were initially set at A = 7Hz and B = 8Hz for two reasons:

(a) the two couplings were expected to be of similar magnitude, and

(b) the peaks of opposite sign started 1Hz past the centre of the spectrum.

The calculated INEPT/binomial spectrum provided a close match to the observed spectrum of $MeSi(GeH_3)_3$. A minor change of the B value to 8.25Hz generated the calculated spectrum shown in Fig. 4.9(b), which compares well with the observed spectrum shown in Fig 4.9(a). Fig 4.9(c) shows the calculated spectrum for the INEPT/INEPT splitting case. The large peak intensities near the middle of the spectra are far more apparent in the INEPT/binomial case than in the case of two INEPT splittings. To confirm that the case where A = 8Hz and B = 7Hz was not a possibility these spectra were also calculated (Fig. 4.10). These spectra are clearly different from the observed spectra, with groups of peaks to the left of their inverted nearest neighbours. With the theoretical peak positions now known it was possible to measure the couplings from the observed spectrum. These coupling constants are listed in Table 4.3 along with those of the other compounds in the series.

Calculated spectra for the cases A_6B_6 and A_9B_3 (Figs. 4.11 and 4.12) show that the match with the observed spectra are again best in the INEPT/binomial case. The measured coupling constants appear in Table 4.3. A comparison of calculated peak positions along with their theoretical and observed intensities for the compounds in the series are listed in Tables 4.4, 4.5 and 4.6. Intensities of the two theoretical spectra are calculated so that the total intensities are comparable. Intensities of the sample spectra were measured, and then scaled so that the outer multiplets were of similar

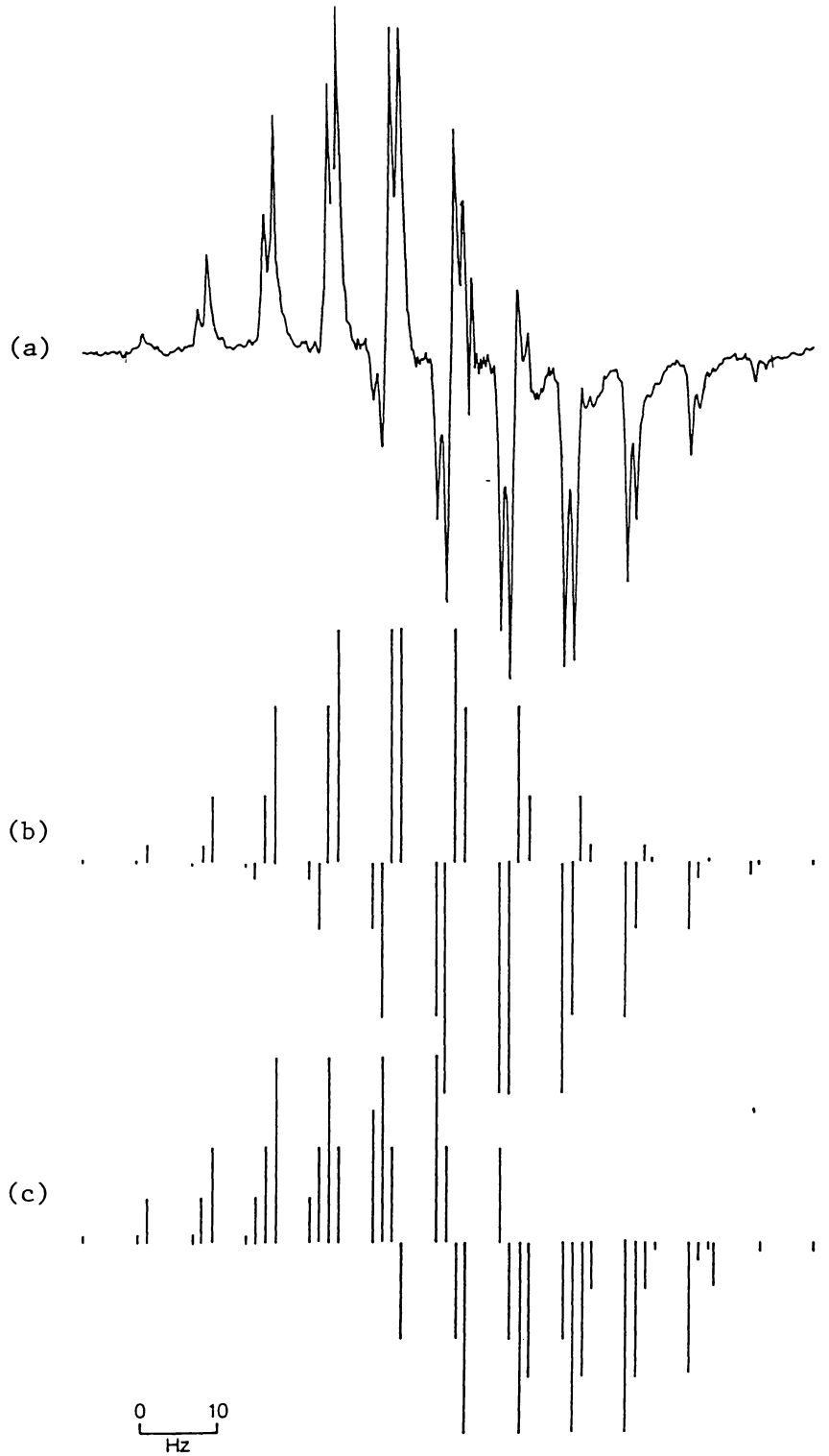

Fig. 4.9 Calculated spectra for an A_3B_9 system along with the observed spectrum of $MeSi(GeH_3)_3$; (a) observed spectrum, (b) calculated spectrum resulting from an INEPT coupling via A followed by a binomial splitting via B, and (c) spectrum resulting from INEPT splittings from both A and B couplings.

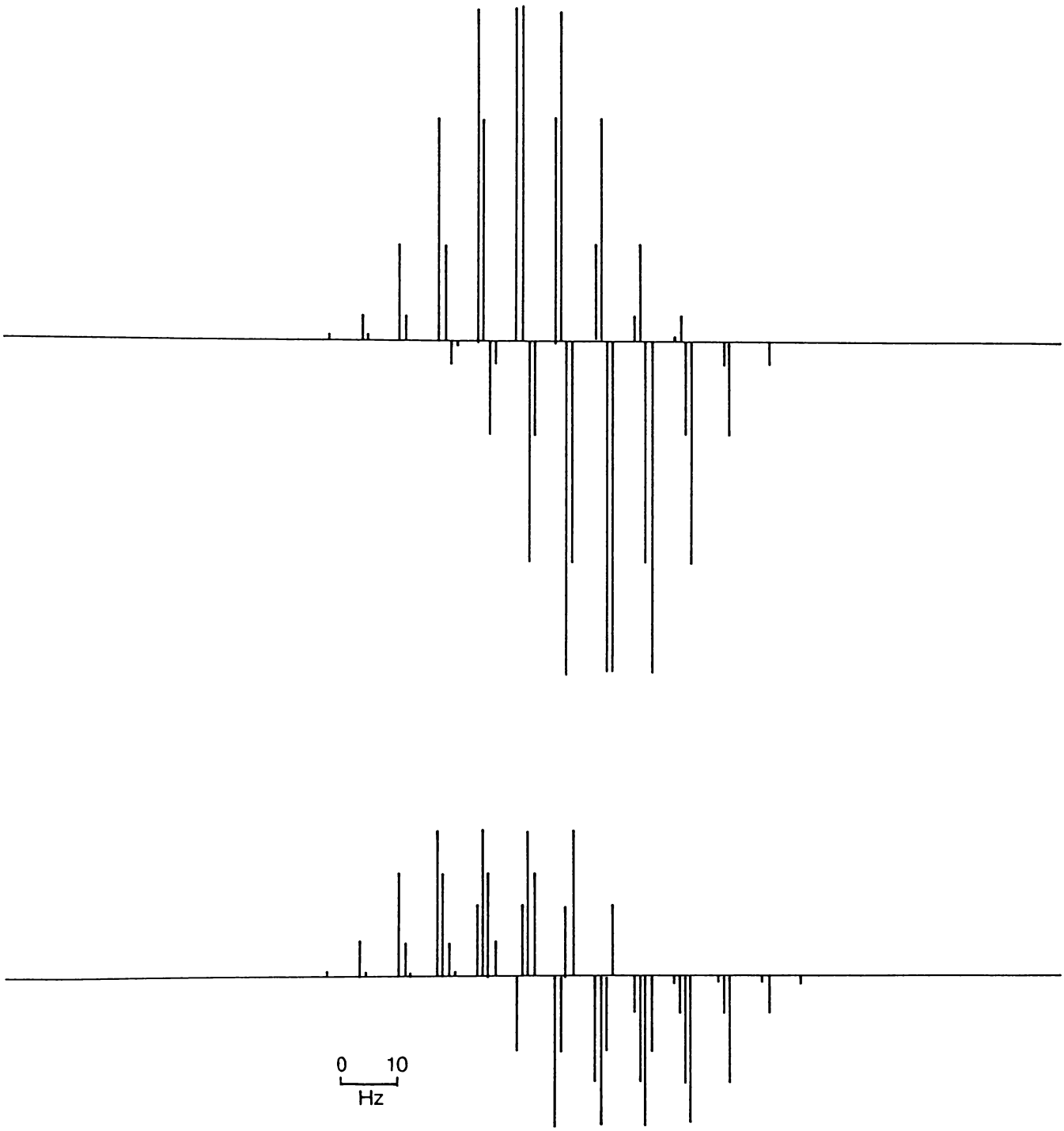

Fig. 4.10 Calculated spectra for an A_3B_9 system, as in Fig. 4.9, but with the couplings A=8Hz and B=7Hz; (a) spectrum resulting from an INEPT coupling via A followed by a binomial splitting via B, and (b) spectrum resulting from INEPT splittings from both A and B couplings.

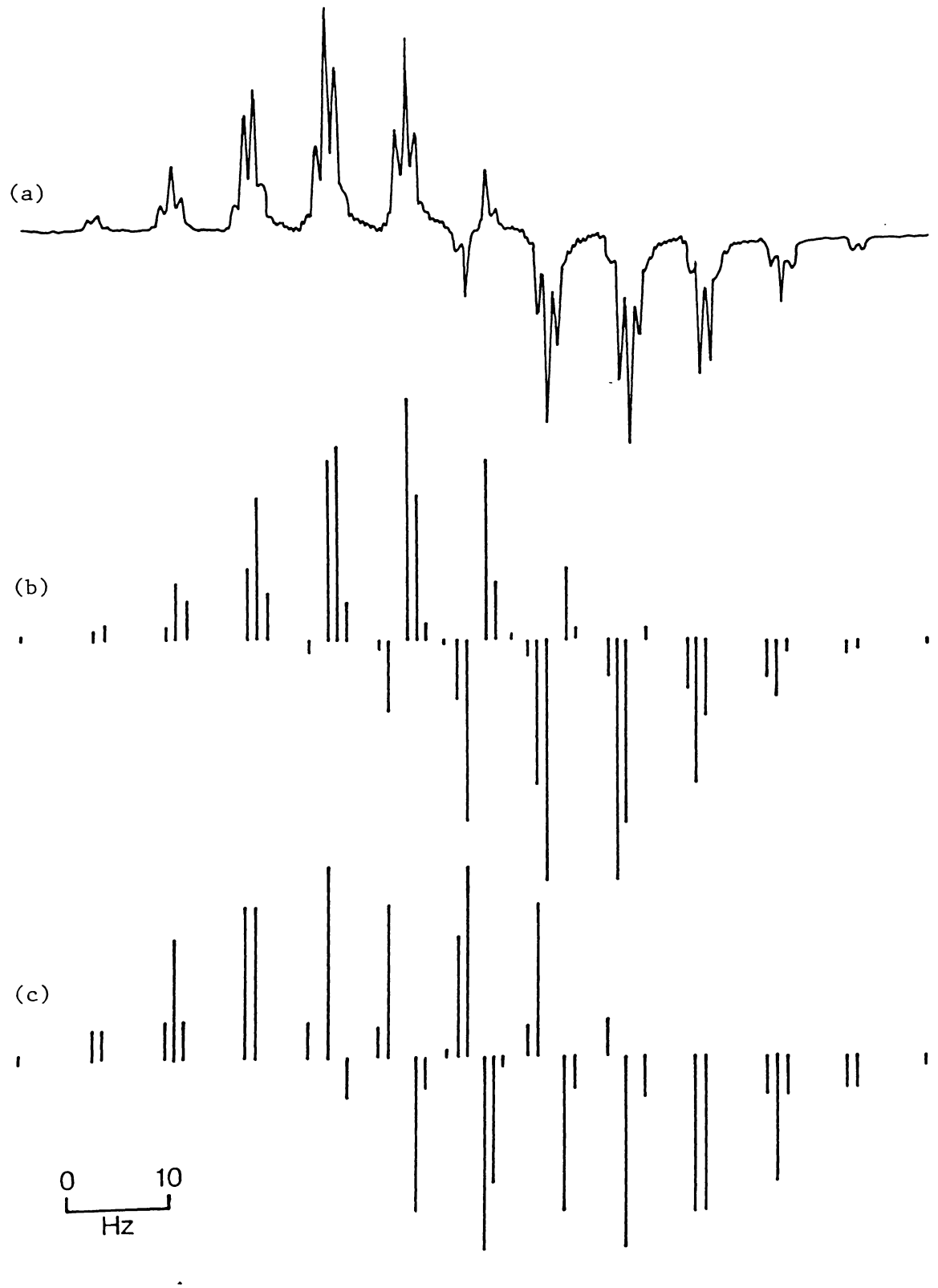

Fig. 4.11 (a) Observed spectrum of $Me_2Si(GeH_3)_2$ along with (b) the calculated spectrum using the INEPT/binomial splitting and (c) the calculated spectrum resulting from an INEPT/INEPT splitting.

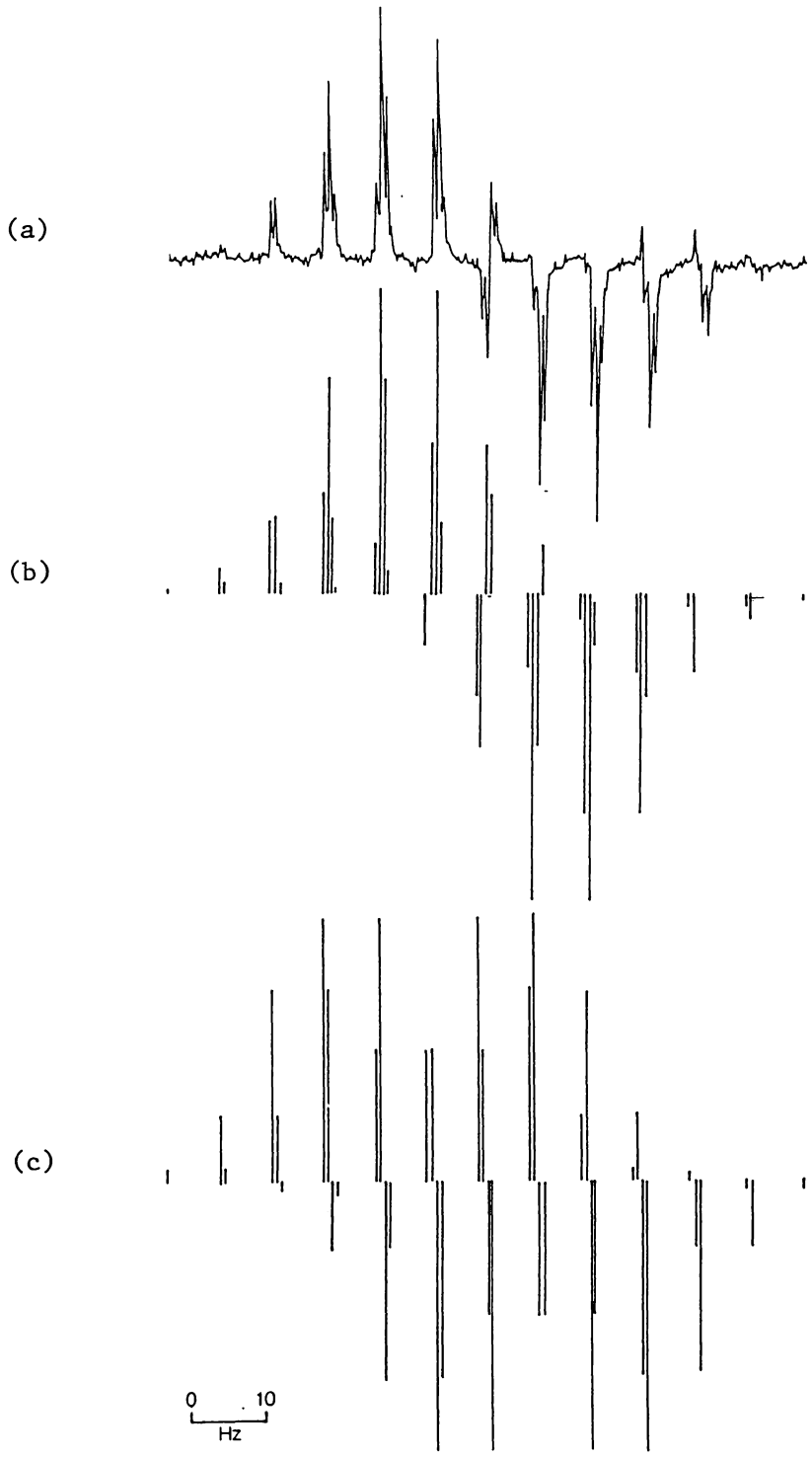

Fig. 4.12 (a) Observed spectrum of $Me_3Si(GeH_3)$ along with (b) the calculated spectrum using the INEPT/binomial splitting and (c) the calculated spectrum resulting from an INEPT/INEPT splitting.

intensity to the INEPT/binomial cases. The error arises from the digital resolution of the observed spectra with data points being 0.12 Hz apart. While this error may arise for one particular peak the overall error in calculated coupling constants amounts to one-seventh this.

Table 4.3 Observed ^2J couplings for the Species $Me_xSi(GeH_3)_{4-x}$ (x=0,1,2,3)

	$^2J_{(Si\text{-}C\text{-}H)}$	$^2J_{(Si\text{-}Ge\text{-}H)}$
$MeSi(GeH_3)_3$	7.00	8.25
$Me_2Si(GeH_3)_2$	7.00	7.95
Me_3SiGeH_3	6.88	7.50
Me_4Si[a]	6.59	-

(a) From ref. 21

4.3 Discussion

Shortly after completing this study Schenker and von Philipsborn published a paper[22] in which they addressed the problem of analysis of INEPT and DEPT spectra for spin systems other than IS_n. Development of computer programs for calculation of density matricies allowed analysis of anything up to six spin systems. They note that ideally the coupling constants should be known, and while they can often be estimated this is a serious restriction for the use of their equations.

More recently Sørenson and Jakobsen[23] have described the analysis of a three spin system using density operators. In this example a ^{15}N INEPT spectrum (see Fig. 4.13) was simulated to determine the one ^2J and two ^3J couplings. The combinations of long-range coupling constants used are listed in Table 4.7.

Table 4.4 Calculated and Observed Peak Intensities for $MeSi(GeH_3)_3$ Using the Calculated Coupling Constants of 7 and 8.25Hz.

Peak Position (in Hz from Centre)	INEPT/ binomial	INEPT/ INEPT	Observed
47.63	1	3.7	n.o.
40.63	1	3.7	4
39.38	9	25.6	10
33.62	-1	3.7	n.o.
32.38	9	25.6	18
31.13	36	73.1	43
26.66	-1	3.7	n.o.
25.37	-9	25.6	n.o.
24.13	36	73.1	18
22.88	84	102.4	43
18.38	-9	25.6	n.o.
17.12	-36	73.1	n.o.
15.88	84	102.4	62
14.63	126	51.2	88
10.13	-36	73.1	-20
8.87	-84	102.4	-30
7.63	126	51.2	124
6.38	126	-51.2	115
1.88	-84	102.4	-72
0.62	-126	51.2	-93
-0.62	126	-51.2	94
-1.88	84	-102.4	73
-6.38	-126	51.2	-130
-7.63	-126	-51.2	-114
-8.87	84	-102.4	33
-10.13	36	-73.1	5
-14.63	-126	-51.2	-128
-15.88	-84	-102.4	-107
-17.12	36	-73.1	n.o.
-18.38	9	-25.6	n.o.
-22.88	-84	-102.4	-89
-24.13	-36	-73.1	-59
-25.37	9	-25.6	n.o.
-26.63	1	-3.7	n.o.
-31.13	-36	-73.1	-39
-32.38	-9	-25.6	-19
-33.62	1	-3.7	n.o.
-39.38	-9	-25.6	-8
-40.63	-1	-3.7	-3
-47.63	-1	-3.7	n.o.

Table 4.5 Calculated and Observed Peak Intensities for Me_3SiGeH_3 Using the Calculated Coupling Constants of 6.88Hz and &.50Hz.

Peak Position (in Hz from Centre)	INEPT/ binomial	INEPT/ INEPT	Observed
42.21	1	2.7	n.o.
35.33	7	18.6	n.o
34.71	3	2.7	n.o.
28.45	20	53.1	22
27.83	21	18.6	16
27.21	3	-2.7	12
21.57	28	74.3	38
20.95	60	53.1	52
20.33	21	-18.6	16
19.77	1	-2.7	n.o.
14.69	14	37.2	30
14.07	84	74.3	78
13.45	60	-53.1	44
12.83	7	-18.6	n.o.
7.81	-14	37.2	12
7.19	42	37.2	45
6.57	84	-74.3	65
5.95	20	-53.1	17
0.93	-28	74.3	-21
0.31	-42	37.2	-29
-0.31	42	-37.2	25
-0.93	28	-74.3	14
-5.95	-20	53.1	-20
-6.57	-84	74.3	-71
-7.19	-42	-37.2	-48
-7.81	14	-37.2	-16
-12.83	-7	18.6	n.o.
-13.45	-60	53.1	-49
-14.07	-84	-74.3	-84
-14.69	-14	-37.2	-19
-19.77	-1	2.7	n.o.
-20.33	-21	18.6	-18
-20.95	-60	-53.1	-54
-21.57	-28	-74.3	-36
-27.21	-3	2.7	-15
-27.83	-21	-18.6	-23
-28.45	-20	-53.1	-19
-34.71	-3	-2.7	n.o.
-35.33	-7	-18.6	n.o.
-42.21	-1	-2.7	n.o.

Table 4.6 Calculated and Observed Peak Intensities for $Me_2Si(GeH_3)_2$ Using the Calculated Coupling Constants of 7Hz and 7.95Hz.

Peak Position (in Hz from Centre)	INEPT/ binomial	INEPT/ INEPT	Observed
44.85	1	3.2	n.o.
37.85	4	12.8	5
36.90	6	12.8	5
30.85	5	16	12
29.90	24	51.2	24
28.95	15	16	11
22.90	30	64	46
21.95	60	64	50
21.00	20	0	12
16.85	-5	16	37
14.95	75	80	92
14.00	80	0	65
13.05	15	-16	8
9.85	-4	12.8	n.o.
8.90	-30	64	30
7.00	100	0	56
6.05	60	-64	26
5.10	6	-12.8	n.o.
2.85	-1	3.2	n.o.
1.90	-24	51.2	-16
0.95	-75	80	-26
-0.95	75	-80	21
-1.90	24	-51.2	4
-2.85	1	-3.2	n.o.
-5.10	-6	12.8	n.o.
-6.05	-60	64	-40
-7.00	-100	0	-75
-8.90	-30	-64	-39
-9.85	4	-12.8	n.o.
-13.05	-15	16	-20
-14.00	-80	0	-64
-14.95	-75	-80	-77
-16.85	5	-16	-31
-21.00	-20	0	-20
-21.95	-60	-64	-55
-22.90	-30	-64	-44
-28.95	-15	-16	-18
-29.90	-24	-51.2	-25
-30.85	-5	16	-9
-36.90	-6	-12.8	-6
-37.85	-4	-12.8	-4
-44.85	-1	-3.2	n.o.

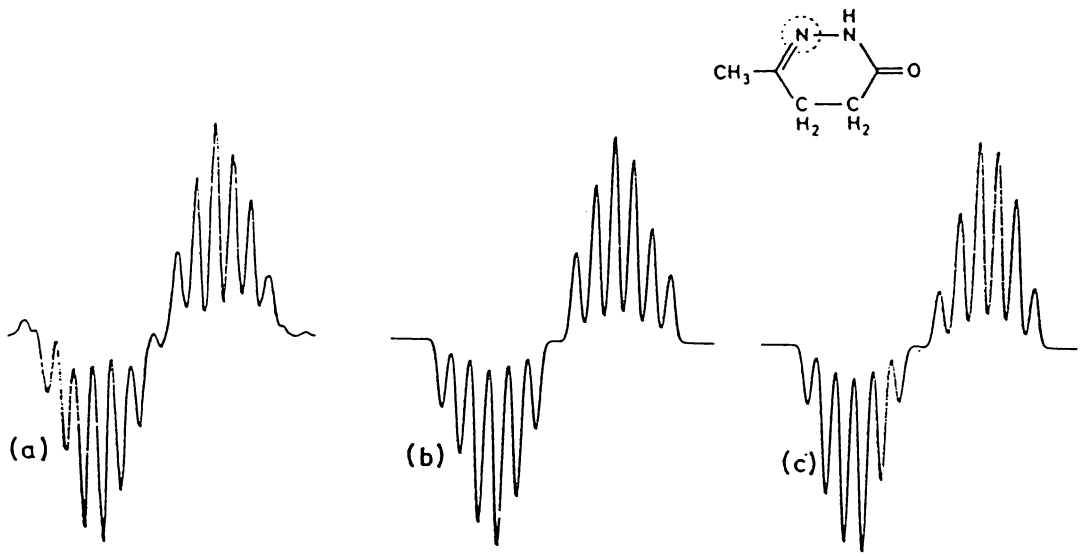

Fig. 4.13 ^{15}N proton-coupled INEPT spectra of of the nonprotonated nitrogen atom in the cyclic hydrazide shown (from ref 23). (a) Experimental spectrum with the timings set for J= 12.5Hz. (b,c) simulated INEPT spectra obtained from density operator calculations using the combinations of coupling constants given in Table 4.~~13~~.7

Table 4.7 Coupling Constants used in INEPT spectra simulation (Fig. 4.13).

Figure	$^2J(^{15}N\text{-}H)$	$^3J(^{15}N\text{-}CH_2)$	$^3J(^{15}N\text{-}CH_3)$
4.13b	7.95Hz	1.91Hz	3.88Hz
4.13c	9.89Hz	3.83Hz	1.97Hz

Use of a stick diagram, such as that used in this work, was able to generate a reasonable fit to the observed spectra when an INEPT/binomial/ binomial combination was used for the $^2J/^3J/^3J$ couplings (see Fig. 4.14). It should be noted that the calculated stick spectra used the J values determined by the authors which they say "apparently represents the correct choice".

Minor changes in the values used would lead to a better cancellation of the opposing peaks.

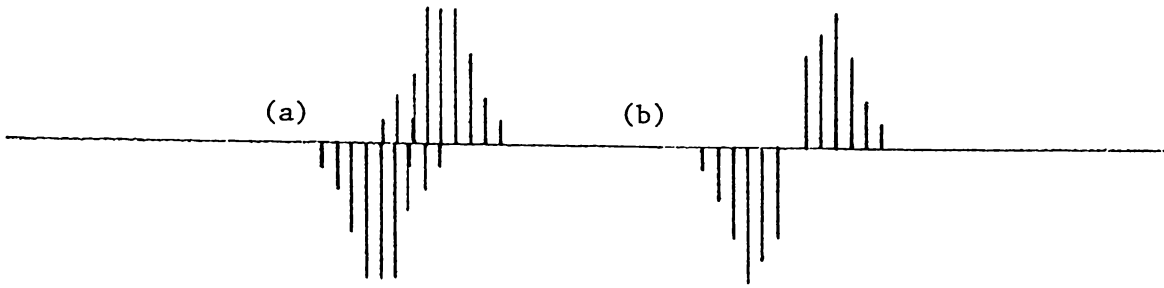

Fig. 4.14 Theoretical spectra calculated using the coupling constants from Table 4.7 for Fig. 13(b); (a) Theoretical spectrum obtained assuming an INEPT ^2J coupling, followed by binomial splitting from each of the two ^3J couplings, and (b) the spectrum obtained from (a) assuming cancellation of opposing peaks when they are within normal linewidth.

This work shows that the relatively simplistic approach used allows for analysis of INEPT spectra without the use of specialised computer programs.

The majority of studies of the $^2J_{(Si\text{-}M\text{-}H)}$ couplings are for situations where M=C, in the methyl-silicon fragment. A parallel behaviour between $^2J_{(Si\text{-}M\text{-}H)}$ and $^1J_{(SiH)}$ indicates that not only are variations in the electronic distribution around the silicon and hydrogen atoms important but also those occurring around the carbon atom in a sense that $^2J_{(Si\text{-}M\text{-}H)}$ increases with the *s* orbital contribution on the silicon as well as on the carbon atom. Other interpretations have involved changes in the bond angles or π bonding. There appears to be no published data of ^2J couplings where germanium is the intervening atom.

The increase in both the ^2J values, with increase in the number of GeH_3 groups, in the series studied is perhaps surprising but without more similar compounds to compare it with it is difficult to define the result as anomalous.

Chapter Four References

1. W.A.Dutton and M.Onyszchuk, *Inorganic Chem.*, **7**, *35*, 1968.
2. S.P.Foster, K-F Leung, K.M.Mackay, and R.A.Thomson, *Aust. J. Chem.*, **39**, *1089*, 1986.
3. Kin-Fai Leung, M.Sc thesis, U. of Waikato, 1985.
4. T.A.Blinka, B.J.Helmer, and R.West, *Advances in Organometallic Chem.*,Vol 23, Academic Press, 1984.
5. S.Li, J.A.Gladysz, and K.L.Servis, *J. Organom. Chem.*, **166**, *317*, 1979.
6. M.Grignon-Dubois, M.Laguerre, B.Barbe, and M.Petraud, *Organometallics*, **3**, *359*, 1984.
7. G.Déléris, M.Birot, J.Dunoguès, B.Barbe, M.Petraud, and M.Lefort, *J. Organom. Chem.*, **266**, *1*, 1984.
8. J.Schraml, *J. Mag. Reson.*, **59**, *515*, 1984.
9. M.Grignon-Dubois, M.Laguerre, B.Barbe, and M.Petraud, *Organometallics*, **3**, *1061*, 1984.
10. M.Grignon-Dubois and M.Laguerre, *Organometallics*, **7**, *1443*, 1988.
11. M.Grignon-Dubois, M.Ahra, M.Laguerre, B.Barbe and M.Petraud *Spectrochimica Acta*, **45A**, *911*, 1989.
12. G.A.Morris and R.Freeman, *J.Am.Chem. Soc.*, **101**, *760*, 1979.
13. D.M.Doddrell, D.T.Pegg, and M.R.Bendall, *J.Magn. Reson.*, **48**, *323*, 1982.
14. D.T.Pegg, D.M.Doddrell, and M.R.Bendall, *J. Chem. Phys.*, **77**, *2745*, 1982.
15. D.P.Burum and R.R.Ernst, *J. Magn. Reson.*, **39**, *163*, 1980.
16. D.T.Pegg, D.M.Doddrell, W.M.Brooks and M.R.Bendall, *J.Magn. Reson.*, **44**, *32*, 1981.
17. M.R.Bendall and D.T.Pegg, *J.Magn., Reson.*, **53**, *272*, 1983.
18. K.M.Mackay, P.J.Watkinson, and A.L.Wilkins, *J. Chem. Soc. Dalton Trans.*, *133*, 1984.
19. P.J.Watkinson, D.Phil. Thesis, U of Waikato, 1984.

20. M.R.Bendall, D.M.Doddrell, W.E.Hull, and D.T.Begg, 'Application Note on D.E.P.T.', Bruker, Analytische Messtechnik, Karlsruhe, 1982.

21. R.West, F.A.Kramer, E.Carberry, M.Kumada, and M.Ishikawa, *J. Organonetallic Chem.*, **8**, *79*, 1967.

22. K.V.Schenker and W. von Philipsborn, *J. Mag. Reson.*, 61, *294,* 1985.

23. O.W.Søresen and H.J.Jakobsen in '*Pulse Methods in 1D and 2D Liquid-Phase NMR (W.Brey Ed.)*', Academic Press, San Diego, 1988.

Chapter 5 Boron Trihalide Adducts

5.1 Introduction

Tervalent boron compounds act as Lewis acids, and a wide variety of complexes are obtained when they are reacted with suitable Lewis bases[1]. While other techniques have proved inadequate for the study of these systems NMR spectroscopy has proved extremely useful[2]. Vibrational spectroscopy has been useful in studying halogen redistribution in the uncomplexed boron trihalides[3X4] but the mixed halogen adducts have lower symmetry and give complex spectra, complicated by overlapping ligand absorptions[5]. Mass spectroscopy techniques are only of use if the donor-acceptor bond is strong enough to remain intact when the sample is ionised. Multinuclear NMR allows study not only of the boron nucleus, but also of appropriate adduct nuclei, e.g. phosphorus, nitrogen. In particular, the technique allows ready examination of the strength of the boron-donor bond[2].

Nöth and Wrackmeyer[2] showed that comparison across a full range of boron-donor complexes is complicated by a number of effects, e.g. steric and π-bonding effects, but found that reasonable comparisons of Lewis acid strengths can be made within limited subgroups. One such grouping is the boron trihalides.

5.1.1 Exchange among the free trihalides

Mixtures of boron trihalides rapidly equilibrate to generate a statistical mix of the full range of mixed trihalides, e.g $BBrCl_2$ and BBr_2Cl, when BCl_3 and BBr_3 are mixed. The ^{11}B chemical shifts of the trihalides are listed in Table 5.1. In their summary of these results Nöth and Wrackmeyer[2] note the divergence of chemical shifts, especially of the mixed trihalides, reported by various groups despite the relatively sharp lines of these signals ($\upsilon_{1/2}$= 3Hz). They suggest that this discrepancy may result from;

(a) incorrect adjustments for different reference compounds used,

(b) the varying concentrations of the starting trihalides, resulting in a different equilibrium point in each case, and that the remaining pure trihalide may possibly affect the boron chemical shift.

Table 5.1 ^{11}B Chemical Shifts[a,b] of Trihalogenboranes. (Cl, Br, I)

BCl_3	41.9-48.0	BClBrI	31.3-31.6
BCl_2Br	44.2-45.8	BBr_2I	26.3-26.5
$BClBr_2$	41.9-44.1	$BClI_2$	17.8-18.1
BBr_3	38.5-44.0	$BBrI_2$	10.3-12.2
BCl_2I	35.4-36.1	BI_3	-5.5- -8.0

(a) This Table lists the range of chemical shifts noted in ref. 2 and references therein.

(b) The narrow ranges generally reflect fewer studies, rather than higher reproducibility.

5.1.2 Mixed halide adducts and halogen exchange in adducts

While this halogen exchange is too rapid to allow the mixed halides to be separated, the adduct of an individual mixed halide may be isolated when a strong adduct bond is formed. Adducts have been formed with a wide range of donors including ethers, amines, dimethylsulfide, phosphines, esters, ureas, ketones, and halides[1]. The latter is a special case where donation of a fourth halide ion generates the tetrahaloborate anion.

Hartmann and Miller[3] have reviewed work carried out with the mixed boron trihalide adducts covering the period up to 1976, while Nöth and Wrackmeyer's book[2] covered the broader field of ^{11}B NMR up to 1977. Hartmann and Miller[3] concluded that *'the mixed boron trihalide adducts hold few surprises in terms of their donor-acceptor behaviour'* but suggest that because of the lack of complicated side reactions the systems are ideal

for studying ligand exchange reactions. Despite this enthusiastic conclusion, and the suggestion that with multinuclear NMR becoming more accessible these systems are open for much more study, little further work has been reported on the trihalide systems.

In the time since the review Miller[6] has carried out a ^{15}N and ^{11}B NMR study of the trimethylamine adducts, Drake and co-workers[7] have studied arsine adducts, and Foret, Korzekwa, and Martin[8] have looked at the 2-substituted pyridine-tribromoborane adducts. Wrackmeyer[9] has used the INEPT pulse sequence to obtain ^{15}N chemical shifts and $^{1}J(^{15}N\text{-}^{11}B)$ data in the amine-borane trihalides, while Minkwitz and Nass[10] have reported the mixed fluorine, chlorine adducts where the donor is $(CH_3)_2NCl$.

All studies have reflected the observation that, within the set of trihalides, the Lewis acid strength increases with the change of halide: fluorine < chlorine < bromine < iodine. This order is the opposite to that which might be expected from the relative electronegativities of the halogens, but was rationalised as resulting from increasing halogen-boron π bonding on going from BI_3 to BF_3. This increase in π bonding would increase the energy required to convert BX_3 from planar to pyramidal configuration and, by returning electron density to B, would decrease the ability of the Lewis ~~acid~~ base to transfer electron density to the boron atom. Recent calculation of the ionisation potentials for the trihalides, from gas-phase X-ray photoelectron spectra[11] has provided experimental evidence for this previously proposed trend in π bonding.

The halogen exchange among the free trihalides is still slow enough to give a sharp peak in the ^{11}B NMR spectrum for each component of a mixture. In mixtures of boron trihalides, redistribution of the halogens is thought to occur via a bridged transition state making use of the formally

unoccupied boron valence shell p_z orbital*. This bridging state can occur with a relatively low activation energy[9].

Addition of a Lewis base D to these mixtures will generate a full range of adducts e.g. $D.BCl_{3-n}Br_n$ (n=0-3). Halogen rearrangement is rapid in ether adducts but is slow when adducts of a stronger base are involved, and occurs only when excess boron trihalide is present[2]. The low energy pathway via p_z orbitals is not available for the coordinatively saturated four coordinate boron compounds. Three possible mechanisms have been proposed for the halogen redistribution in such adducts.

1. Dissociation of the halide ions.

The reaction

$$D.BX_3 \rightleftharpoons D.BX_2^+ + X^- \qquad \text{.....(5.1)}$$

while occuring in the tetrahaloborates has not been unambiguously established as a pathway for neutral adducts.

2. Dissociation of the donor-acceptor bond

The reaction

$$D.BX_3 \rightleftharpoons D + BX_3 \qquad \text{.....(5.2)}$$

followed by halogen exchange of the trihalides, is thought to be the rate determining step in many adducts of weak donors.

---

* This orbital is used in B-X π bonding but is still accessible after a relatively small loss of bonding

3. Associated bridging mechanism

The reaction of an adduct with free boron trihalide has, as a proposed first step, a species with a single halogen bridge which could then

$$D.BX_3 + BY_3 \rightleftharpoons D.BX_2X \rightarrow BY_3 \qquad .....(5.3)$$

proceed via a four centre transition state, or an ion pair, to a final dissociation giving a mixed halogen species.

This chapter reports on a study of the halogen exchange in the boron trihalide adducts of triphenylphosphine. This is classified as a 'soft' donor, so that in the adducts, some donor bond breaking might be expected to occur and halogen scrambling might occur via either mechanism 2 or 3 described above. As a result of observations made within these systems the study was extended to include the adducts formed by other representative Lewis bases containing Group 15 atoms, i.e. Ph_3As, Me_3N and Et_3N. Table 5.2 lists the ^{11}B and ^{31}P chemical shifts, and coupling constants, of the compounds in this group, so far reported[(2)(6)(12)].

5.2 Experimental

5.2.1 NMR Techniques

As with other boron NMR studies of halide adducts, ^{11}B was the isotope observed in this work. Both NMR-active isotopes of boron, ^{10}B and ^{11}B, have a magnetic moment I >1/2 which results in line broadening that often hides any fine structure in the spectra. The lower spin of ^{11}B ($^3/_2$), along with its higher resonance frequency, lower quadrupolar moment and greater receptivity, make this isotope the one most generally observed in boron studies. All ^{11}B NMR spectra were run on a JEOL FX90Q operating at 28.75MHz in the Fourier Transform mode. A 90° tip angle (21μs) was used, with a repetition rate of 1.5 sec. 8K data points were used with a 5000Hz window giving a resolution of ±1.2Hz. The spectra are referenced to external

$Et_2O.BF_3$ with an error of ±0.5ppm. Coupling constants are quoted with an error of ±1.2Hz.

Table 5.2. Chemical Shifts and Coupling Constants of Trihalogenoborane Adducts of the Lewis bases PPh_3, Ph_3As, Me_3N, and Et_3N.[a)b)]

(a) PPh_3 Adducts

Adduct	δ ^{11}B	δ ^{31}P	J(^{31}P-^{11}B) (Hz)
$PPh_3.BF_3$	0.4-2.5		165
$PPh_3.BCl_3$	3.8-4.2	-1.7	131, 154, 157
$PPh_3.BCl_2Br$	-1.0		154
$PPh_3.BClBr_2$	-7.0		151
$PPh_3.BBr_3$	-14.0 - -14.4	-5.3	147

(b) Amine Adducts

Adduct	$\delta^{11}B$	$\delta^{15}N$	J(^{15}N-^{11}B) (Hz)
$Me_3N.BF_3$	-0.2 - 0.8, 0.6*	-342.0	-18.7
$Me_3N.BF_2Cl$	4.5 - 5.2, 5.2*	-338.0	-18.6
$Me_3N.BF_2Br$	4.4*	-340.4	-18.5
$Me_3N.BFCl_2$	6.5 - 8.3, 8.2*	-335.9	-17.5
$Me_3N.BFBr_2$	3.7*	-339.1	-17.4
$Me_3N.BCl_3$	9.4-10.5, 10.2*	-334.0	-16.5
$Me_3N.BCl_2Br$	5.8, 6.7*	-334.6	-16.1
$Me_3N.BClBr_2$	1.3, 2.2*	-335.6	-15.7
$Me_3N.BCl_2I$	-3.2*	-336.0	-15.4
$Me_3N.BBr_3$	-3.1 - -3.9, -3.3*	-337.0	-15.2
$Me_3N.BClBrI$	-9.8*	-336.7	-14.7
$Me_3N.BBr_2I$	-17.0*	-339.8	-14.3
$Me_3N.BFI_2$	-19.0*	-346.5	-14.3
$Me_3N.BClI_2$	-24.8*	-340.7	-13.9
$Me_3N.BBrI_2$	-33.9*	-343.4	-13.2
$Me_3N.BI_3$	-54.0 - -54.4, -54.2*	-347.8	-12.1

	$\delta^{11}B$		$\delta^{11}B$
$Et_3N.BF_3$	0.0 - 0.2	$Et_3N.BBr_3$	-5.1
$Et_3N.BCl_3$	10.0	$Et_3N.BI_3$	-59.8

cont...

Table 5.2.(cont.) Chemical Shifts and Coupling Constants of Trihalogenoborane Adducts of the Lewis bases PPh_3, Ph_3As, Me_3N, and Et_3N.[a)(b)]

	$\delta^{11}B$		$\delta^{11}B$
(c) Ph_3As Adducts			
$Ph_3As.BF_3$	2.8	$Ph_3As.BClBr_2$	-7.6
$Ph_3As.BCl_3$	5.3	$Ph_3As.BBr_3$	-15.4 - 15.9
$Ph_3As.BCl_2Br$	-0.7		

(a) All ^{11}B shifts from ref. 2 except those marked with an asterisk which are from ref. 6

(b) ^{31}P shifts from ref. 12, ^{15}N shifts from ref. 6.

The number of scans collected varied depending on the reaction being followed. For fast reactions enough scans to obtain a S/N ratio of 2:1 for the largest peaks were used, especially in the early stages of the reaction, to minimise time averaging of the observed signals. The minimum time used to collect this signal was thirty seconds (15 scans), but in general the signal was collected for two minutes (60 scans). The time mentioned in the reaction runs is the time at the end of data accumulation in each case.

Because of the varied number of scans collected, often within one experiment, it is difficult to compare directly the intensities of a particular peak throughout the run. In describing the reaction runs it is therefore assumed that the total adduct signal intensity remains the same throughout the experiment, as the Lewis base was the limiting reagent and all adducts remained in solution. At any one time the adduct signals are described as a percentage of all adduct signals present in the sample. Calculation of signal area was by the "cut and weigh" method. The error is estimated as ±3%. For the free trihalides, whenever individual signals were observable, no change in the ratio of the intensities was apparent during the experiments.

The ^{31}P spectra were run on either a JEOL FX90Q spectrometer at 36.27MHz or a Bruker AM400 at 162MHz. Because of the inherently better sensitivity of ^{11}B compared with ^{31}P (1:0.4) the reactions were followed using ^{11}B NMR but ^{31}P NMR was used to confirm coupling constants in the adducts and as a check for any other phosphorus-containing compounds in the systems. The ^{31}P spectra are referenced to external 85% H_3PO_4.

5.2.2 Preparation of Ph_3P adducts

Aldrich BBr_3, and BCl_3 (10% in CH_2Cl_2) were used without further purification. Fluka BI_3 was recrystallised from pentane[13].

$Ph_3P.BBr_3$:- 0.35g (13mmol) of Ph_3P, dissolved in 7.5ml of pentane and 1.5ml of benzene, was added to a solution of 0.25g (10mmol) of BBr_3 in 5ml of dry pentane. The adduct formed as colourless needles which were collected and washed with pentane. Yield 0.35g (7mmol)(70%).

$Ph_3P.BI_3$ was similarly prepared by adding a solution of 10mmol Ph_3P to 10mmol BI_3 in pentane. Yellow needles were formed and washed with pentane. Yield 0.5g (7.6mmol)(75%).

$Ph_3P.BCl_3$ was prepared in a Schlenk tube, under N_2 by adding BCl_3 in CH_2Cl_2 dropwise to a solution of Ph_3P in benzene. Colourless needles were formed. The solvent was pumped off and the product washed three times with pentane, the solvent being pumped off each time.

The identity of the $Ph_3P.BX_3$ products was established by IR and Raman spectroscopy prior to the NMR study[14].

5.3 Results

5.3.1 PPh_3 adducts of the Trihalides

The adducts, prepared as described above, were dissolved in CH_2Cl_2 and the ^{11}B and ^{31}P NMR spectra obtained. The results are listed in Table 5.3. The ^{11}B results compare well with the literature values previously obtained for $PPh_3.BCl_3$ and $PPh_3.BBr_3$. The new result, for $PPh_3.BI_3$, shows a very similar range of ^{11}B shifts for the PPh_3 adducts as that reported[2] for $Et_3N.BX_3$. The ^{31}P shift and ^{11}B-^{31}P coupling constant continues the trend in chemical shift, and coupling constant, apparent in the $PPh_3.BCl_{3-n}Br_n$ systems.

Table 5.3 Observed ^{11}B and ^{31}P Chemical Shifts and ^1J Coupling Constants.

Adduct	$\delta^{11}B$	$\delta^{31}P$	$J(^{11}B$-$^{31}P)$ (Hz)
$PPh_3.BCl_3$	3.9	-1.3	154
$PPh_3.BBr_3$	-14.7	-4.8	147
$PPh_3.BI_3$	-72.2	-15.5	124

5.3.2 Mixed Trihalide Reactions

To investigate the mixed halide adduct species, a number of reactions were carried out where the free trihalides were mixed, allowed to equilibrate, and then a deficit of PPh_3 was added to the mixture. These reactions are described below.

5.3.2.1 BCl_3 and BBr_3

Equimolar samples of BCl_3 and BBr_3 were mixed and allowed to equilibrate for thirty minutes. Four peaks, in the ratio 1:3:3:1, were observed in the ^{11}B spectrum at 46.6, 45.2, 42.8, and 39.0 ppm. These are assigned as the previously observed[2] peaks for BCl_3, BCl_2Br, $BClBr_2$, and BBr_3 respectively. Two small peaks (ca. 15% of the total intensity) at 31.0 and 30.3ppm were also present. These stayed constant throughout the

experiment and have not been definitely assigned, but are thought to be hydrolysis products.

The changes in adduct signals that occurred when Ph_3P (25% of equimolar ratio) was added to this equilibrium mixture is shown in Fig 5.1. After three minutes three doublets, centred at 3.9ppm (J=154Hz), -1.3ppm (J=151Hz), and -7.5ppm (J=149Hz) are observed. After ten minutes a fourth doublet centered at -14.7ppm (J=147Hz) is visible. The doublet at 3.9ppm, the high field component of which is coincident with the low field component of the -1.3ppm doublet, matches the reported[2] shift of $PPh_3.BCl_3$. The doublet at -14.7ppm may be similarly assigned[2] to $PPh_3.BBr_3$. Previous work[12X15] has shown that the coupling constant between boron and the adduct nucleus provides a good correlation of bond strength, and that the trend is toward a smaller coupling constant with heavier halides. This, along with the previously observed stepwise chemical shift change with halide replacement, allows assignment of the doublet at -1.3ppm to $PPh_3.BCl_2Br$ and that at -7.5ppm to $PPh_3.BClBr_2$. This assignment is further supported by the peak intensities that show an increase in the proportions of the heavier halide adducts as the reaction proceeds.

$PPh_3.BCl_2Br$ was the dominant adduct after three minutes, but after ten minutes it had been reduced in amount while $PPh_3.BClBr_2$ increased. By this time PPh_3BCl_3 had virtually disappeared and $PPh_3.BBr_3$ made its first appearance. By the end of the experiment, after two hours, the dominant adduct was PPh_3BClBr_2, while $PPh_3.BBr_3$ had increased to 17% of the total adduct signal observed. The ratio of the intensities of these adduct signals as the reaction proceeded are listed in Table 5.4.

Immediately on addition of PPh_3, the free trihalide peaks coalesced into a broad peak ($\upsilon_{1/2}$=130Hz) centered at 43ppm and remained this way throughout the experiment. This suggests that the rate of halide exchange,

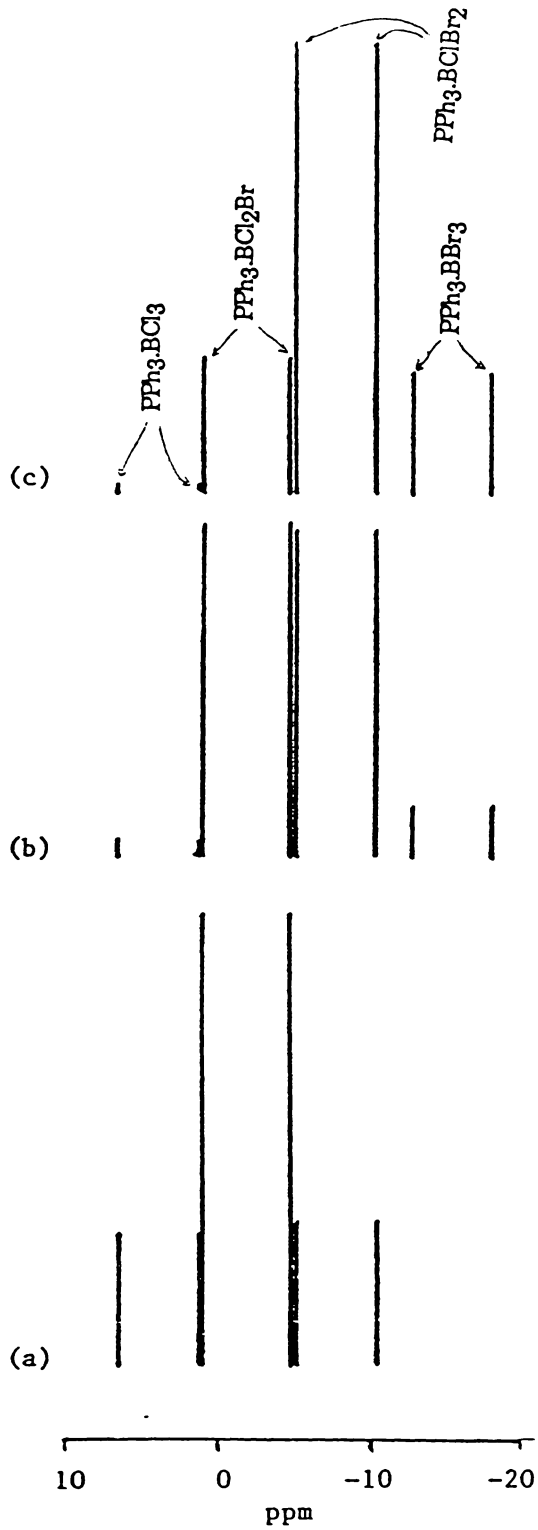

Fig. 5.1 Schematic diagram of adduct peak intensity vs time in the reaction where PPh_3 was added to a pre-equilibrated mix of BCl_3 and BBr_3: (a) 3min after addition, (b) 10min after addition, and (c) 120min after addition.

Table 5.4 Adduct Signal Intensities vs. Time in Reactions where PPh_3 is Added to Equilibrated Mixtures of Two Trihalides.

1. BCl_3/BBr_3 Mixture

$BCl_3 : BCl_2Br : BClBr_2 : BBr_3$ 1:3:3:1

Time after addn. (min.)	Adduct $PPh_3.BCl_3$	$PPh_3.BCl_2Br$	$PPh_3.BClBr_2$	$PPh_3.BBr_3$
3	18	62	20	0
10	2	46	45	7
120	1	19	63	17

2. BCl_3/BI_3

(a) $BCl_3 : BCl_2I : BClI_2 : BI_3$ 1:2:2.5:4

	$PPh_3.BCl_3$	$PPh_3.BCl_2I$	$PPh_3.BClI_2$	$PPh_3.BI_3$
2	0	17	50	33
15	0	0	34	66
30	0	0	19	81
90	0	0	4	96
120	0	0	0	100

(b) $BCl_3 : BCl_2I : BClI_2 : BI_3$ 10:5:2:1

2	0	63	37	0
15	0	25	63	12
30	0	12	68	20
60	0	0	60	40

3. BBr_3/BI_3

$BBr_3 : BBr_2I : BBrI_2 : BI_3$ 1:5:11.5:14

	$PPh_3.BBr_3$	$PPh_3.BBr_2I$	$PPh_3.BBrI_2$	$PPh_3.BI_3$
1	0	38	40	22
3	0	22	46	32
10	0	12	35	53
180	0	0	26	74

within the trihalides, had increased sufficiently, on the NMR time scale, to generate an averaged signal.

5.3.2.2 BCl_3 with BI_3

Two experiments were run with this system. In the first reaction the trihalides were mixed in a BCl_3:BI_3 ratio of ca. 1:3 to produce the free trihalide peaks BCl_3, BCl_2I, $BClI_2$, and BI_3 in the ratio of 1:2:2.5:4. PPh_3 (25% molar equivalent) was added and the changes that occurred were similar to the BCl_3/BBr_3 experiment (see Fig 5.2)* . The changes in halide adduct intensities in this system are tabulated in Table 5.4. Assignment of the mixed adduct peaks are made on the criteria described above, thus the doublet at -13.7ppm (J=147Hz) is assigned as $PPh_3.BCl_2I$ and that at -39.0ppm (J=136Hz) as $PPh_3.BClI_2$.

As in the BCl_3, BBr_3 system the Cl-rich adducts were quickly replaced by the I-rich ones. $PPh_3.BCl_3$ was not observed in this experiment, and $PPh_3.BCl_2I$ had disappeared within fifteen minutes. The reaction was dominated by the $PPh_3.BI_3$ adduct ninety minutes after the reaction commenced.

In an attempt to observe $PPh_3.BCl_3$ in this system a free trihalide ratio of 8:1 (BCl_3/BI_3) was used (Fig 5.3). This experiment started with the free trihalides BCl_3, BCl_2I, $BClI_2$, and BI_3, in the ratio of 10:5:2:1. PPh_3 (25% molar equivalent) was added and the reaction followed. Despite this strong bias to the lighter halide $PPh_3.BCl_3$ was still not observed. The initial spectrum showed only the two mixed halide adducts, with $PPh_3.BI_3$ appearing after fifteen minutes. After one hour of reaction all $PPh_3.BCl_2I$ had disappeared, but $PPh_3.BClI_2$ was still dominant compared to $PPh_3.BI_3$. The changes in adduct formation are tabulated in Table 5.4. When compared

* To avoid overcrowding in this and following figures not all spectra run are included. Details of all spectra are noted in the Tables. Note also the varying S/N which on occasions may highlight an apparent growth in signal, e.g. the impurity peak in Fig. 5.2(c), when in reality the relative intensity has remained the same throughout.

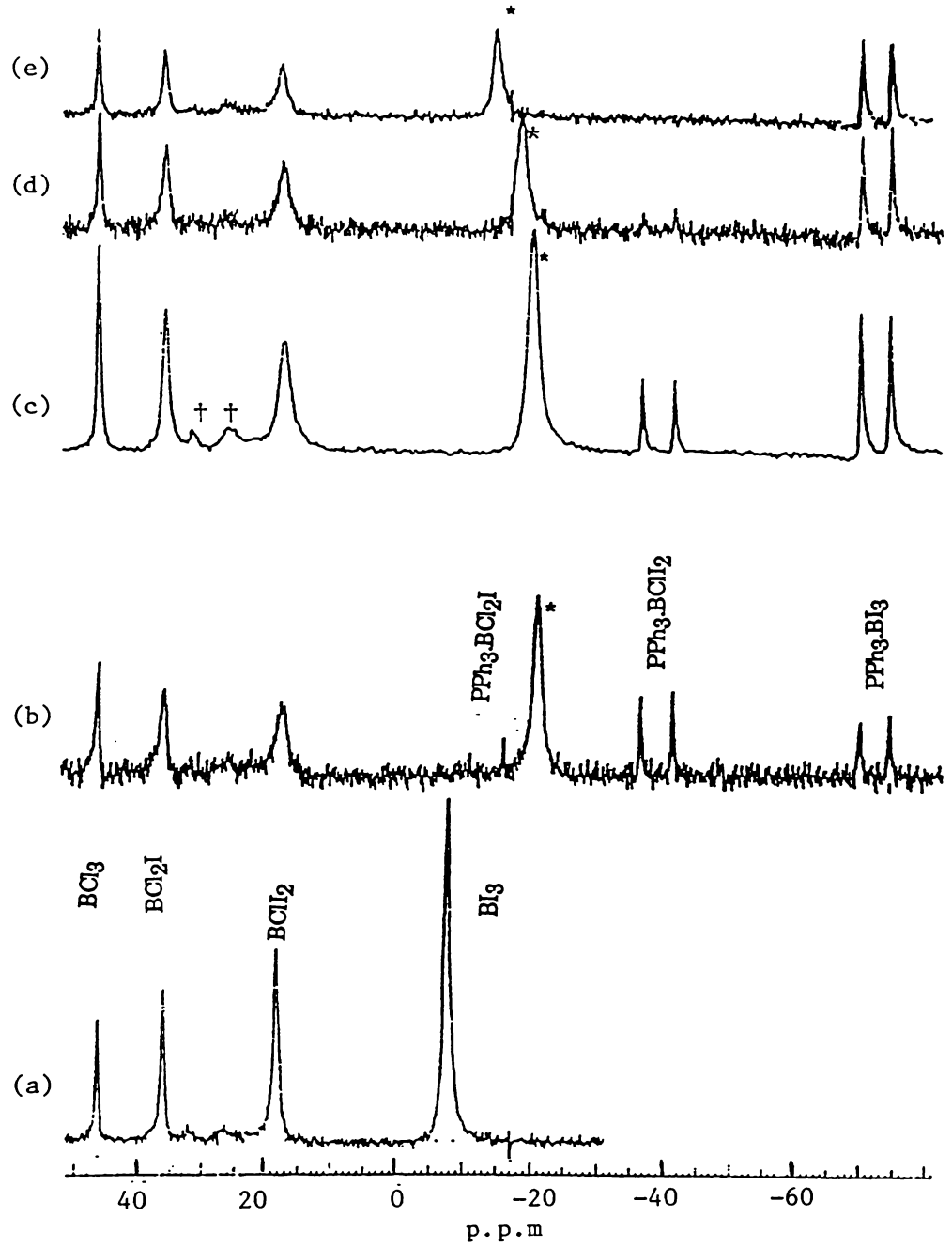

Fig. 5.2 Reaction of Ph_3P with an equilibrated mixture of BCl_3 and BI_3 (1:3 ratio): (a) ^{11}B NMR spectrum of the equilibrated trihalides, (b) 2min. after addition of Ph_3P, (c) 15min. after addition, (d) 90min. after addition, (e) 120min. after addition. The peak marked with an asterisk is tentatively assigned as BI_3. For discussion on the movement of this peak see Section 5.~~2.2.5~~ 4.4. † Impurity.

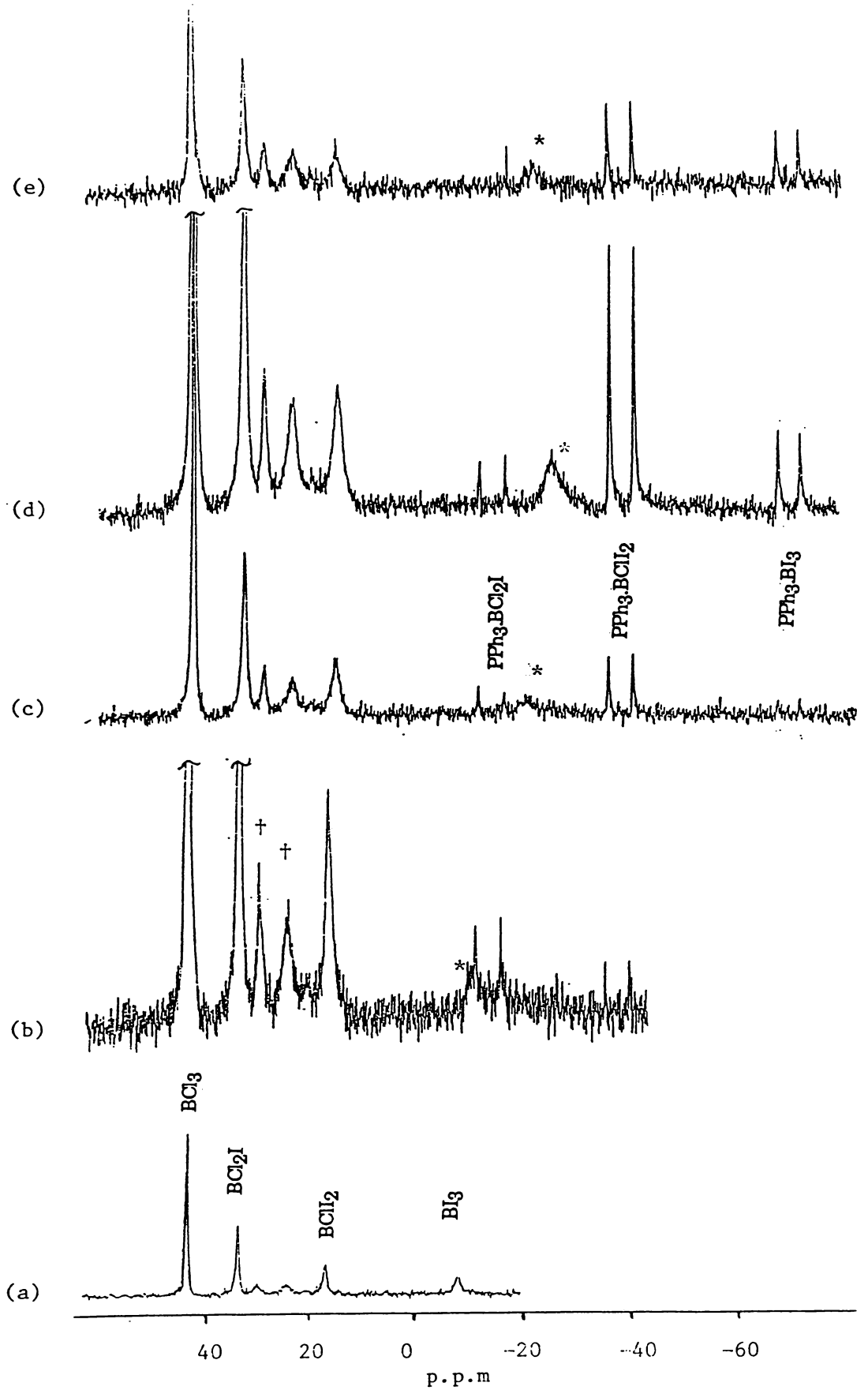

Fig. 5.3 Reaction of Ph_3P with an equilibrated mixture of BCl_3 and BI_3 (8:1 ratio): (a) ^{11}B NMR spectrum of the equilibrated trihalides, (b) 2min. after addition of Ph_3P, (c) 15min. after addition, (d) 30min. after addition, (e) 60min. after addition. Note again the movement of the peak marked with an asterisk. † Impurity.

to the first reaction of this system it is apparent that the initial trihalide balance, with its bias towards the light halide, has dramatically altered the overall rate of formation of the heavier halide adducts. The reaction was not carried through to equilibrium, so it is not certain whether this reaction, too, would have resulted in the heavy halide adduct only.

In contrast to the BCl_3/BBr_3 reaction, the free trihalide signals of BCl_3, BCl_2I, $BClI_2$, and BI_3 did not coalesce, but there were some rather large changes in chemical shifts as the reaction progressed. These chemical shift changes are listed in Table 5.5. The signals for both BCl_3 and BCl_2I remained constant, at 46.4 and 36.3ppm respectively, in both reactions. The signal at *ca.* 18ppm, attributed to $BClI_2$, moved by only 0.5ppm in the first

Table 5.5 ^{11}B Chemical Shifts for the Free Halide Signals vs. Time in Reactions Where PPh_3 is added to Equilibrated BCl_3/BI_3 Mixtures.

Run 1. BCl_3 : BCl_2I : $BClI_2$:BI_3 1:2:2.5:4

	BCl_3	BCl_2I	$BClI_2$	"BI_3"
Time (min.)		Chemical Shifts		
0	46.4	36.3	18.4	-7.2
2	46.4	36.3	17.9	-20.9
15	46.4	36.3	17.9	-18.2
30	46.4	36.3	17.9	-16.3
60	46.4	36.3	17.9	-14.3
90	46.4	36.3	18.0	-12.4
120	46.4	36.3	18.0	-12.1

Run 2. BCl_3 : BCl_2I : $BClI_2$:BI_3 10:5:2:1

0	46.4	36.3	18.4	-7.9
2	46.4	36.3	18.4	-10.5
15	46.4	36.3	17.9	-21.1
30	46.4	36.3	17.5	-25.4
60	46.4	36.3	17.8	-21.5

reaction (within the error of the experiment) while in the second experiment it ranged over 0.9ppm. The signal at -7.3ppm changed dramatically with time. In the first reaction it moved upfield to -20.9ppm after two minutes and then slowly moved back downfield to -12.1ppm after two hours, still 5ppm from its starting position. In the second reaction it moved more slowly upfield, but reached a position at -25.4ppm after thirty minutes, before starting to move downfield again. With no other trihalide signal present in this region, and with the hydrolysis product signals at 30.3 and 26.4ppm remaining stationary throughout the reaction, it is assumed that this signal is a result of BI_3 interacting with some other species in the system. This phenomenon is discussed further in Section 5.4.2.

5.3.2.3 BBr_3 and BI_3

A 1:8 ratio of BBr_3/BI_3 was equilibrated to give a spectrum of the free trihalides $BBr_3/BBr_2I/BBrI_2/BI_3$ in the ratio 1:5:11.5:14. PPh_3 (25% molar equivalent) was added and the reaction followed with time (Fig 5.4). The adduct signal intensity changes are listed in Table 5.4. The two new adduct peaks are assigned as $PPh_3.BBr_2I$ at -30.6ppm (J=140Hz) and $PPh_3.BBrI_2$ at -49.8ppm (J=132Hz). The reaction follows a similar pattern to those described above, with the heavier halide adducts dominating as time increased. No $PPh_3.BBr_3$ adduct is observed, with the two mixed halide adducts accounting for 80% of the adduct signal at the initial stages. $PPh_3.BI_3$ increases to become 74% of total adduct signal after a reaction time of three hours. By this time no $PPh_3.BBr_2I$ is present in the system. The free trihalide peaks immediately coalesced into a broad peak ($\upsilon_{1/2}$ = 650Hz) centered at 7ppm. With time this became broader ($\upsilon_{1/2}$=1100Hz) with its center at approximately 10ppm.

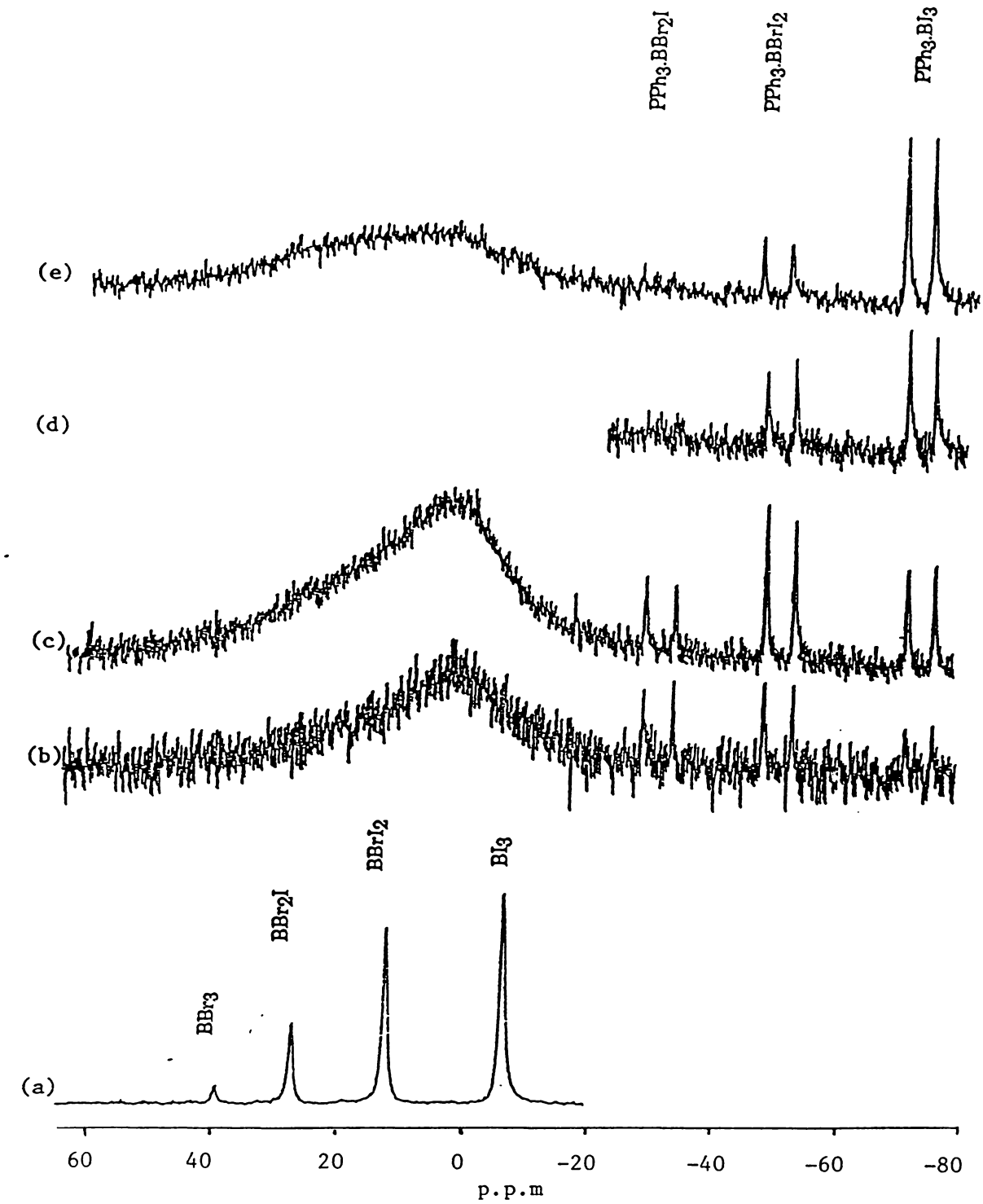

Fig. 5.4 Reaction of Ph_3P with an equilibrated mixture of BBr_3 and BI_3 (1:3 ratio): (a) ^{11}B NMR spectrum of the equilibrated trihalides, (b) 1min. after addition of Ph_3P, (c) 3min. after addition, (d) 10min. after addition, (e) 180min. after addition.

5.3.2.4 BCl_3, BBr_3 and BI_3

Fig 5.5 shows the spectrum of a reaction where all three trihalides were equilibrated before PPh_3 was added. The only adduct not previously assigned is that of PPh_3.BClBrI. This is found to have a chemical shift of -21.7ppm and ^1J = 142Hz. The chemical shifts and coupling constants of all the PPh_3 boron trihalide adducts are summarised in Table 5.9.

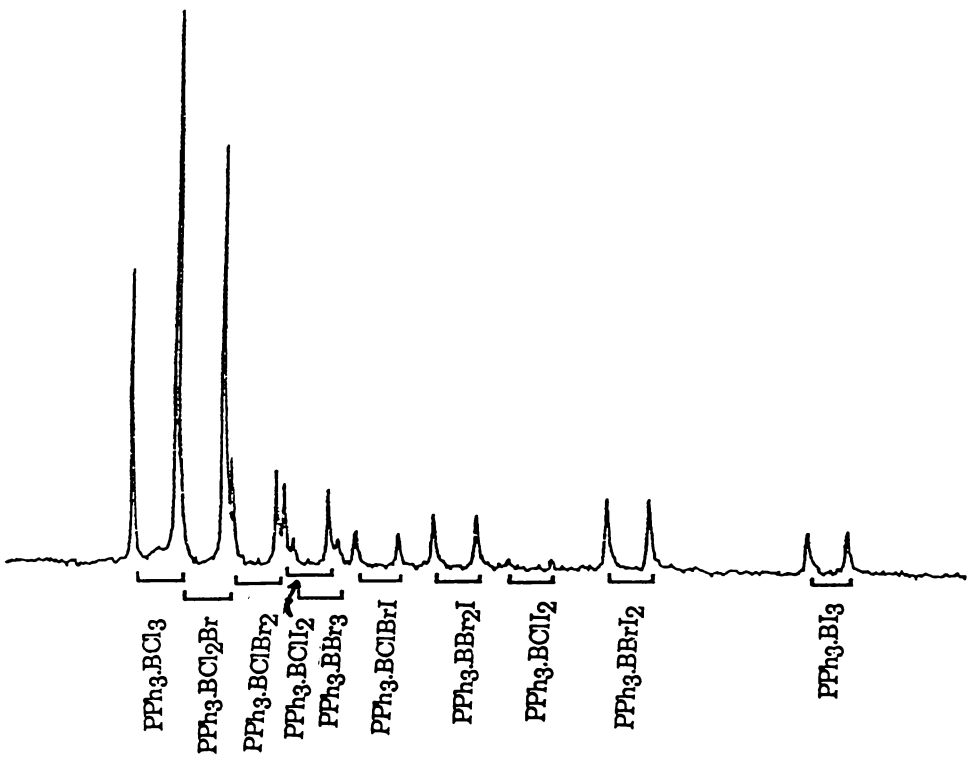

Fig.5.5 ^{11}B NMR spectrum of the adduct region from a mixture of BCl_3, BBr_3, and BI_3 with Ph_3P showing signals for all possible mixed halide adducts. The only signal not previously assigned is for Ph_3P.BClBrI.

5.3.2.5 Free Trihalide Signal Studies

In an effort to better understand the changes seen in the trihalide region during the BCl_3/BI_3 reaction (Section 5.3.2.2) two further reactions were carried out with the BBr_3/BI_3 system. In the first, a BBr_3/BI_3 ratio of 1:1.5 gave trihalide signals for BBr_3, BBr_2I, $BBrI_2$, and BI_3 in the ratio 1:3:3:2. The sample was then cooled to -40°C and PPh_3 (5% molar equivalent) added. The BBr_3, BBr_2I, and $BBrI_2$ signals coalesced into one broad envelope with obvious peaks at 26.6 and 9.5ppm. A broad signal ($\upsilon_{1/2}$= 250Hz) was also apparent at -19.5ppm (Fig.5.6(b)).

Peaks for the adducts of $PPh_3.BBr_2I$, $PPh_3.BBrI_2$, and $PPh_3.BI_3$ were present in the ratio 3:3:2 immediately after the addition of PPh_3, with no measureable change in intensities during the twenty minutes the reaction was followed.

In the second experiment, BBr_3 and BI_3 were mixed in a 1:4 ratio and allowed to equilibrate. The free trihalide signals for BBr_3, BBr_2I, $BBrI_2$, and BI_3 were present in the ratio 1:2.5:3.5:3. The mixture was then cooled to -40°C which broadened the free trihalide signals by a factor of three, to $\upsilon_{1/2}$= 100Hz., without coalescing. No change in chemical shift was apparent. PPh_3 (5% molar equivalent) was then added to the low temperature mixture (Fig 5.7).

After three minutes at -40°C the spectrum showed that the free trihalide signals had further doubled in linewidth ($\upsilon_{1/2}$= 200Hz), the signal for $BBrI_2$ moved upfield to 10.8ppm, and that for BI_3 moved to -10.0ppm. Adduct signals for BBr_2I and $BBrI_2$ were present in a 1:1 ratio. After thirteen minutes at -40°C no further change had occurred, so the sample was warmed to -20°C. After two minutes at that temperature the spectrum showed a coalescence of the BBr_3 and BBr_2I signals. The first indications of $PPh_3.BI_3$ were apparent at this time.

After fifteen minutes at -20°C the sample was again cooled to -40°C and a further spectrum run. This showed the BI_3 signal had continued to move

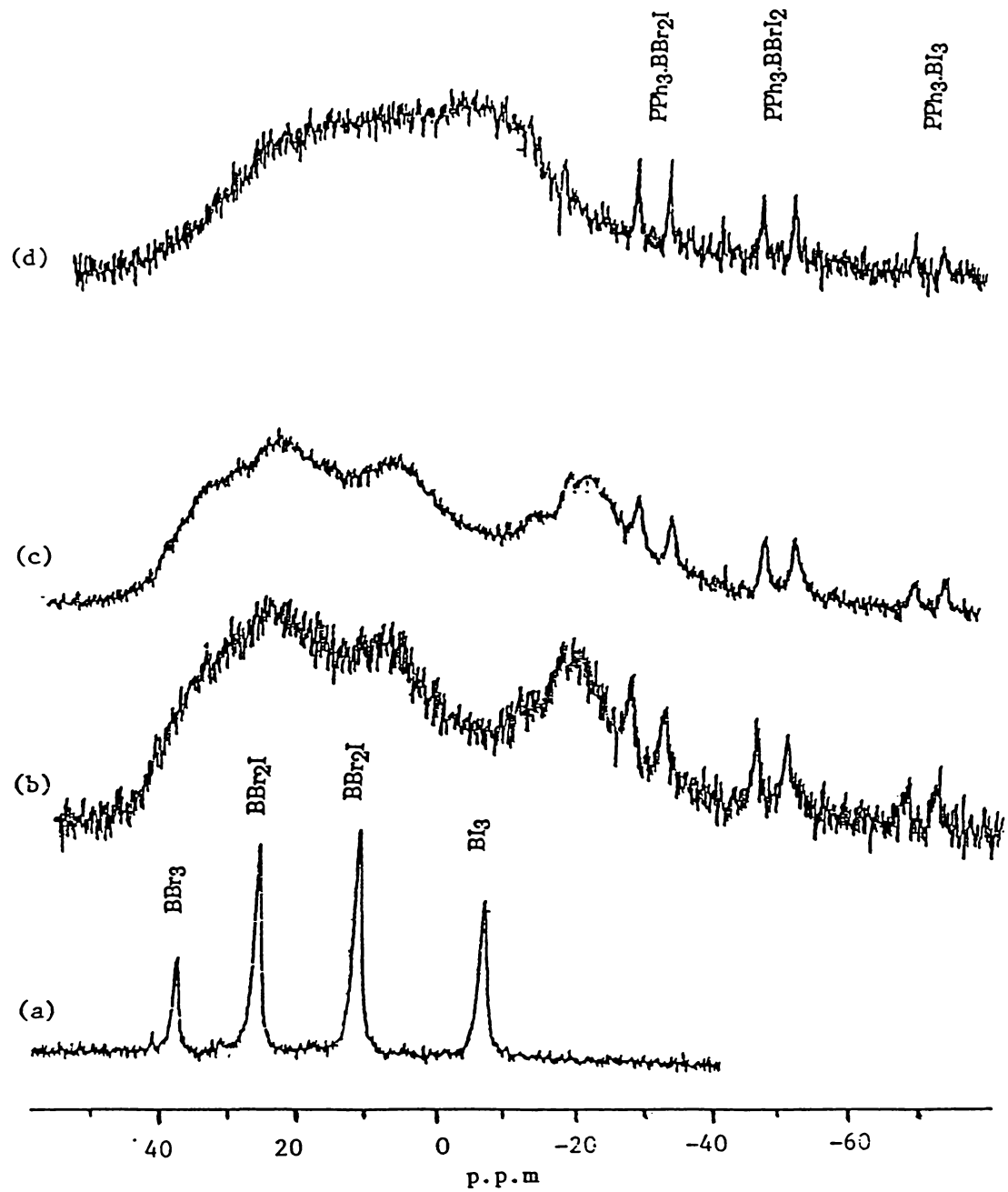

Fig. 5.6 Reaction where a 5% molar equivalent of Ph_3P was added to an equilibrated mixture of BBr_3 and BI_3 (1:1.5 ratio): (a) ^{11}B NMR spectrum of the equilibrated trihalides, (b) 10min. after the sample was cooled to -40°C and Ph_3P added, (c) -40°C spectrum 20min. after the addition of Ph_3P, (d) R.T. spectrum of (c).

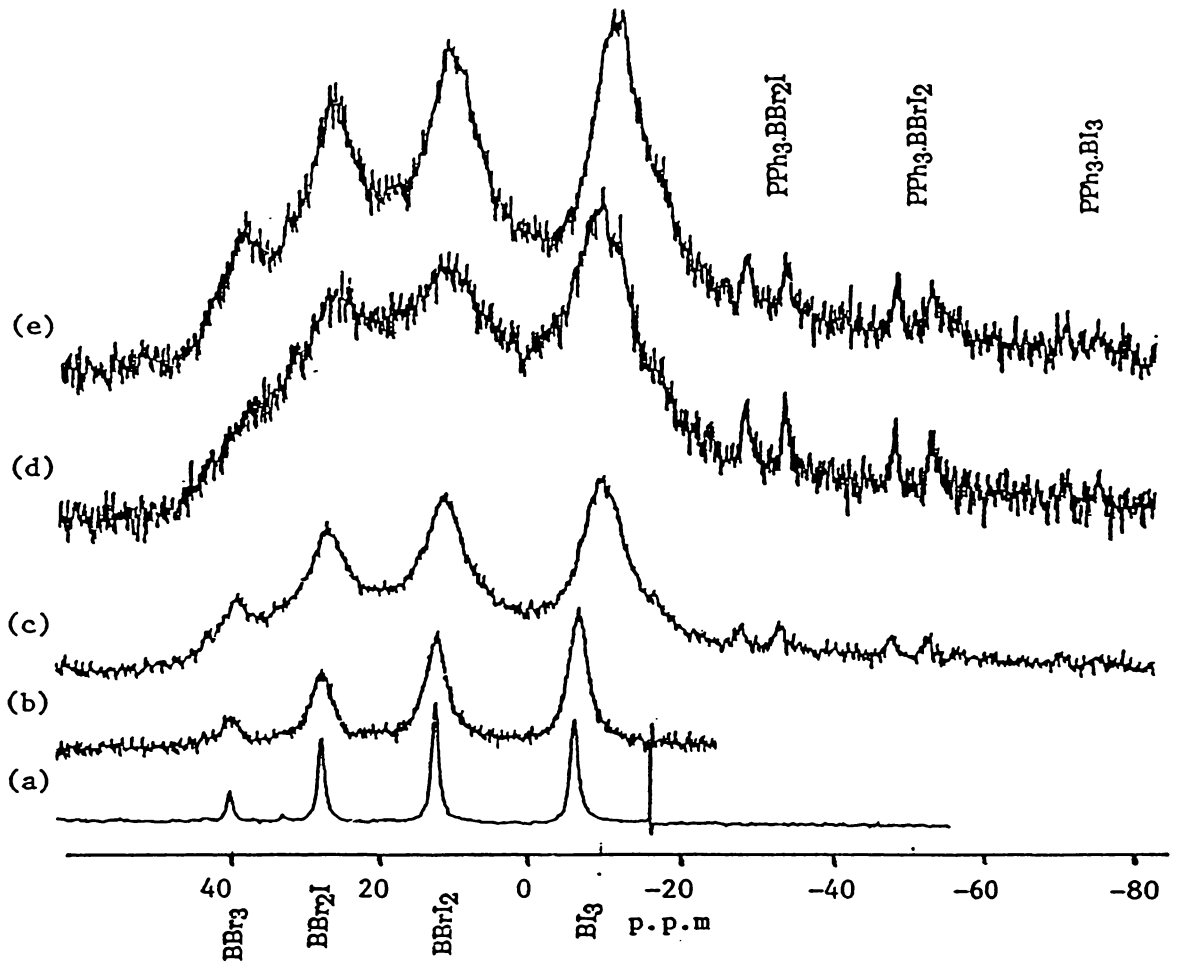

Fig. 5.7 Second reaction of Ph_3P (5% molar equivalent) with an equilibrated mixture of BBr_3 and BI_3 (1:4 ratio): (a) R.T ^{11}B NMR spectrum of the equilibrated trihalides, (b) -40°C spectrum of (a), (c) 3min. after addition of Ph_3P, (d) 15min. after addition, 13min. of which were at -40°C. The last 2min. at -20°C, the temperature at which this spectrum was run. (e) After a further 15min. at -20°C the temperature was lowered to -40°C and this spectrum run. Total reaction time 30min.

upfield, to -11.5ppm, while the other trihalide signals sharpened ($\upsilon_{1/2}$= 200Hz) to a width similar to the width previously observed at this temperature. The first, small, indications of $PPh_3.BI_3$ were apparent in this spectrum. The sample was finally warmed to R.T. where the trihalide signals coalesced into one broad signal ($\upsilon_{1/2}$ = 1400Hz) centered at 0ppm, while the adduct concentrations for $PPh_3.BBr_2I$, $PPh_3.BBrI_2$, and $PPh_3.BI_3$ were in the ratio 2:2:1.

This reaction confirmed the results seen earlier in the BCl_3/BI_3 system. As described in Section 5.3.2.2 rather large shifts in the signals from the uncoordinated heavier trihalide occurred on addition of PPh_3 to the system. In systems where neighbouring halides were mixed i.e. BCl_3/BBr_3 and BBr_3/BI_3, exchange within the trihalides was speeded up to the extent that at room temperature a broad coalesced signal, although not yet an averaged signal, resulted. The reactions described in this section indicate that lowering the temperature a modest amount slows the exchange in the uncomplexed trihalide to a rate where once more individual signals are observable. This has allowed observation of an upfield shift of the heavy trihalide in a similar fashion to that observed in the BCl_3/BI_3 system. Possible reasons for this shift are discussed in detail in Section 5.4.2.

5.3.3 Exchange of BX_3 with $PPh_3.BY_3$

The reactions described in Section 5.3 looked at the addition of donor to a pre-equilibrated trihalide mixture. The reactions that occurred were therefore, at least in the initial stages, controlled by the rates of formation of the individual trihalide adduct. To observe what might occur when one trihalide adduct was exposed to a second trihalide, a series of reactions was carried out where $PPh_3.BX_3$ was dissolved in CH_2Cl_2 in an NMR tube, BY_3 was added to the solution, and the change in these systems over time was monitored.

5.3.3.1 X heavier than Y

An equimolar amount of BBr_3 was added to $PPh_3.BCl_3$ in CH_2Cl_2. Within six minutes of mixing no $PPh_3.BCl_3$ was evident in the mixture, and only $PPh_3.BCl_2Br$ (66% of the adduct signal) and $PPh_3.BClBr_2$ (34%) were present. The proportion of $PPh_3.BCl_2Br$ decreased with time to approximately 20% of the total signal after three and a half hours, while $PPh_3.BCl_2Br$ increased to 56%, and $PPh_3.BBr_3$ appeared and increased to 22%. The changes in adduct signal are listed in Table 5.6. Two signals at 44.6 and 26.7ppm were the only signals present in the free trihalide region. These remained constant throughout the reaction, and because of their position, and linewidth, are tentatively assigned as hydrolysis products.

In a further reaction with this system BBr_3 (35% deficit) was added to $PPh_3.BCl_3$ (Fig 5.8 and Table 5.6). In this experiment it took seven minutes for the $PPh_3.BCl_3$ adduct signal to disappear with $PPh_3.BCl_2Br$ being the dominant signal at that time. After fifteen minutes the three adducts $PPh_3.BCl_2Br$, $PPh_3.BClBr_2$ and $PPh_3.BBr_3$ were present in an approximate 2:2:1 ratio. Forty minutes after the start of the experiment $PPh_3.BClBr_2$ and $PPh_3.BBr_3$ were the only adduct signals were present, and they were in a 1:2 ratio.

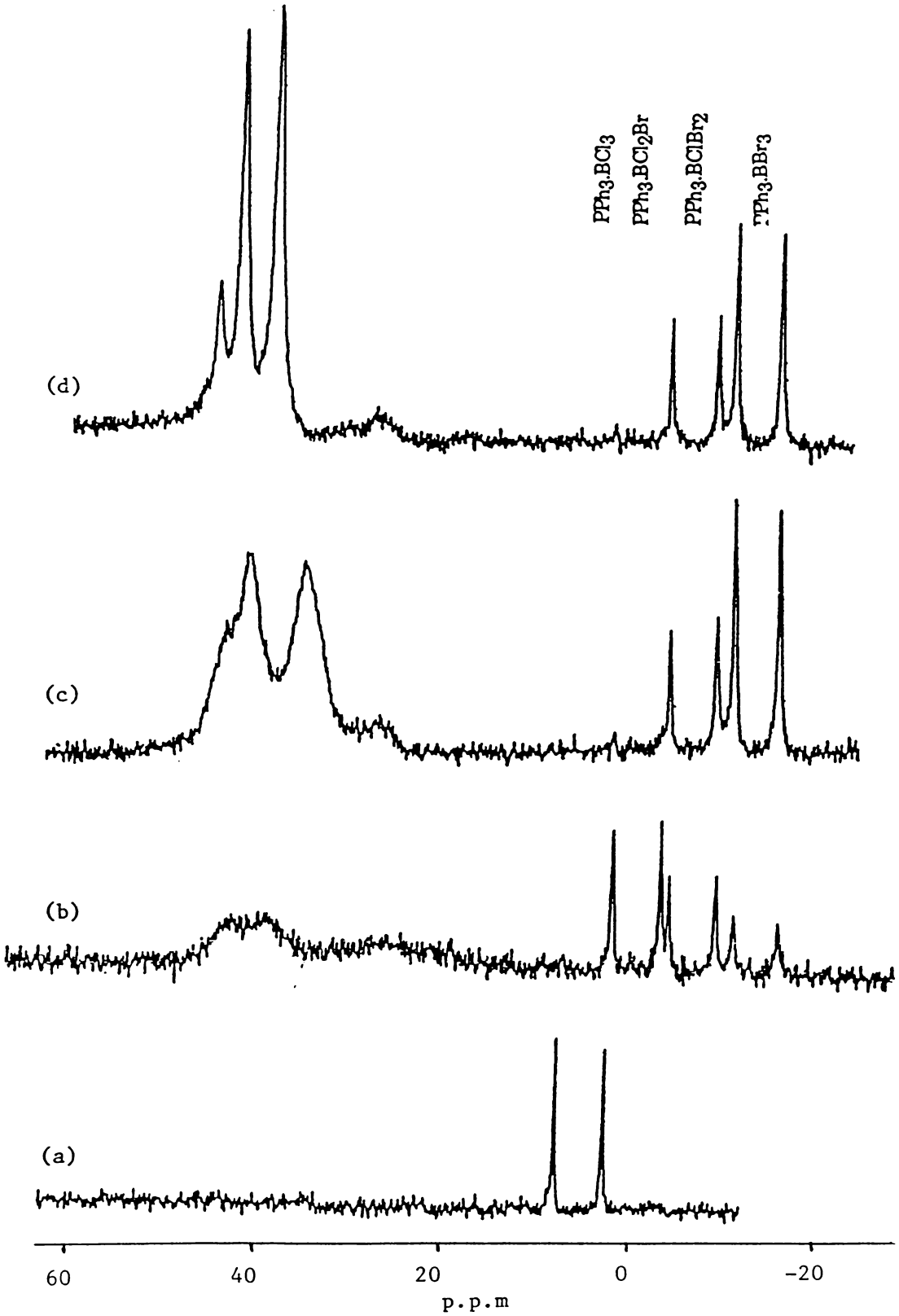

Fig. 5.8 Reaction of BBr_3 with $Ph_3P.BCl_3$: (a) ^{11}B NMR spectrum of $Ph_3P.BCl_3$, (b) 10min. after addition of a 35% deficit of BBr_3, (c) 30min. after addition, (d) 40min. after addition.

Table 5.6 Changes in Adduct Signal Ratios (%) with Time in Reaction Mixtures $PPh_3.BX_3 + BY_3$ (Y heavier than X).

1. $PPh_3.BCl_3 + BBr_3$

Run 1. 1:1 ratio, $PPh_3.BCl_3$:BBr_3	Adduct			
Time (min.)	$PPh_3.BCl_3$	$PPh_3.BCl_2Br$	$PPh_3.BClBr_2$	$PPh_3.BBr_3$
6	0	66	34	0
9.5	0	52	37	11
13.5	0	43	43	14
18.5	0	40	48	12
22	0	35	51	14
32	0	32	55	14
35	0	26	62	12
42	0	26	60	14
48.5	0	27	57	16
82	0	22	60	18
155	0	21	56	23
210	0	22	56	22
Run 2 1:0.65 ratio, $PPh_3.BCl_3$:BBr_3				
1	71	29	0	0
2	71	29	0	0
7	0	67	20	13
10	0	50	32	18
15	0	36	40	24
20	0	14	52	34
25	0	22	30	48
30	0	4	32	64
40	0	0	37	63

cont...

Table 5.6 (cont.) Changes in Adduct Signal Ratios (%) with Time in Reaction Mixtures $PPh_3.BX_3 + BY_3$ (Y heavier than X).

2. $PPh_3.BBr_3 + BI_3$ (equimolar)

	$PPh_3.BBr_3$	$PPh_3.BBr_2I$	$PPh_3.BBrI_2$	$PPh_3.BI_3$
4	71	28	0	0
9	48	44	8	0
13	41	46	13	0
16.5	33	50	17	0
20	35	48	17	0
23	33	48	19	0
27	32	50	18	0
50	31	37	22	0
110	29	42	24	5

3. $PPh_3.BCl_3 + BI_3$ (equimolar)

	$PPh_3.BCl_3$	$PPh_3.BCl_2I$	$PPh_3.BClI_2$	$PPh_3.BI_3$
4	0	77	23	-
9	0	46	42	12
14	0	31	53	16
20	0	18	64	18
27	0	12	63	25
30	0	10	67	23
36	0	0	70	30
41	0	0	67	33
44	0	0	68	32
49	0	0	69	31
52	0	0	67	33
211	0	0	57	43

The major difference between this experiment and the earlier one with more BBr_3 occurred in the free trihalide region. While, in the early stages, no signals were apparent in this region, as was the case in the first experiment, after ten minutes signals began to appear. Initially these were broad ill-defined lumps, but after forty minutes they sharpened into three signals at 45.0, 42.4, and 38.4ppm coinciding with earlier observations of BCl_2Br, $BClBr_2$ and BBr_3 respectively.

A similar reaction was carried out with equimolar amounts of BI_3 and $PPh_3.BBr_3$. Four minutes after mixing $PPh_3.BBr_3$ and $PPh_3.BBr_2I$ were present in a 71:28 ratio. $PPh_3.BBrI_2$ was evident after nine minutes and the first indications of $PPh_3.BI_3$ appeared after almost two hours. $PPh_3.BBr_3$ decreased to be 33% of the total adduct signal intensity after sixteen and a half minutes, at which concentration it remained for the rest of the experiment. $PPh_3.BBr_2I$ increased to 50% of adduct signal after sixteen and a half minutes, then slowly decreased while $PPh_3.BBrI_2$ increased (see Table 5.6). No other signals were observed in the reaction mixture.

The series was completed by following the changes that occurred after mixing equimolar amounts of BI_3 and $PPh_3.BCl_3$ (Fig.5.9 and Table 5.6). No $PPh_3.BCl_3$ was observed in the reaction, with $PPh_3.BCl_2I$ and $PPh_3.BClI_2$ accounting for 77% and 23% of the adduct signal intensity after four minutes. After thirty minutes $PPh_3.BCl_2I$ had disappeared, while PPh_3BI_3, present after nine minutes, increased to be 43% of the adduct signal after three and a half hours.

Free trihalide signals were apparent in this experiment as they had been in the earlier experiment using a deficit of BBr_3. What was notable in this experiment was the movement of some of these trihalide signals with time. The signals for BCl_3 and BCl_2I remained in their normally observed positions of 46.4 and 35.7ppm respectively although the signal for BCl_2I was broadened by a factor of three. The signal at next highest field to these two first appeared at 14.2ppm and gradually moved downfield to be at 21.8ppm after fifty-two minutes. A fourth signal started at -51.4ppm and moved downfield to be at -22.1ppm after fifty-two minutes. This shift with time is tabulated in Table 5.7. Possible causes for these shifts in signals are discussed in Section 5.4.2.4.

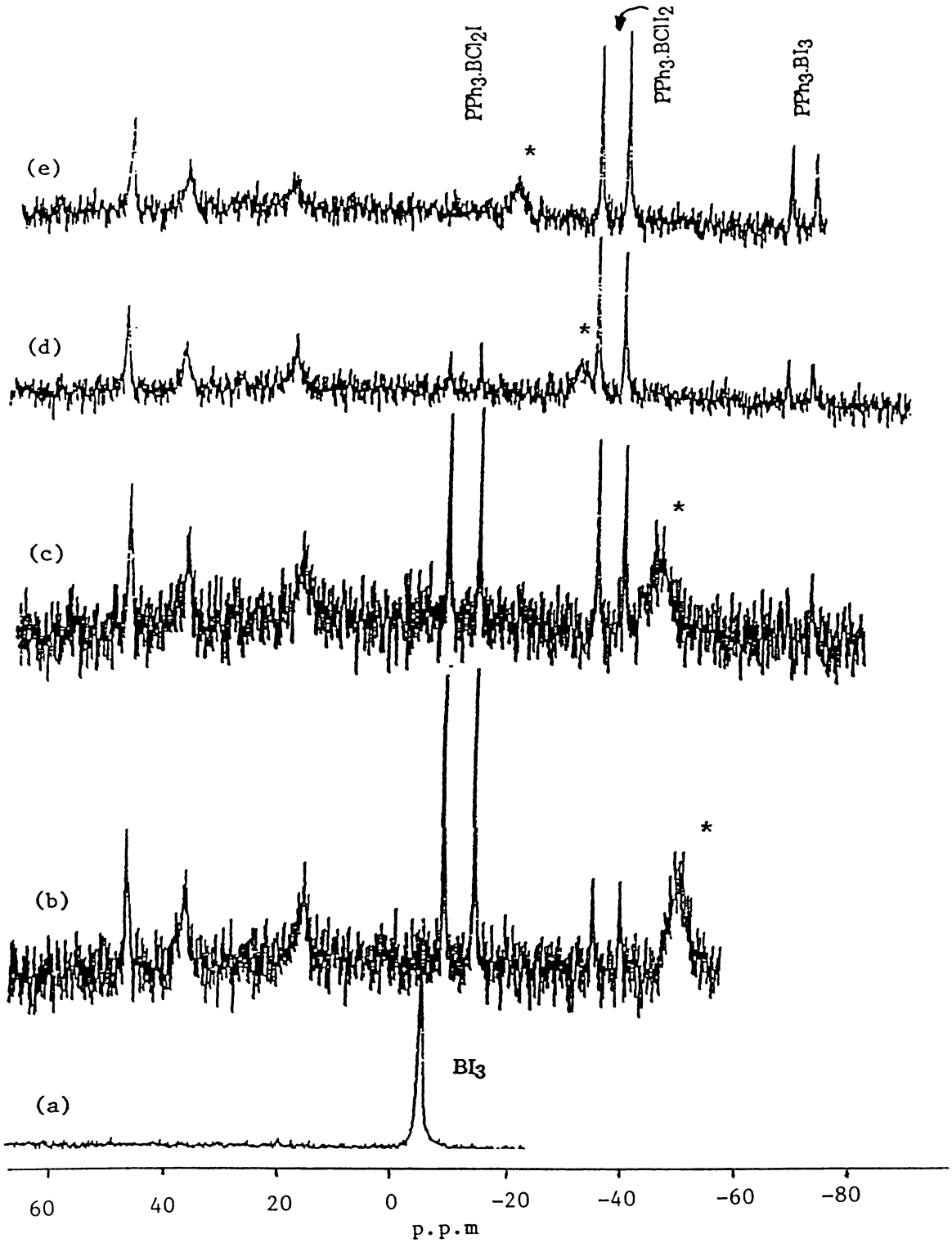

Fig. 5.9 Reaction of BI_3 with $Ph_3P.BCl_3$: (a) ^{11}B NMR spectrum of BI_3, (b) 4min. after addition of an equimolar amount of $Ph_3P.BCl_3$, (c) 9min. after addition, (d) 20min. after addition, (e) 49min. after addition. Note the movement over time of the singlet peak marked with an asterisk.

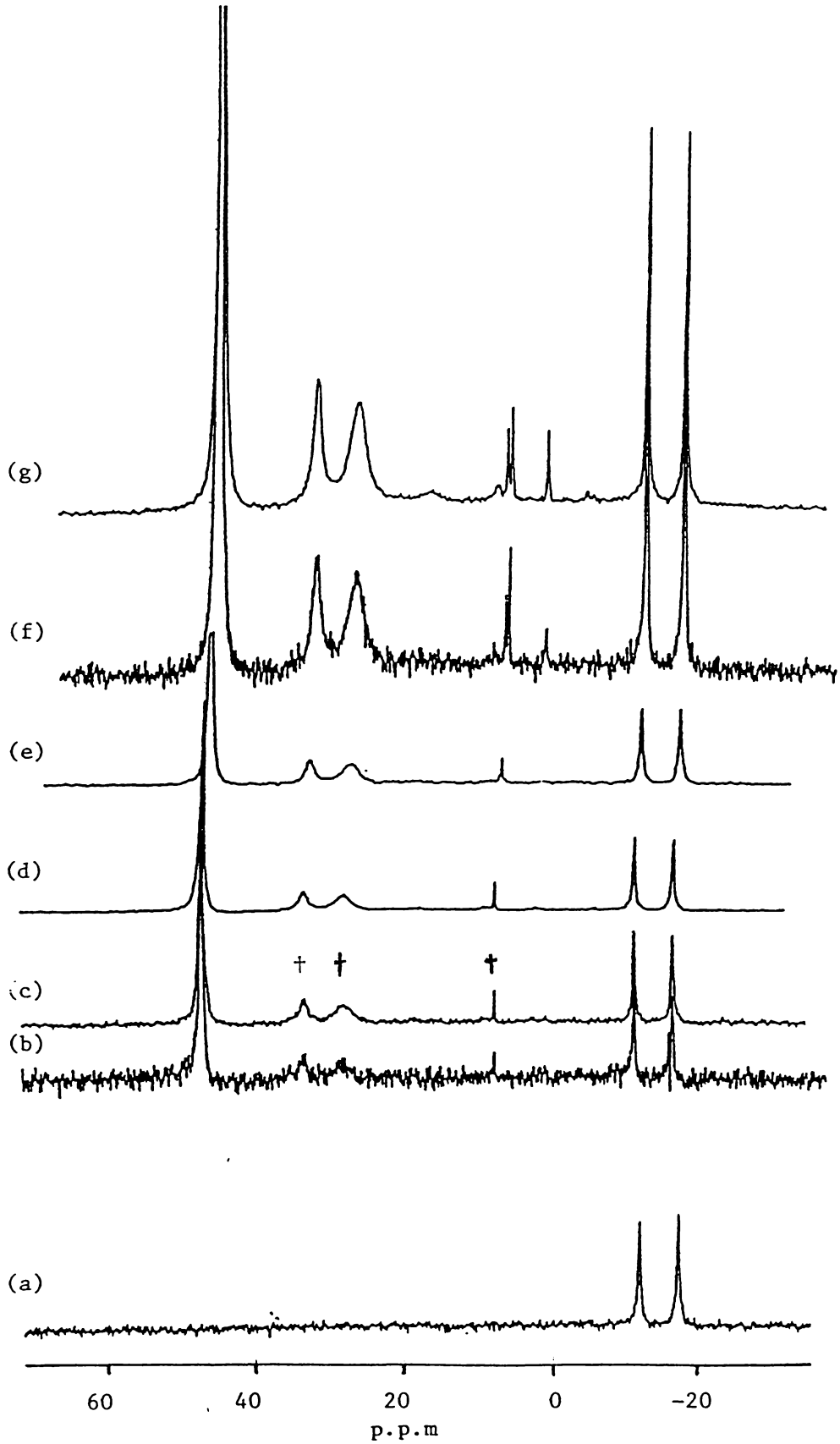

Fig. 5.10 ^{11}B NMR spectra of the reaction of BCl_3 and $Ph_3P.BBr_3$: (a) $Ph_3P.BBr_3$, (b) immediately after addition of BCl_3, (c) 30min. after addition, (d) 1hr. after addition, (e) after 2hrs., (f) after 3hrs., and (g) after 6hrs. † Impurity.

Table 5.7 Chem. Shift of the Upfield Singlet vs. Time in the Reaction Mixture $PPh_3.BCl_3 + BI_3$.

Time (min.)	$\delta(^{11}B)$
4	-51.4
9	-47.9
14	-42.1
20	-33.8
27	-30.0
30	-27.0
36	-25.3
41	-24.3
44	-22.8
49	-22.4
52	-22.1

5.3.3.2 X lighter than Y

In this experiment an equimolar amount of BCl_3 was added to a solution of $PPh_3.BBr_3$ in CH_2Cl_2 (Fig 5.10). This reaction proceeded at a considerably slower rate than those described in the previous section and it should be noted that the list of adduct intensities in Table 5.8 are listed against a time in hours, not minutes. A spectrum run immediately after addition of BCl_3 showed, besides the adduct signal, a sharp signal for the free BCl_3 and two broad peaks at 31.7 and 27.1ppm. These two signals amounted to approximately 15% of the BCl_3 signal intensity and remained constant throughout the experiment* . They are believed to be hydrolysis complexes. It was three hours after the reaction commenced before any adduct signal other than the original $PPh_3.BBr_3$ appeared. The new signal was $PPh_3.BCl_3$ and formed 14% of the total adduct signal. After six hours this had increased to 16%. After twenty-two hours the first indications of $PPh_3.BCl_2Br$ were apparent and after seventy hours all four adducts were

* Change in Y-gain between spectra misleadingly suggests growth in these peaks during the course of the experiment.

present although the mixed halide adducts accounted for less than 30% of total adduct signal at this time. The signal for BCl_3 had shifted slightly upfield to 37.9ppm after seventy hours. No other adduct signal was apparent. The adduct signal intensity variations vs. time are listed in Table 5.8.

Table 5.8 Variation in Signal Intensities vs Time in the Reaction $PPh_3.BBr_3 + BCl_3$.

	Adduct			
Time (hrs.)	$PPh_3.BCl_3$	$PPh_3.BCl_2Br$	$PPh_3.BClBr_2$	$PPh_3.BBr_3$
2	0	0	0	100
3	14	0	0	86
6	16	0	0	84
22	25	11	0	64
70	36	22	5	37

In contrast to the runs with X heavier than Y, the obvious difference in this reaction was the very slow appearance of any other adduct signal. In all cases where X was heavier than Y mixed adduct signals were evident immediately on mixing, while in this case the first new adduct did not appear until three hours into the reaction. It is also of interest that this signal was for $PPh_3.BCl_3$, and that the mixed adduct signals did not appear for some time later. The overall length of the reaction probably meant that hydrolysis products had some effect on the overall course of the reaction, and thus a sealed tube reaction would be required to achieve more definitive results from this experiment.

5.3.3.3. X=Y

In an effort to understand the shift of the free trihalide signals observed earlier successive increments of BCl_3 were added to a solution of $PPh_3.BCl_3$ (Fig 5.11). The adduct signal did not change position, but the position of the

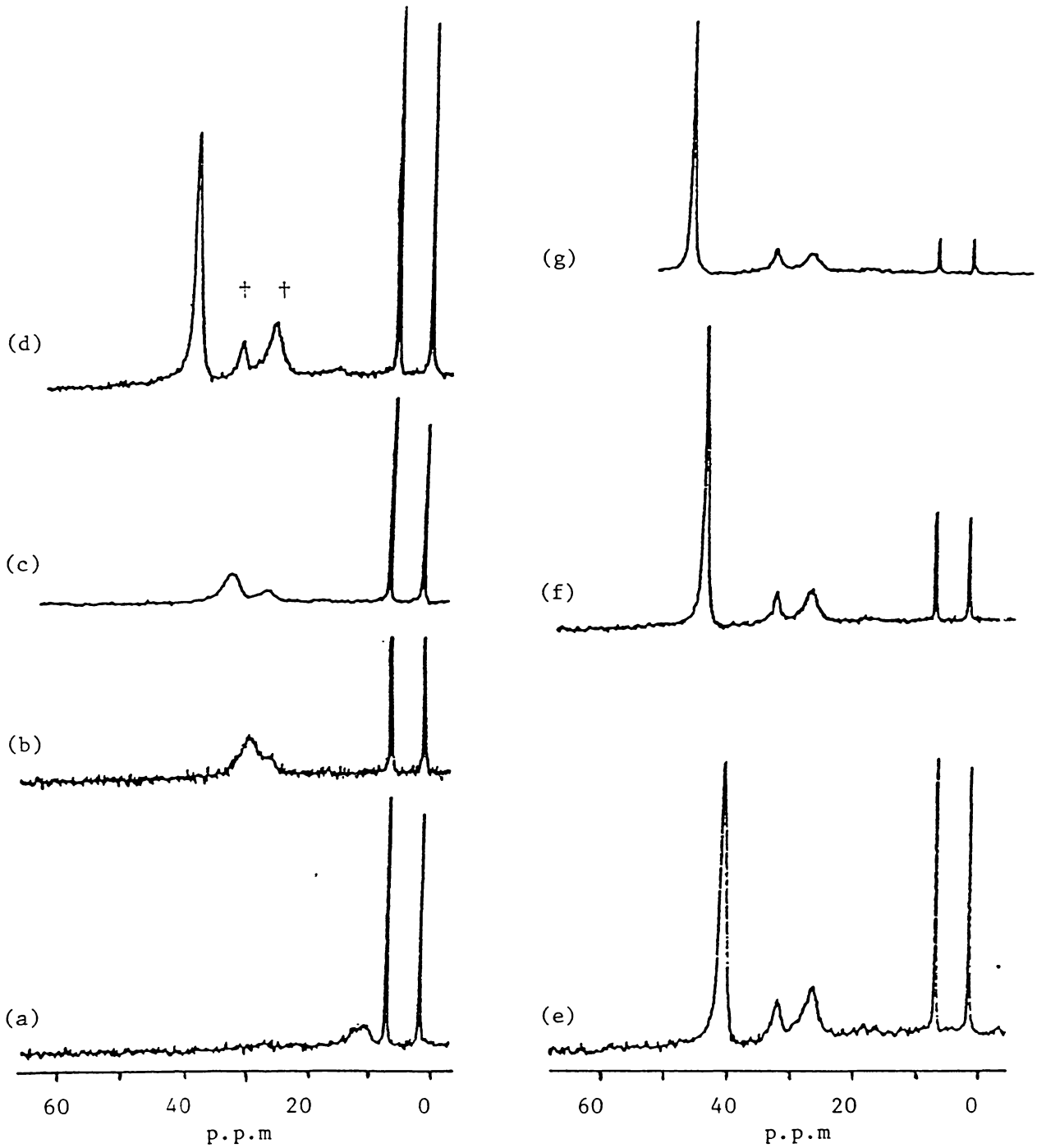

Fig. 5.11 Spectra showing the change in position of the 'free' halide peak at varying ratios of $BCl_3/PPh_3.BCl_3$: (a) 0.3:1, (b) 0.4:1, (c) 0.5:1, (d) 0.8:1, (e) 1:1, (f) 2:1, (g) 4:1. † Impurity.

other signal in the system was dependent on the mole ratio of BCl_3 to adduct. With only a small excess of BCl_3 in the system a broad peak was observed at 10.1ppm. As the amount of BCl_3 in the system was increased this signal sharpened and moved downfield, to be at 44.8ppm with a 1.5:1 $BCl_3/PPh_3.BCl_3$ mole ratio. This signal shift is plotted against the mole ratio in Fig. 5.12.

This result, in addition to the anomalous signal shifts observed in earlier exchange reactions suggest that the free trihalide is in some way interacting with the adduct in the system, and that that the anomolous signals result from a signal that is an average of the trihalide and some other species in the system. A possible cause for this is discussed further in Section 5.4.2.4.

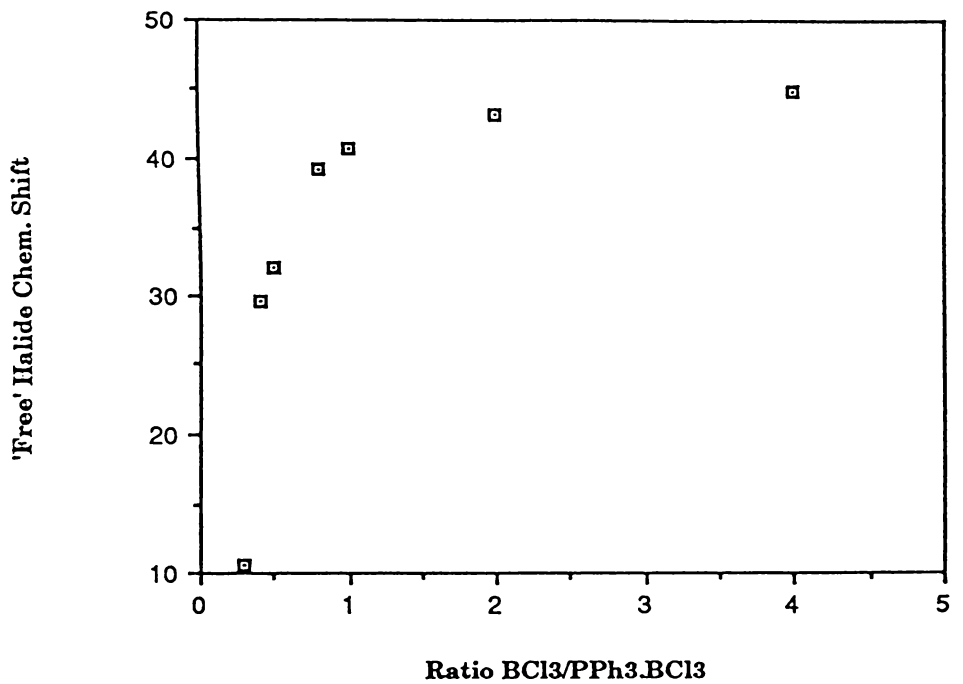

Fig. 5.12 Plot of the 'free' halide chemical shift at varying mole ratios of $BCl_3/PPh_3.BCl_3$. Data from Fig. 5.11.

5.4 Discussion of PPh_3 Adduct Systems

5.4.1 NMR Data

The above reactions have generated the triphenylphosphine-boron trihalide complexes for all the possible combinations of Cl, Br and I. The observations are summarised in Table 5.9. The stepwise change in chemical shifts and coupling constants, as halides are exchanged, are shown in Figs. 5.13 and 5.14 respectively.

Table 5.9 ^{11}B Chemical Shifts and ^{11}B-^{31}P Coupling Constants for the PPh_3-Trihalogen Adducts. (Halogen = Cl, Br, or I)

Adduct of	$\delta\ ^{11}B$	$\Delta\delta$	$^1J(^{11}B$-$^{31}P)$ (Hz)	$\delta\ ^{31}P$
BCl_3	3.9	42.3	154	-1.3
BCl_2Br	-1.4	46.4	151	-2.3
$BClBr_2$	-7.5	50.3	149	-3.5
BCl_2I	-13.7	50.0	147	
BBr_3	-14.7	53.7	147	-4.8
BClBrI	-21.7	53.1	142	
BBr_2I	-30.6	57.0	140	
$BClI_2$	-38.9	57.3	136	
$BBrI_2$	-49.8	60.8	132	
BI_3	-72.2	64.7	124	-15.5

Chemical Shifts. Mooney et.al.[16] concluded that the complexation shift $\Delta\delta$ (the difference in chemical shift between the free trihalide and the corresponding adduct) provided a measure of the donor-acceptor interaction in boron-trihalide adducts equivalent to the information obtained from vibrational spectra and thermochemical studies, with the larger $\Delta\delta$ corresponding to the stronger bond. Muylle and co-workers[17] in their study of arylphosphine and -arsine adducts confirmed this trend for these

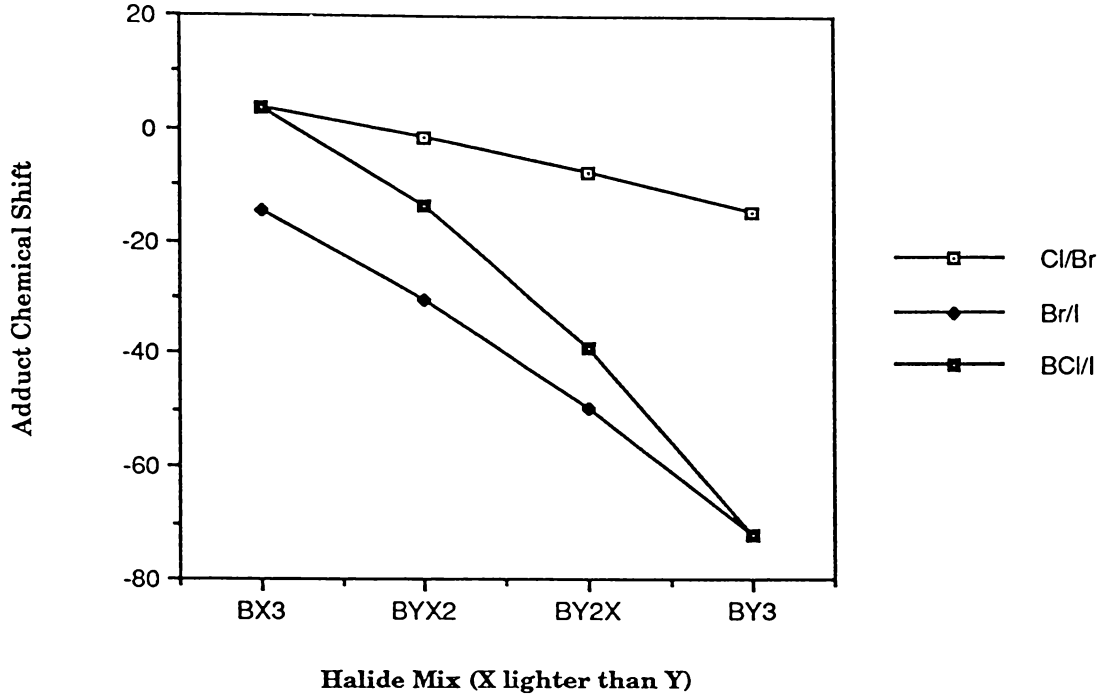

Fig. 5.13 Plot of adduct chemical shift against halide mix for the three mixes Cl/Br, Br/I, and Cl/I.

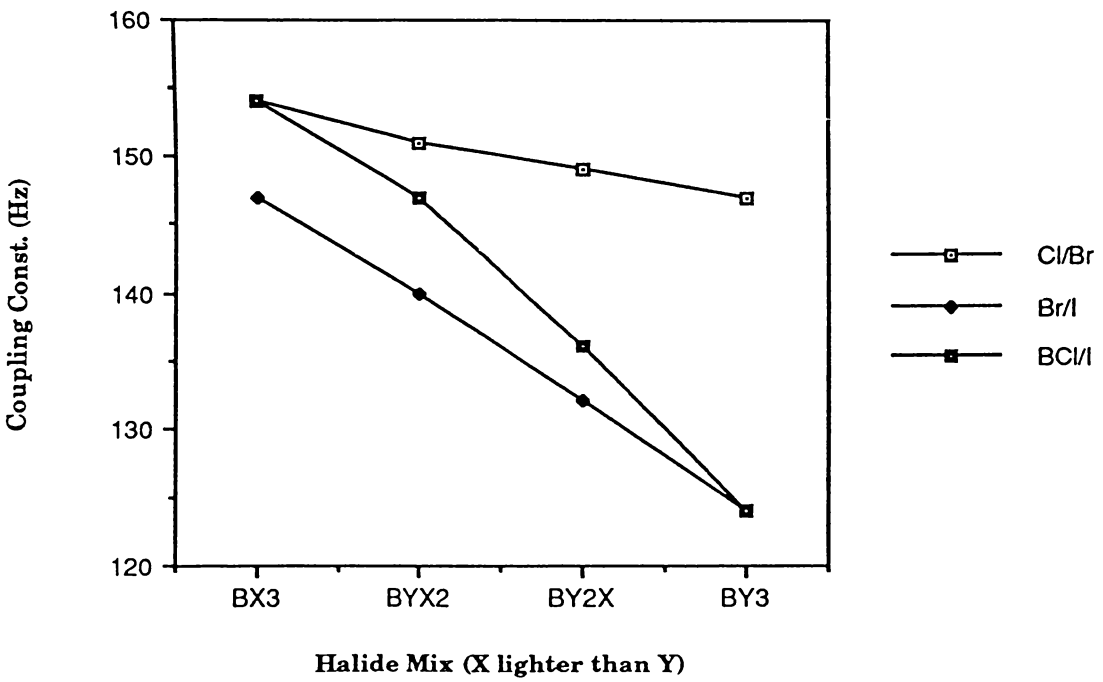

Fig. 5.14 Plot of J(^{11}B-^{31}P) against halide mix for the three mixes Cl/Br, Br/I, and Cl/I.

complexes. As the fourth bonding electron pair will increase the shielding of the boron nucleus, it is to be expected that the stronger P-B bond will result in the greater complexation shift.

On this basis the observed data show the most stable complex is $PPh_3.BI_3$, with the least stable being $PPh_3.BCl_3$. This trend parallels the generally accepted sequence of acceptor strength (Lewis acidity) of the boron halides.

With the amount of work carried out on the boron adduct systems it is perhaps surprising that very few crystal structure determinations have been carried out to allow direct comparison of the bond length and angles with the observed NMR data. The only phosphines for which crystal structures have been completed are the series $Me_3P.BX_3$ (X= Cl,Br,I)[18]. Data from these crystal structures are listed in Table 5.10 along with the $\Delta\delta$ values for these compounds. The data shows that the B-P bond length reduces as $\Delta\delta$ increases, as might be expected. The changes in bond length between the trichloride and tribromide adducts are only marginally significant with no change between the tribromide and triiodide adducts. They are therefore not useful in predicting any trends in bond strength. Thus $\Delta\delta$ may be a better measure - certainly a more accessible one, especially for adducts of mixed halides.

Table 5.10 Crystallographic and NMR Data of the $Me_3P.BX_3$ Adducts

	$Me_3P.BCl_3$	$Me_3P.BBr_3$	$Me_3P.BI_3$
B-P Bond Length	1.957(5)	1.924(12)	1.918(15)
X-P-X Bond Angles (°)	111.4	110.3	110.7
C-P-C Bond Angles (°)	107.9	107.2	107.8
δ ^{11}B (ppm)	10.0	-3.5	-54.0
$\Delta\delta$ (ppm)	35.0	43.5	48.0

Comparison of the $\Delta\delta$ values in Tables 5.9 and 5.10 indicate that PPh_3 forms a stronger adduct bond than the PMe_3 donor for each of the trihalides.

Coupling Constants. A number of efforts have been made to correlate J with the dative bond strength. In their review of spin-spin coupling constants between boron and phosphorus in phosphinoboranes, Nöth and Wrackmeyer[2] point to the lack of any apparent correlation between J and the dative bond strength, despite the large number of adducts studied. Studies by Rudolph and Schultz[19] of the adducts of $F_{(3-n)}H_nP$, $Me_{(3-n)}H_nP$, $(Me_2N)_{3-n}F_nP$ (n=0,1,2,3) and F_2XP (X=F,Cl,Br) with BH_3 concluded that an increase of $J(^{31}P\text{-}^{11}B)$ parallels increased stability in the complexes. With boron trihalides as acceptors the coupling constants decreased with increased stability. All coupling constants were assumed to be positive, although a suggestion was made that in some circumstances sign reversal may account for anomolous trends. With very few signs determined this is still an area of considerable doubt.

Muylle[17] rationalised the decreasing trend of J in the arylphosphine adducts of the trihalides by consideration of the change in the Ph-P-Ph bond angles as the complex is formed. According to the theory of Pople and San try[20,21] the J value will vary with this angle, with J decreasing as the angle increases toward 109°. While no crystal structures of the arylphosphine-boron trihalide adducts are available, comparison of data available for compounds where Ph_3P is forming a donor bond with sulphur, or with oxygen, show that this angle does indeed increase on formation of a complex[17]. The proposal that the stronger bond will therefore generate the bigger angle change leads to the suggestion that the trends in chemical shift will be opposite to that of the J values. With no data to show what change in this angle is occurring, if any, as the halide changes on the boron nucleus, it is impossible to quantify the overall effect on the J values. The theory takes

no account of what changes are occurring at the boron nucleus as the halide is changed.

The most complete set of NMR data for boron trihalide complexes comes from the work of Miller[6] with the Me_3N complexes. This provides an interesting comparison with the phosphorus adducts as there may be expected to be nothing other than a direct σ bond between boron and nitrogen. A plot of the comparable couplings in that series (Table 5.2) with the data in Table 5.9 shows a nearly linear relationship (Fig 5.15). This tends to support a proposal that the boron nucleus is having the greater effect on the overall J value. Miller proposed that as J was, in its most simple form, an indication of the amount of *s* character in the bond, the fact that the BI_3 adduct had the smallest value, was an indication that the sign of the observed ^{11}B-^{15}N must be negative. Determination of absolute signs of J in these systems may help to clarify these apparent anomalies.

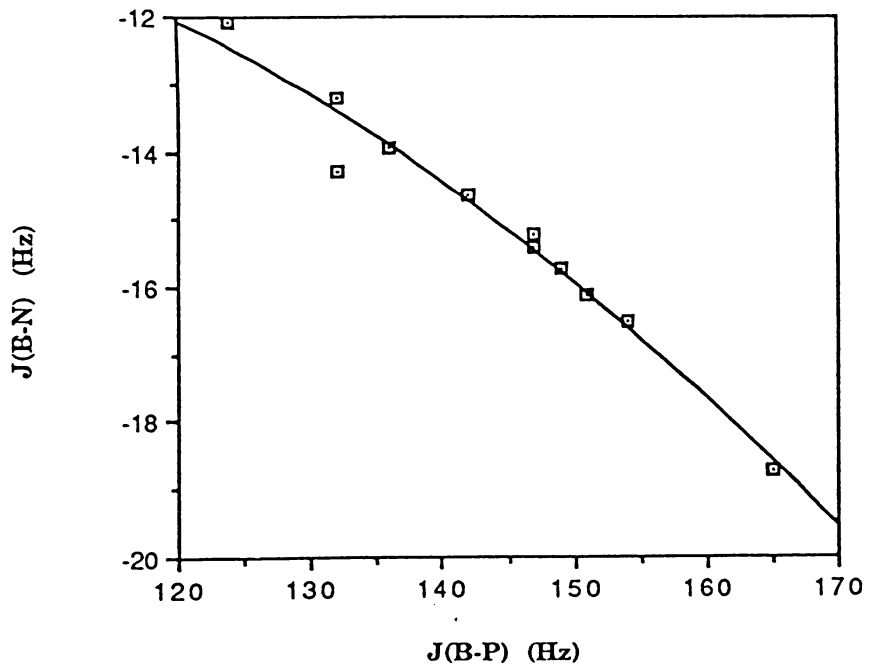

Fig. 5.15 Plot of $J(^{11}B$-$^{31}P)$ in Ph_3P trihalide adducts against $J(^{11}B$-$^{15}N)$ in the equivalent NMe_3 adducts. (data from Tables 5.2 and 5.9)

Miller considered a number of possible correlations between his observed data and factors that might provide information about the properties of the dative bond. While assuming that the complexation shift was a good indicator of bond strength, other correlations were not so apparent. As with most previously observed complexes pairwise additivity was assumed. The calculated reduced couplings were plotted against the sum of the Pauling electronegativities (Cl=3.16, Br=2.96, and I=2.66), and the sum of the van der Waal radii. Fig 5.16 shows Miller's data with;

(a) the least squares fit line drawn by Miller to omit the BF_3 adduct which Miller described as anomalous,

(b) with a simple second order exponential including all points.

The latter provides a better fit and suggests that while electronegativity is not the sole factor involved in correlation with J it is a useful indicator.

A plot of the observed $J(^{15}N\text{-}^{11}B)$ (see Table 5.2) vs the sum of the electronegativities shows a good second order fit, for all except the adduct of BFI_2 (Fig 5.17). The value for this last compound is described by Miller as being tentative and therefore may reasonably be treated with caution until more definite data is obtained. A plot of the $J(^{31}P\text{-}^{11}B)$ values in Table 5.10 against the sum of the electronegativities again shows a reasonably smooth second order curve similar to that observed in the Me_3N adducts (Fig 5.18).

Although these curves are second order, the straight-line correlation between the Me_3N and the PPh_3 adducts indicate that the factors affecting J are common in both cases and that more complicated back bonding to phosphorus is not the cause.

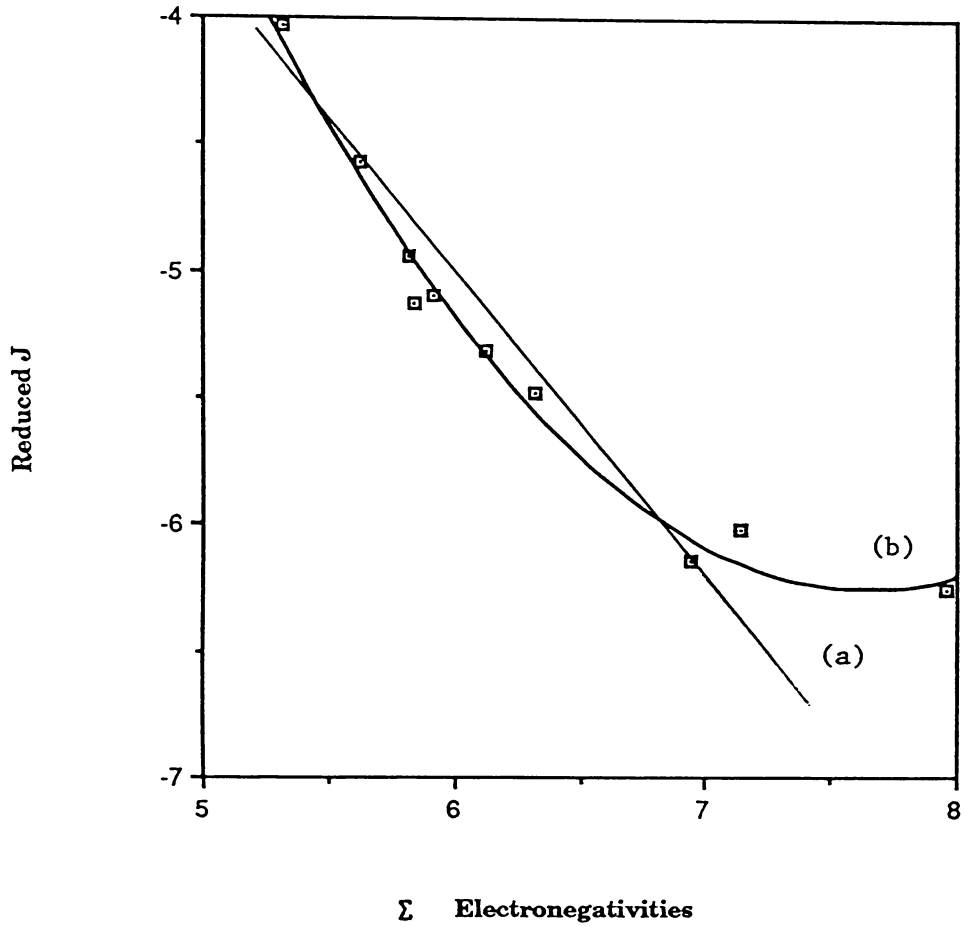

Fig. 5.16 Plot of reduced J against the sum of the halogen electronegativities in NMe_3 trihalide adducts, taken from Ref 6, and showing: (a) the least squares fit line for all adducts other than BF_3 which Miller described as anomalous. (b) a second order exponential including all adducts.

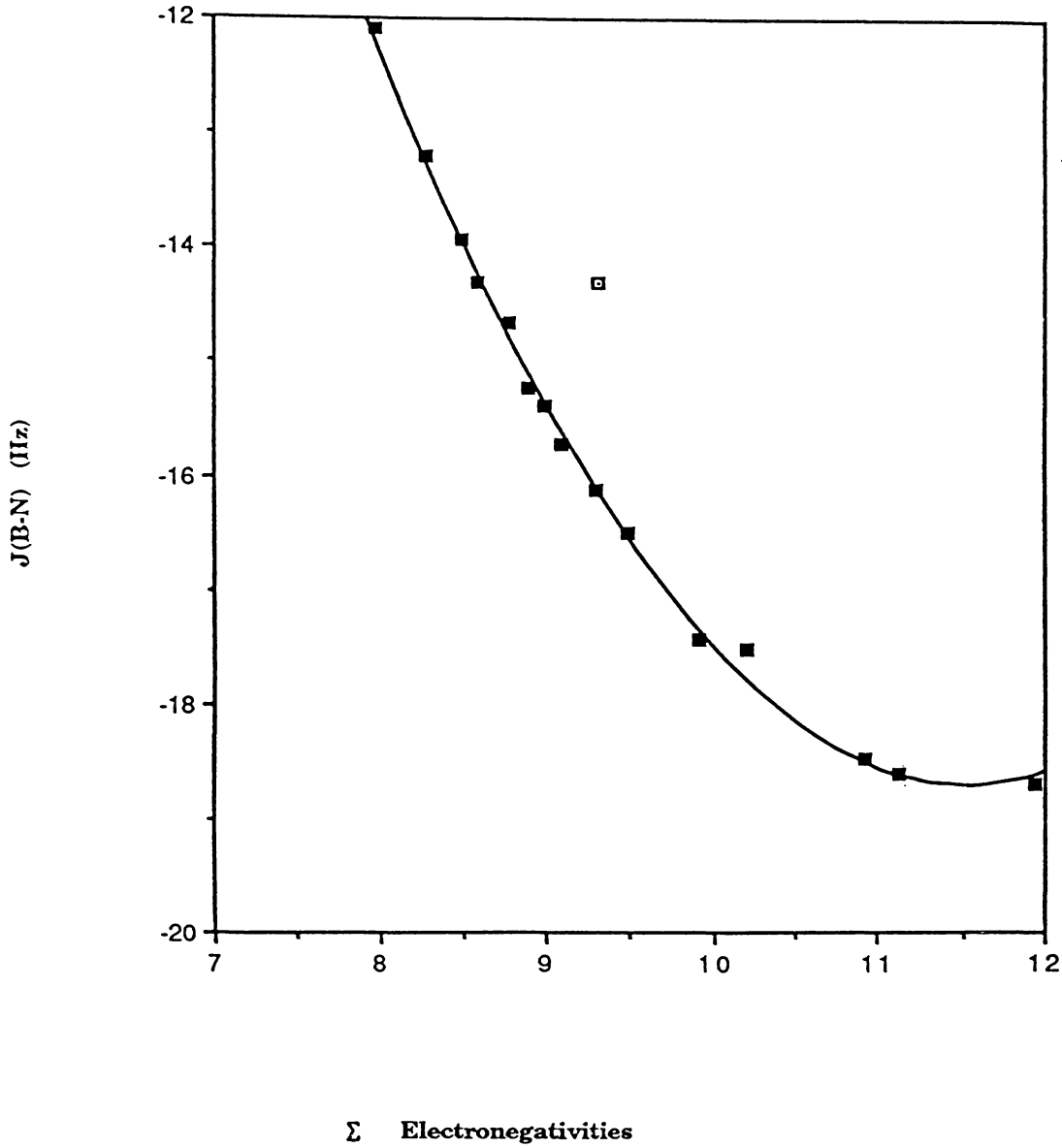

Fig. 5.17 Plot of $J(^{11}B\text{-}^{15}N)$ against the sum of the halogen electronegativities for the NMe_3 trihalide adducts. Data from ref.6. A second order curve for all data except $NME_3.BFI_2$, described as tentative, shows reasonable fit.

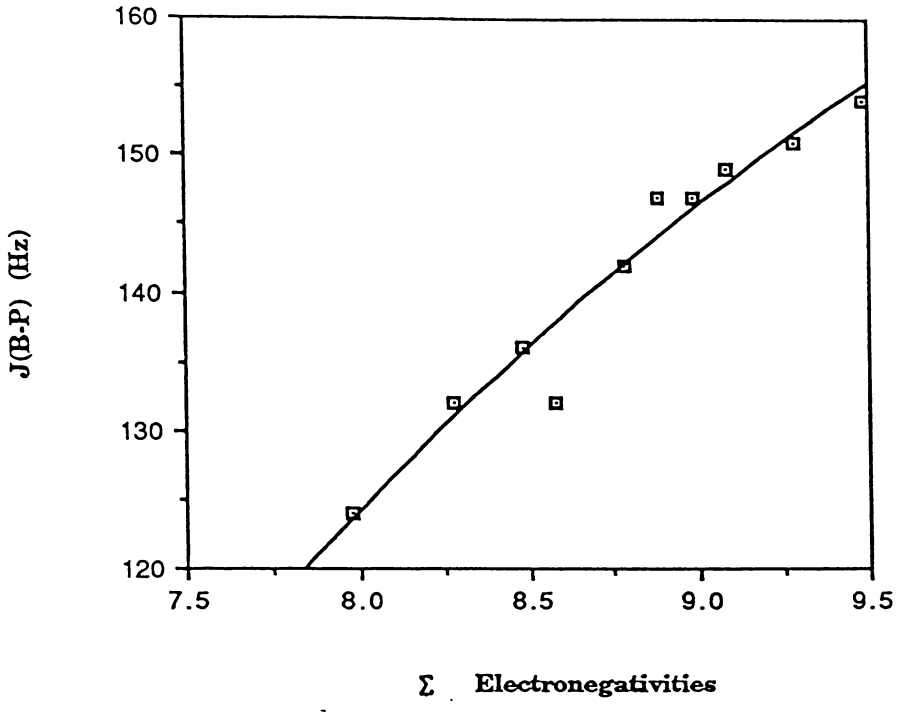

Fig. 5.18 Plot of $J(^{11}B-^{31}P)$, in the Ph_3P adducts (Table 5.10), against the sum of the halogen electronegativities. Curve fit is a second order exponential.

5.4.2 Formation of the Mixed Halide Adducts

A 1:1 mixture of BCl_3 and BBr_3 was pre-equilibrated to give a 1:3:3:1 ratio of mixed trihalides. When a 25% equivalent of PPh_3 was added, the earliest observation showed, that of the possible adducts $PPh_3.BCl_3$ (A), $PPh_3.BCl_2Br$ (B), $PPh_3.BClBr_2$ (C), and $PPh_3.BBr_3$ (D), the formation of (A),(B), (C) and (D) was in the approximate ratio of 1:6:1:0. As discussed in the experimental section, the reactions were so fast that ^{31}P data could not be obtained during the course of the reaction but it is assumed that all PPh_3 was complexed. On this assumption the above results show that (after three minutes);

(a) the initial trihalide ratio was substantially changed in the adducts

(b) there was a 2:1 preference for Cl over Br in the adducts formed initially.

There followed a progressive loss of Cl and a gain of Br in the adducts, with (A) diminishing almost to zero, (B) declining, (C) increasing, and (D) appearing then increasing, so that the ratio of Cl:Br in the adducts dropped to about 1:1 after ten minutes and decreased further to about 1:2 after two hours. In each ratio the distribution of halides is not statistical but favours the mixed halide species (B) and (C) over (A) and (D). For BCl_3/BI_3 the changes were similar but more pronounced. The $PPh_3.BCl_3$ adduct was not observed, even with an eight-fold excess of Cl in the initial halide mixture, and the proportion of I in the adducts increased markedly with time, rising to 100% when the reaction was carried to completion.

These changes were also paralleled in the BBr_3/BI_3 system, even when only a small amount of PPh_3 was added to the system (see Section 5.3.2.5). These trends are readily apparent in Table 5.4.

These results may be rationalised as follows;

(i) initial adduct formation favours the lighter trihalide,

(ii) the adducts, once formed, undergo exchange processes which replace the lighter halogen by the heavier.

The above suggests that the P-B bond most easily formed is that to the lighter trihalide, but as the heavier trihalides form the strongest bonds (see the discussion on chemical shifts above) they will predominate as the initial complexes formed undergo halogen exchange.

5.4.3 Reactions between BX_3 and $PPh_3.BY_3$

The exchange reactions discussed in Sections 5.3.1 - 5.3.3 saw similar halogen exchange within the adducts as that observed in the pre-equilibrated trihalide systems. In the experiments where X was heavier than Y stepwise replacement by the heavier halide is apparent. In the one experiment with X lighter than Y, i.e. when BCl_3 was reacted with

$PPh_3.BBr_3$ the reaction was extremely slow and a new adduct signal appeared only after about three hours. This signal was of $PPh_3.BCl_3$, and it was not until after the appearance of this signal that any of the mixed halide signals became apparent.

5.4.4 Behaviour of the free trihalide signals

Nöth and Wrackmeyer[2] expressed surprise at the wide range of reported signals for the mixed trihalides, and one suggestion for the cause of this spread was that the presence of varying amounts of starting trihalides in a system may have an effect on the chemical shifts.The two experiments with BCl_3/BI_3 mixes, using quite different ratios of the two starting halides, indicate that this is not the cause of any difference in observed chemical shifts. The first mix with a 1:3 ratio of BCl_3:BI_3 resulted in a ratio of 1:2:2.5:4 for the four trihalides BCl_3, BCl_2I, $BClI_2$, and BI_3, while an 8:1 starting mix generated the trihalides in the ratio 10:5:2:1. Although the equilibrium compositions of the trihalide mixtures are quite different, the chemical shift of each mixed trihalide signal remained unchanged. This theory also does not describe the dramatic shift in the BI_3 signal observed during the course of the reactions. This upfield shift of the trihalide signals is most pronounced when lighter halide adducts are present.

While coalescence of the free trihalide signals masked any change in the BCl_3/BBr_3 system the BBr_3/BI_3 system was studied more closely (see Section 5.3.2.5). In this case cooling the sample to -40°C allowed observation of upfield movement of the $BBrI_2$ and BI_3 signals when a 5% molar equivalent of PPh_3 was added to the equilibrated mixture.

Brown *et al*[22] reported a triethylamine boron trichloride adduct having the stoichiometry $Et_3N(BCl_3)_2$, observed at a temperature of -70°C, and they proposed two possible structures for it. One was a halogen bridged compound Et_3N-BCl_2-Cl-BCl_3, the other an ion pair $Et_3N.BCl_2^+.BCl_4^-$. Of the two they considered the former the most likely. Identification of the anions

$B_2F_7^-$ [23], $B_2F_6Cl^-$ and $B_2Cl_7^-$ [24] lend support to the formation of the halogen-bridged compound. I suggest that the shift to higher field of the BI_3 signal in the reaction above, and its resulting broadening, is the result of this signal being an averaged signal resulting from the equilibrium (compare equation 5.3)

$$PPh_3.BX_3 + BY_3 \rightleftharpoons PPh_3\text{-}BX_2\text{-}X\text{-}BY_3.$$

This equilibrium would lie furthest to the right when BY_3 was the best acceptor and X the best donor halide. The stronger the X...BY_3 interaction in this adduct form, the closer we might expect the boron chemical shifts to be to boron in the 1:1 adduct. Thus when Cl, the stronger donor halogen is present, as in $PPh_3.BCl_3$, the strong acceptor e.g. BI_3 is most likely to have the greatest upfield shift. Experimentally this was observed in the reactions described above. Even when only $PPh_3.BI_3$ was present the BI_3 signal was shifted upfield.

5.4.5 Halogen Exchange Pathway

The observations reported in Section 5.3 may now be discussed in terms of the three mechanisms that have been suggested for halogen redistribution (see Section 5.1.2.1);

(a) X^- dissociates (equation 5.1)

No signal was seen for an intermediate of the type $D.BX_2^+$, nor was there any shift in position of the observed adduct signals, that might indicate an averaged signal from the adduct with a $D.BX_2^+$ species. Thus the dissociation of the halide ions (equation 5.1) may be rejected as a mechanism for exchange in these systems.

(b) Donor-acceptor dissociation (equation 5.2)

If the donor-acceptor bond dissociation pathway of equation 5.2 is the exchange mechanism, this would mean that the most stable adduct (i.e. the one with the greatest complexation shift) would dominate within an exchanging system even if it is not the adduct most easily formed. All

changes in adduct signal strength in the experiments carried out in Sections 5.3 may be rationalised on the basis that the lighter halide adducts are;

(i) the most readily formed and

(ii) most easily dissociated.

The first of these effects may be considered as a kinetic effect while the second is a thermodynamic effect.

The observed final mix of adducts would depend on the starting ratio of trihalides and on the amount of PPh_3 added. The two BCl_3/BI_3 experiments (Section 5.3.2.1) show this situation. The mix of adducts first observed in these two experiments is quite different in each case. Although the heavier halide adducts are present at a higher proportion than their free trihalide analogs the change with time is toward a dominance of the iodine containing adduct. In the first experiment, which started with an excess of BI_3 this is rapidly achieved. In the second experiment even though BI_3 made up only 6% of the starting trihalide mixture it amounted to 40% of the adduct mix after 60min.

The experiment where BCl_3 is added to $PPh_3.BBr_3$ (Section 5.3.2.) clearly shows that the first step, at least, was dissociation of the adduct bond, as no step-wise exchange of halide occurs until after the formation of $PPh_3.BCl_3$.

(c) Associated bridging (equation 5.3)

Formation of a 2:1 adduct is the first step in the associated bridging mechanism (equation 5.3) which then leads to halide exchange through a possible four centre transition state. Such a transition state is likely to have a preferred direction of substitution, and observations in this work may be explained on the assumption that the exchange leads to a heavier halide adduct. The only anomaly in the observations is the BCl_3 + $PPh_3.BBr_3$ experiment where, because this method of halide exchange can only lead to heavier halide adducts, there must be some form of adduct dissociation to form the $PPh_3.BCl_3$ adduct before halide scrambling through an associated

bridging mechanism can occur. The strength of the heavy halide adduct bond causes this first step to be slow and explains the overall slowness of this reaction.

In summary all the observations in Section 5.3 may be explained by the ready dissociation and reforming of the donor-acceptor bond (eqn. 5.2), with halogen equilibration occurring among the free trihalides

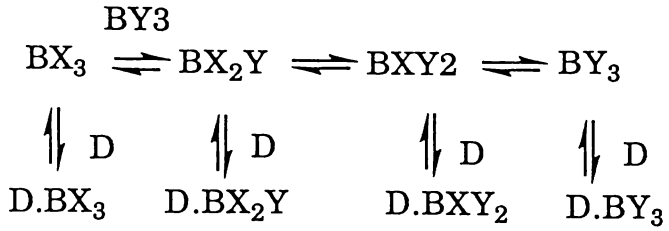

however the anomalous shifts in the free trihalide signals (Section 5.4.4) may be accounted for by the formation of a 2:1 adduct as required in the first step of eqn. 5.3. This may indicate that this exchange is also contributing to the overall exchange. In particular the results of the early stages of the BCl_3/BI_3 reactions, where the kinetically favoured $PPh_3.BCl_3$ is not observed at all, is more easily explained by a rapid formation of a 2:1 adduct of the form $PPh_3.BCl_3.BI_3$ which then undergoes rapid halogen exchange.

Which of the two mechanisms is preferred may posssibly be answered by a Raman, I.R. study to look for the four-centre transition state. Observation, or otherwise, of this transition state would be a much simpler task than attempting the convoluted mathematics involved in trying to solve the numerous exchange constants resulting from a system of multiple bond breaking.

5.5 Amine Adducts

A preliminary study was made to look for possible shifts in uncoordinated BX_3 signals in the presence of amine adducts.

5.5.1 Mixtures of $Me_3N.BCl_3$ with BCl_3

Spectra were run on samples containing different mole ratios of BCl_3 and $Me_3N.BCl_3$. The results are plotted in Fig 5.19(a) and show that with mole ratios of less than 1:1 the chemical shift of the observed trihalide signal rapidly moves upfield. With a 3.4:1 excess of BCl_3 the signal still remains 1ppm to high field of the usual position for BCl_3.

5.5.2 Mixtures of BX_3 with $Et_3N.BX_3$

In a similar manner to the experiment for $Me_3N.BCl_3$ varying mole ratios of BCl_3 and $Et_3N.BCl_3$ were observed, and the change in chemical shift of the trihalide signal is plotted against the mole ratio in Fig 5.19(b). A similar experiment for BBr_3 and $Et_3N.BBr_3$ is shown in Fig 5.19(c). Both these experiments showed a similar pattern to that shown in the $Me_3N.BCl_3$ system. Even at a mole ratio of 15:1 BBr_3:$Et_3N.BBr_3$ the trihalide signal is still upfield of the normal BBr_3 signal position.

5.5.3 Discussion of the Amine Adduct Systems

In these qualitative studies measurement of mole ratios was not extremely accurate. Nevertheless it is clear that large movements in the chemical shift of the 'free' trihalide signal occur as trihalide is added to a solution of the adduct until the mole ratio of trihalide to amine is approximately 2:1. At this point the change in chemical shift slows but has still not reached the normal position for free trihalide even at surprisingly high mole ratios.

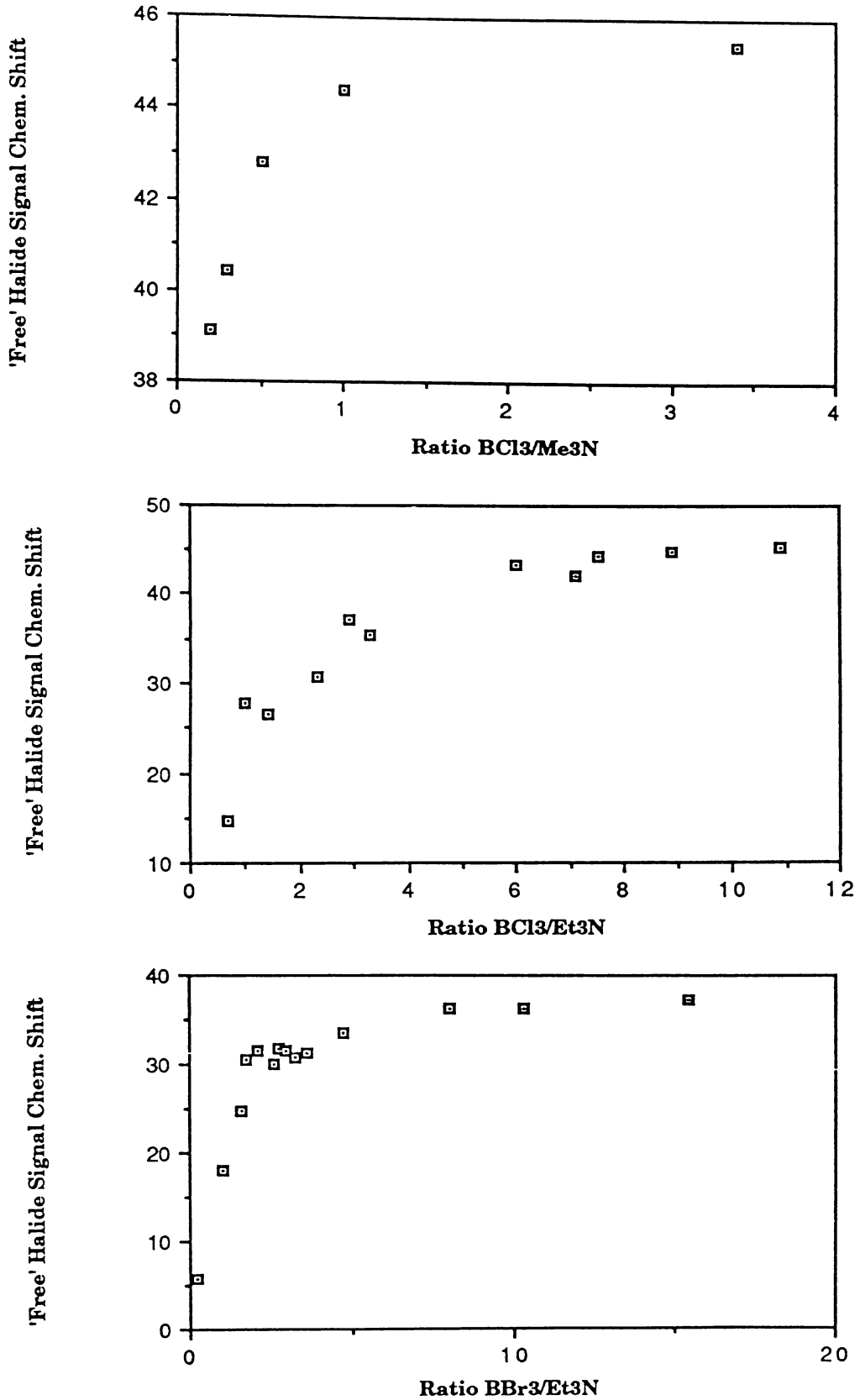

Fig. 5.19 Plot of trihalide peak chemical shift at varying mole ratios of trihalide and adduct. (a) $Me_3N.BCl_3$ and BCl_3, (b) $Et_3N.BCl_3$ and BCl_3, and (c) $Et_3N.BBr_3$ and BBr_3.

The change in slope around the 2:1 mole ratio lends strength to the proposal of a 2:1 adduct as described earlier in the PPh_3 systems. The possibility arises that the variation in free trihalide signal chemical shift figures published by different authors, and noted by Nöth and Wrackmeyer[2], might stem from some weak adduct formation in solution.

5.6 Ph_3As Adducts

A qualitative survey of the Ph_3As adducts commenced with the mixing of an approximate 1:1 mole equivalent of BCl_3 and BBr_3 and allowing them to equilibrate before adding Ph_3As to the mixture. The ^{11}B spectrum showed three peaks, at 0.3, -8.0, and -16.0ppm, with the peaks at higher field sharper than those at low field. Further addition of BCl_3 to the mixture resulted in the loss of the peak at 0.3ppm and the appearance of two new peaks, at 7.9 and -0.2ppm. Again the higher field peaks were sharpest. These peaks were within ±0.5ppm of the previously quoted figures (see Table 5.2) for the Ph_3As adducts, except the peak for BCl_3 which was at 2.5ppm to low field of the previously reported figure. This sample was allowed to stand overnight and when the spectrum was rerun the low field signals had sharpened and moved, to be at 6.0 and -0.8ppm for the BCl_3 and BCl_2Br adducts respectively.

A second mixture using an excess of BCl_3 over BBr_3 was allowed to equilibrate and addition of Ph_3As resulted in the adduct mix shown in Fig. 5.20(a). While the sharp signals for $Ph_3As.BClBr_2$ and $Ph_3As.BBr_3$ have remained at their previously observed positions, the signal for $Ph_3As.BCl_3$ is now found at 5.1ppm and that for $Ph_3As.BCl_2Br$ at -1.1ppm. The low field adduct signals are again broad. On lowering the temperature of this sample to 0°C each signal splits into two peaks that sharpened on further cooling to -40°C (Fig. 20(c)). The resultant pairs of peaks were in an approximate 1:6 ratio. The peak for $Ph_3As.BCl_3$ has been split into a peak at 6.9ppm (minor) and a peak at 4.8ppm (major). For $Ph_3As.BCl_2Br$ the two peaks are at 0.8ppm (minor) and -1.2ppm (major), with those for $Ph_3As.BClBr_2$ at

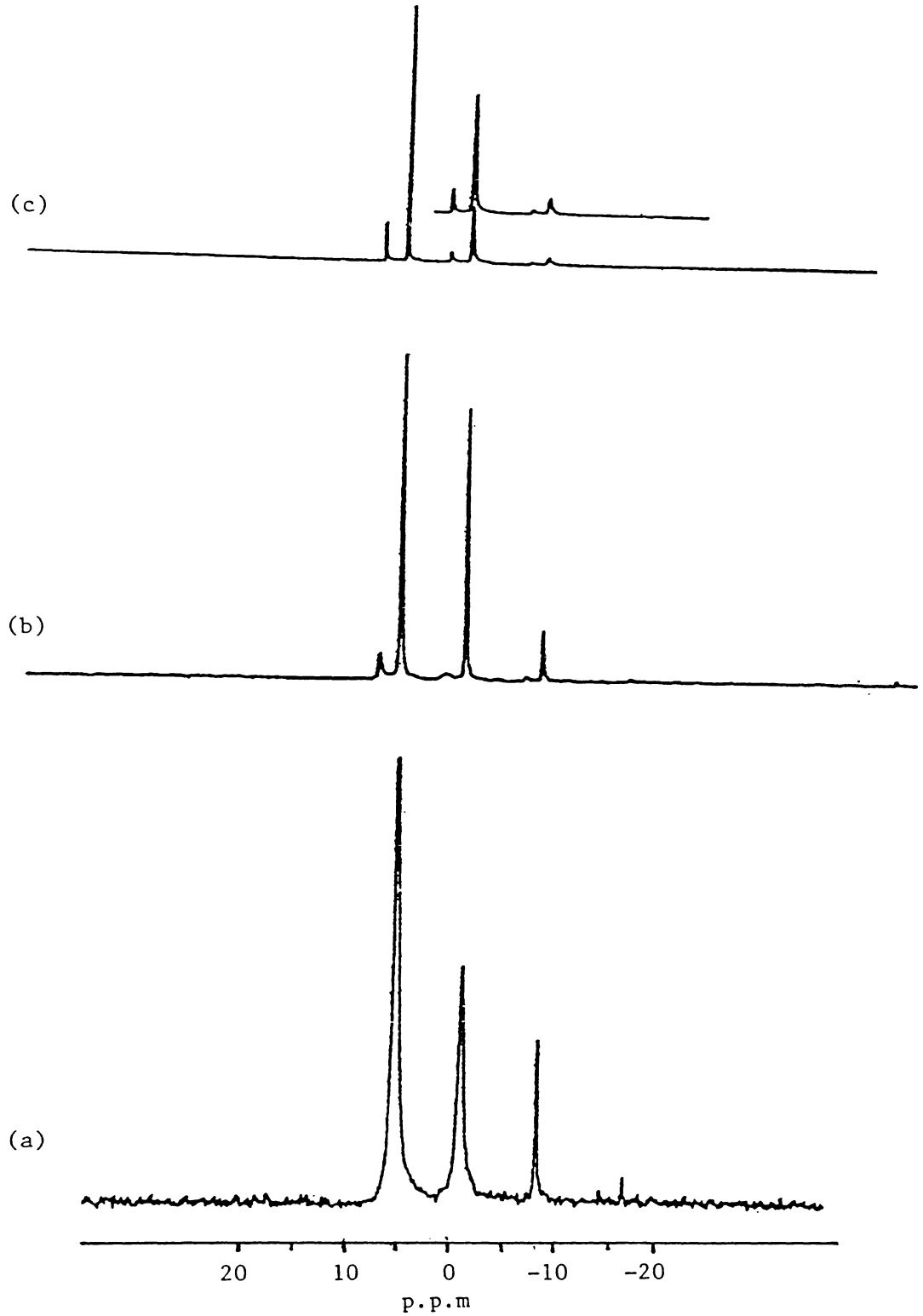

Fig. 5.20 (a) R.T. ^{11}B NMR spectrum of adduct signals resulting from the addition of Ph_3As to an equilibrated mix of BCl_3 and BBr_3. (b) Spectrum run at 0°C. (c) Same sample at -40°C. See Section 5.6 for a discussion of these spectra.

-6.4ppm (minor) and -8.1ppm (major). $Ph_3As.BBr_3$ is not clearly defined in this spectrum.

A sample of $Ph_3As.BCl_3$ made in the NMR tube by adding equimolar amounts of Ph_3As and BCl_3 gave a signal at 5.4ppm. When cooled to 10°C this signal broke into two peaks, a small peak at 6.8ppm and a major peak at 5.1ppm. Further cooling, to -50°C, resulted in the sharpening of these peaks ($\upsilon_{1/2}$<3Hz) and a shift to 6.9 and 4.8p.pm.

Figs. 5.21 and 5.22 follow a reaction containing varying mixes of BCl_3 and Ph_3As. A 1:2 mixture of BCl_3:Ph_3As generated a spectrum, at 0°C, containing two peaks, at 6.9 and 4.9p.pm, in a 1:2 ratio. Further addition of Ph_3As altered this to a 1:1.75 ratio of peak intensities (Fig. 5.21(a)). Addition of BCl_3 to this system resulted in a signal at 5.4ppm at R.T. Cooling to -20°C resulted in the two peaks, 6.9 and 4.9ppm, in a 1:14 ratio (Fig. 5.21(b)).

A further addition of BCl_3 resulted in a R.T. signal at 8.0ppm that had a shoulder at 9.5ppm (Fig. 5.21(c)). Two small, broad peaks, at 31.7 and 27.0ppm, are similar to those observed in the PPh_3 adduct systems and are probably hydrolysis products. Cooling of this sample narrowed the peak at 10°C (Fig. 5.21(d)), but at -20°C a very broad peak, centered at 7.2ppm was observed (Fig. 5.21(e)). Further cooling (Figs. 5.21(f) and 5.21(g)) resulted in a sharp peak at 4.7ppm and a weak broad peak at 26.5ppm. There was no indication of any peak at 6.9ppm.

A final addition of BCl_3 resulted in a R.T. peak at 23.1ppm (shoulder at 26.3ppm) and a small peak at 31.7ppm (Fig. 5.22(b)). Warming the sample to 30°C sharpened the 23.1ppm peak without shifting it (Fig. 5.22(a)). Cooling the sample resulted in a transition state at -20°C (Fig. 5.22(e))which at -50°C had resolved into a sharp peak at 4.8ppm and a broad peak at 39.3ppm (Fig. 5.22(g)).

In an experiment with BBr_3 a slight excess of Ph_3As was added to the halide. A sharp signal was observed at -15.9ppm, as had been the case in the mixed halide sample mentioned above. When cooled to -40°C a signal, 1/8th

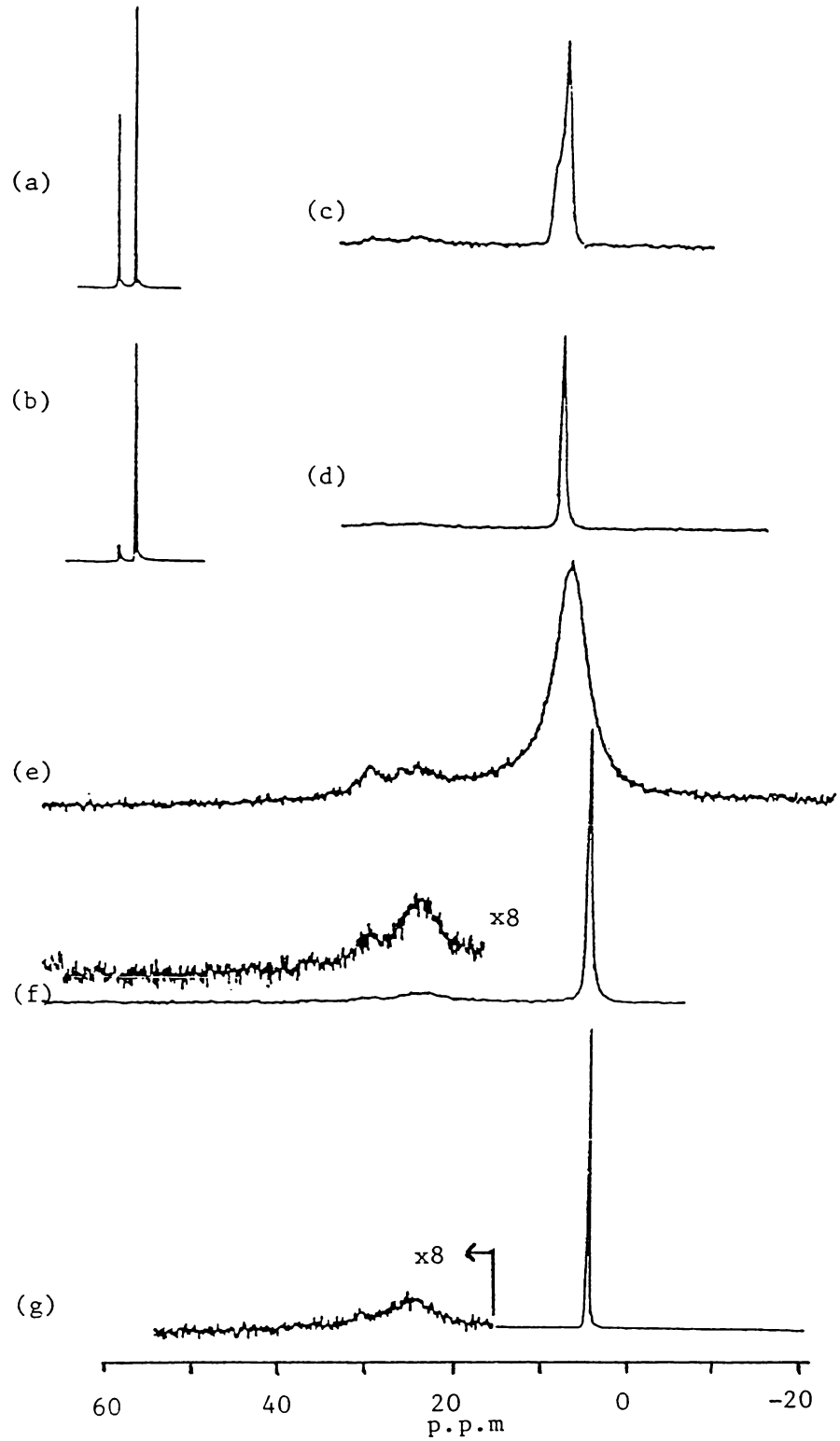

Fig. 5.21 Variable temperature ^{11}B NMR spectra of mixtures of BCl_3 and Ph_3As: (a) 0°C spectrum of 1:2 mix, (b) -20°C spectrum after addition of more BCl_3, (c) R.T spectrum after further addition of BCl_3, (d) same sample at 10°C, (e) Spectrum run at -20°C, (f) -30°C, and (g) -40°C.

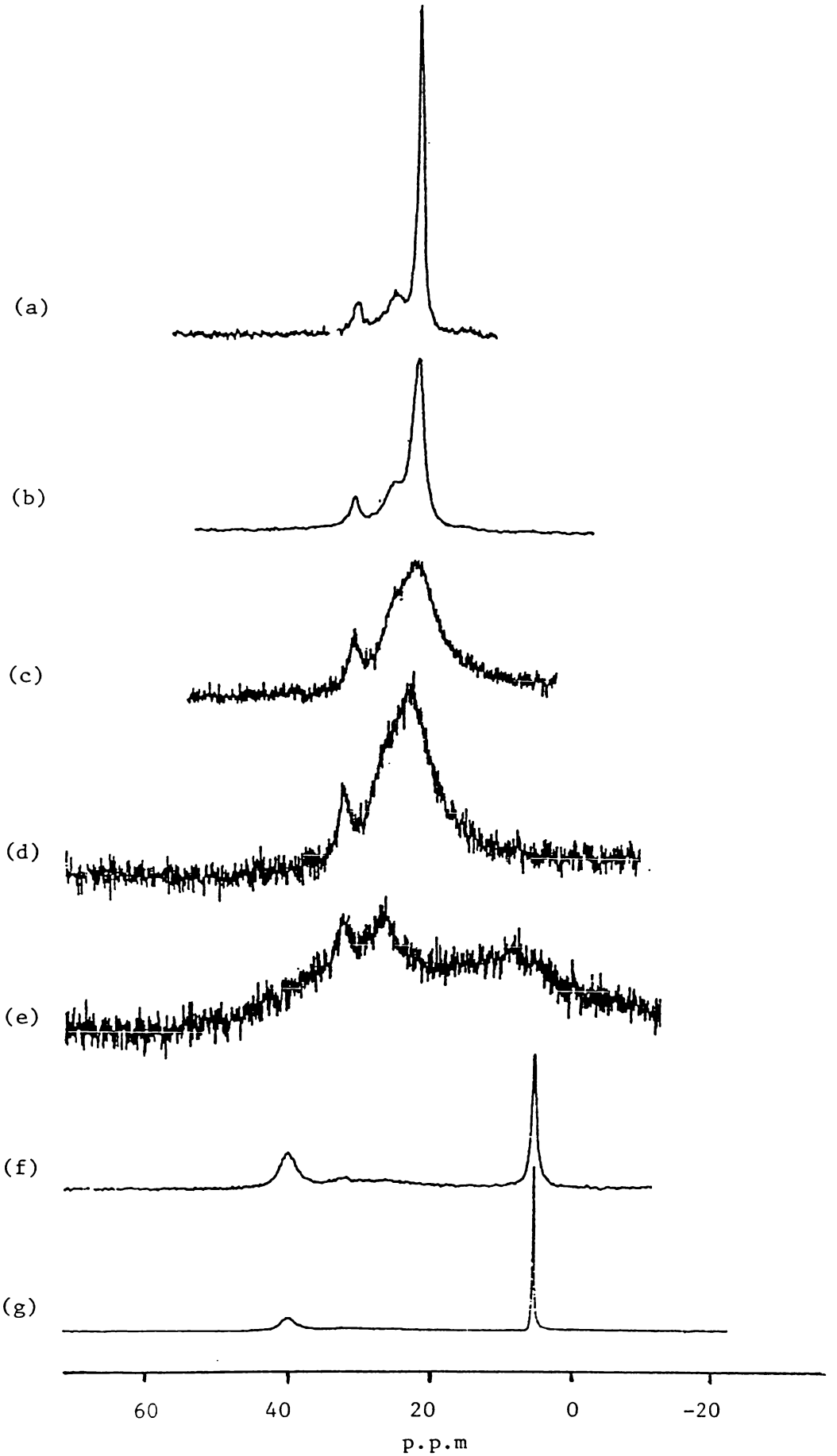

Fig. 5.22 A further addition of BCl_3 to the sample shown in Fig. 5.21 resulted in ^{11}B NMR spectra at the following temperatures: (a) 30°C, (b) R.T., (c) 0°C, (d) -10°C, (e) -20°C, (f) -40°C, and (g) -50°C.

the size of the -15.9ppm signal, was apparent at -24.2ppm.

5.6.2 Summary of Ph_3As Adducts

The different chemical shifts observed for $Ph_3As.BCl_3$ at R.T., along with the splitting of the signals at lower temperature indicate the presence of two species in solution and that the R.T. signals are not the true chemical shifts of the Ph_3As adducts. Nöth and Wrackmeyer[2] quote chemical shifts (taken from data by Hartman and Schrobilgen) for the tetrahalide anions BCl_4^-, BCl_3Br^-, $BCl_2Br_2^-$, $BClBr_3^-$ and BBr_4^- as 6.5, 2.9, -3.8, -12.6, and -24.1 ppm respectively, in CH_2Cl_2 solution. It has been noted[25] that for the tetrahaloborate ions the pairwise additivity model of Vladimiroff and Malinowsky[26] provides the best empirical model for chemical shifts. Using this model Hartman and Schrobilgen[27] obtained calculated chemical shifts that were within 0.5ppm of the observed result. The small peaks obtained in the cooled samples in this work agree well with the published figures for BCl_4^- and BBr_4^- but do not match in the case of the mixed halide species. The published work used symmetric tetra-*n*-butyl ammonia as the counter-ion. The unsymmetric Ph_3As, presumably forming Ph_3AsH^+ used in this work may be expected to interact with the dipole of the unsymmetric mixed tetrahalides to result in a different chemical shift in these species. This effect would be greatest in the least symmetric species, $BCl_2Br_2^-$. Assuming the smaller peaks may be assigned to the tetrahalide species the correct chemical shifts of the Ph_3As adducts are listed in Table 5.11.

Table 5.11. Observed Chemical Shifts of the Ph_3As Adducts.

Adduct	$\delta(^{11}B)$	Adduct	$\delta(^{11}B)$
$Ph_3As.BCl_3$	4.8	$Ph_3As.BClBr_2$	-8.1
$Ph_3As.BCl_2Br$	-1.2	$Ph_3As.BBr_3$	-15.9

These experiments suggest that there is a competing reaction

occurring within the systems. Alongside the reaction of Ph_3As with BCl_3 to form the adduct there is a reaction that generates BCl_4^-. When there is a deficit of Ph_3As in the system adduct formation dominates, and the signal observed at R.T. is a signal that is the average of the adduct signal and a signal that is concentration dependent, similar to those observed in the PPh_3 and amine adduct systems. When Ph_3As is in excess in the system, the resultant R.T. signal is the time average of the adduct and the tetrahalide anion.

There was no indication of tetrahalide ions in the PPh_3 adduct systems even though similar handling techniques were used for both systems. It is probable that the amount of moisture in the stock BCl_3 solution used increased as the series of experiments progressed and may have reached a critical level in these latter experiments.

This work has been carried out under conditions that have not excluded all moisture from the system. Certainly the purification of BCl_3 was not carried out to the extent used by Briscoe and Robinson[28] when they were determining its molecular weight. Their purification involved fractional distillation in low temperature columns, followed by three months standing over mercury, further fractionation, standing over sodium amalgam for a further three months and a final fractionation in a vacuum! Other authors studying the boron trihalide adducts do not comment on any specific purification steps and it is unlikely that the moisture level in the systems studied here is much different to that in other systems reported. If that is the case this work highlights the interaction of the moisture in the adduct systems. Obviously considerable care must be taken to ensure the dryness of the systems. Vacuum lines used in sample preparation would need to be greaseless as BCl_3 in particular reacts with vacuum grease. Until this type of sample preparation was carried out it would be difficult to be certain that moisture was not having a catalytic effect in any of the halide exchange systems discussed in this work.

Chapter 5 References

1. J.Emri and B.Györi, *Comprehensive Coordination Chemistry*, ed. G. Wilkinson, R.D.Gillard and J.A.McCleverly, Pergamon, Oxford 1987 Vol. 3, Chap 24.
2. H.Nöth and B.Wrackmeyer, *NMR14*, ed. P.Diehl, E. Fluck, and R. Kosfeld, Springer-Verlag, 1978, p85.
3. J.S.Hartman and J.M.Miller, *Adv. Inorg. Chem. and Radiochem.*, **21,** *147*, 1978.
4. J.Aron and T.A.Ford, *S. African J. Chem.*, **35,** *129,* 1982.
5. B.Benton-Jones, M.E.A.Davidson, J.S.Hartman, J.J.Klassen, and J.M.Miller, *J. Chem Soc. Dalton Trans, 2603.* 1972.
6. J.M.Miller, *Inorg Chem.*, **22,** *2384,* 1983
7. (a) J.M.Chehayber and J.E.Drake, *Inorganica Chimica Acta,* **112,** *209*, 1986
   (b) J.E.Drake, L.N.Khasrou, and A.Majid, *Can. J. Chem.*, **59,** *2417*, 1981
8. C.J.Foret , K.R.Korzekwa, and D.R.Martin, *J. Inorg. Nucl. Chem.*, **42** *1223* 1980.
9. B.Wrackmeyer, *J. Mag Reson.*, **66,** *172,* 1986.
10. R.Minkwitz and R.Nass, *Z. Anorg. Allg. Chem.*, **549,** *195*, 1987.
11. D.B.Beach and W.L.Jolly, *J Phys. Chem.*, **88,** *4647*, 1984.
12. E.Muylle and C.P.van der Kelen, *Spectrochimica Acta,* **32A,** *599,* 1976.
13. Harmon and Cummings, *J. Am. Chem. Soc.,* **87,** *539,* 1965.
14. M.J.Taylor, Auckland University, personal communication.
15. J.M.Miller and T.R.B.Jones, *Inorg. Chem.*, **15**, *284*, 1976.

16. P.N.Gates, E.J.McLauchlan, and E.F.Mooney, *Spectrochimica Acta* **21**, *1445,* 1965.

17. E.Muylle, C.P.van der Kelen, and E.G.Claeys, *Spectrochimica Acta* **32A**, *1149,* 1976.

18. D.L.Black and R.C.Taylor, *Acta Cryst.*, **B31**, *1116,* 1975.

19 R.W.Rudolph and C.W.Schultz, *J. Am. Chem. Soc.*, **93,** *6821,* 1971.

20. J.A.Pople, and D.P.Santry, *Molec. Phys.*, **8**, *1*,1964.

21. J.F.Nixon, and A.Pidcock, *Annual Review NMR Spectroscopy*, Academic Press N.Y., **2** ,*354*, 1969.

22. H.C.Brown, P.F.Stehle and P.A.Tierney, *J. Am. Chem. Soc.* **79**, *2021* 1957.

23. J.S.Hartman, and P.Stilbs, *J.C.S. Chem. Comm. 566*, 1975.

24. N.C.Craig , J.Prananta, S.J.Reinanum, J.S.Sprague and P.S.Stevens, *J.Am. Chem. Soc.*, **108** *4378,* 1986.

25. B.F.Spielvogel and J.M.Purser, *J. Am. Chem. Soc.*, **93**, *4418*, 1971.

26. T.Vladimiroff and E.R.Malinowski, *J. Chem. Phys.*, **46**, *1830*, 1967.

27. J.S.Hartman and G.J.Schrobilgen, *Inorg. Chem.*, **11**, *940,* 1972.

28. H.V.A.Briscoe and P.L.Robinson, *J. Chem. Soc.*, *696*, 1925.

Chapter 6 Tin Halide Exchange Systems

6.1 Introduction

NMR has been extremely useful in the study of a number of halide exchange systems. As noted in the previous chapter the mixed boron trihalides cannot be isolated, but are readily studied using NMR. The mixed germanium tetrahalides (see Chapter 3) are similarly observed[1] using NMR. Watkinson[2] was able to use ^{73}Ge NMR to study halide exchange in mixed nucleus systems $GeX_4 : MY_y$ (y = 4 for M = Si, Sn; y = 2 for Hg; X,Y = Cl or Br).

For tin, mixing between the tin tetrahalides was one of the earliest studies of exchanging systems[3]. More recently Coddington and Taylor[4] have studied exchange in the Sn(II) halide systems (SnX_3^-) and found a nuclear shielding order opposite to that present in Sn(IV) halide systems (see Table 6.1).

Table 6.1 Chemical Shifts of Tin Chlorides and Bromides

Tin(II) Halide Ions[a]	δ/ppm	Tin(IV) Halides[b]	δ/ppm
$(SnCl_3)^-$	-26	$SnCl_4$	-150±2
$(SnCl_2Br)^-$	33	$SnCl_3Br$	-263±3
$SnClBr_2)^-$	87	$SnCl_2Br_2$	-385±1
$(SnBr_3)^-$	142	$SnClBr_3$	-508±1
		$SnBr_4$	-638±1

(a) Ref. 4. Spectra run at -60°C.

(b) Ref. 3

Workers in this Department[5][6] were looking at the synthesis of the unsymmetric $[R_3MCo(CO)_3M'R'_3]^-$ anions where M,M' were Group 14 elements and R,R' = Cl, Br, and $Co(CO)_4$. One experiment reacted Et_4NSnCl_3 with $Br_3SnCo(CO)_4$ in an attempt to generate

$\{Br_3SnCo(CO)_3SnCl_3\}^-$. A crystal structure[6] analysis resulted in the structure shown in Fig. 6.1, but refinement below an R factor of 0.069 could not be achieved apparently because of random occupation of the halogen sites. This, in turn, indicated that halide exchange was occurring within the molecule and I undertook a ^{119}Sn NMR study in an attempt to clarify the situation.

6.2 Experimental

The ^{119}Sn NMR spectra were run on the Bruker AM400 at Auckland University at an observation frequency of 149.215MHz. 8K data points were collected over an 83,333Hz window to provide a resolution of 10.17Hz/point. The proton coupled spectra were collected using a 90° tip angle and a 0.5s relaxation delay. The spectra were referenced to external $^nBu_3SnCl$ taken to have a chemical shift of 150ppm w.r.t. Me_4Sn. The number of scans collected are noted in the figure captions. Samples were run as CH_2Cl_2 solutions in sealed 8mm O.D. tubes placed concentrically within 10mm O.D. tubes.

Run 1. Et_4NSnCl_3 (0.213g; 0.6mmoles) in CH_2Cl_2 (10mls) was added to a solution of $Br_3SnCo(CO)_4$ (0.319g; 0.6mmoles) in CH_2Cl_2 (10mls). After 30min no further changes were apparent in the infrared spectra. The solvent was removed and the mixture extracted with hexane which yielded a trace of unreacted $Br_3SnCo(CO)_4$. The ^{119}Sn spectrum obtained from a CH_2Cl_2 solution of the product is shown in Fig. 6.2.

As the Cl/Br ratio of the product is not necessarily the same as that of the starting materials an electron probe analysis was carried out on the product. This resulted in atomic percentage values that gave an approximate empirical Co:Sn:Cl:Br ratio of 1:2:2:4. This bias towards Br was also apparent in a Fast Atom Bombardment (FAB) mass spectrum obtained at the same time. The mass spectrum indicated that a mixture of anions was present but the complicated spectrum was difficult to assign.

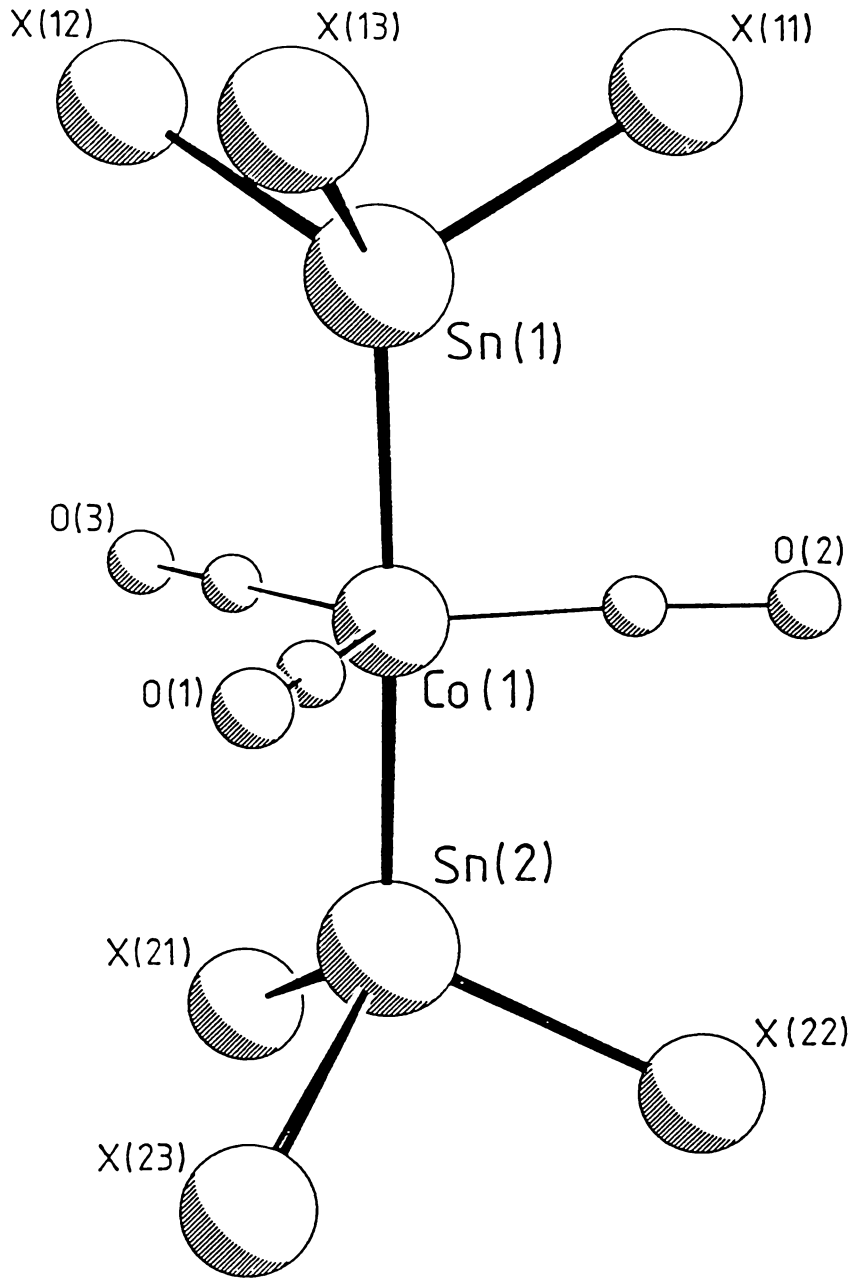

Fig. 6.1 A view of the anion of $Et_4N[Br_2ClSnCo(CO)_3SnClBr_2]$, (X = disordered Br, Cl in the ratio 2:1). Some bond lengths (Å) are: Co(1)-Sn(1) = Co(1)-Sn(2) = 2.464(3); Sn-X = 2.498(3) (average, range 2.467-2.541); bond angles; Sn(1)-Co-Sn(2) = 177.9(1)°; X-Sn-X = 99.4(1)° (average, range 96.5-102.7°).

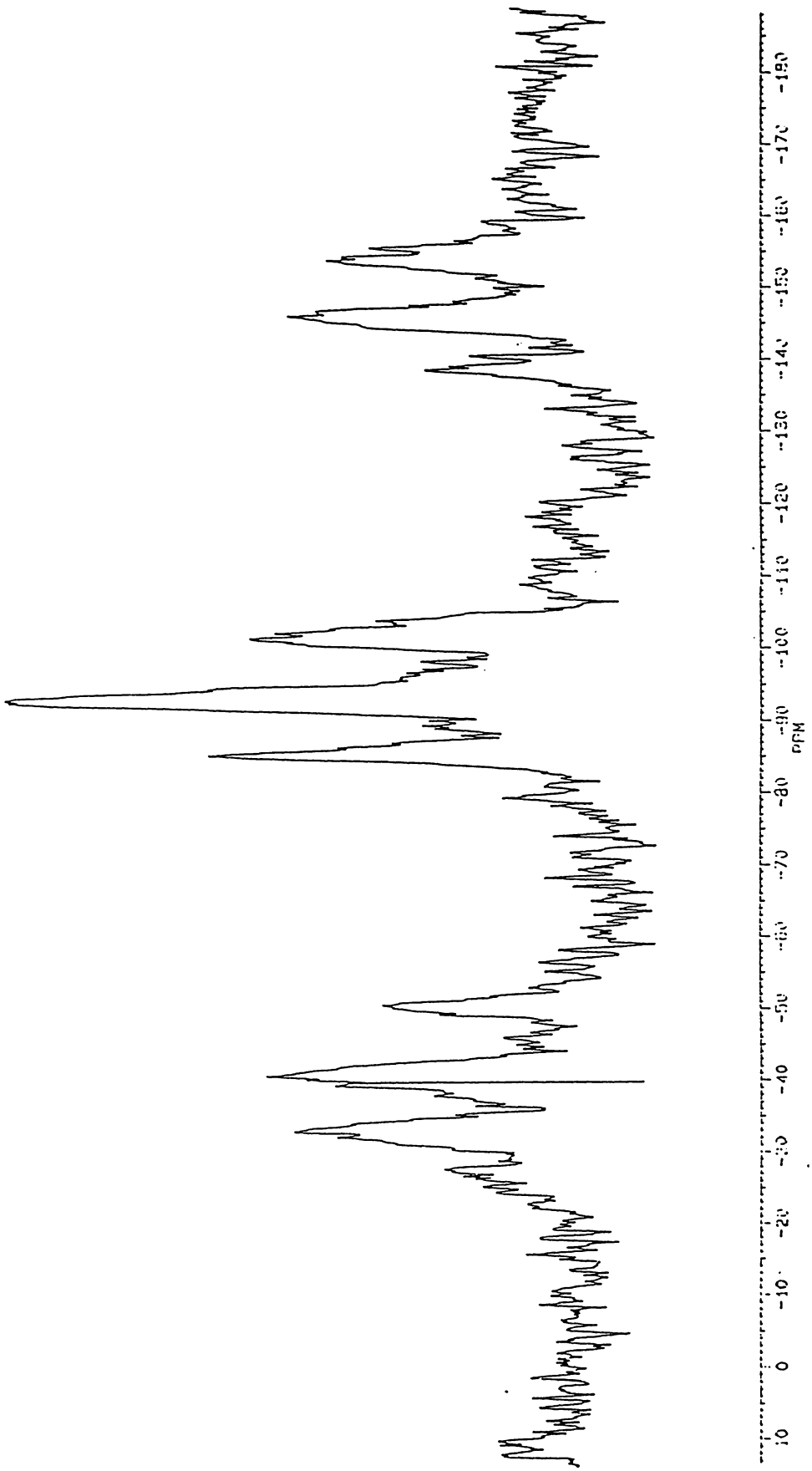

Fig. 6.2 The ^{119}Sn NMR spectrum of a CH_2Cl_2 solution of Et_4NSnCl_3 and $Br_3SnCo(CO)_4$. 6034 scans of 8K data points were collected over an 83,333Hz window.

Run 2. Equimolar amounts of Et_4NSnBr_3 and $Cl_3SnCo(CO)_4$ were stirred in CH_2Cl_2. After removal of the solvent, and washing with hexane, the product was dissolved in CH_2Cl_2 and the ^{119}Sn NMR spectrum (Fig. 6.3) obtained.

Run 3. A 1:3 ratio of the Et_4N^+ salts of $\{Cl_3SnCo(CO)_3SnCl_3\}^-$ and $\{Br_3SnCo(CO)_3SnBr_3\}^-$ were mixed in CH_2Cl_2. Table 6.2 lists the peak intensities of the resultant ^{119}Sn NMR spectrum.

The chemical shifts listed in Table 6.2 have an error of ±2ppm, while the intensity data are based on measured peak height and are accurate to ±10%. In the case of the symmetric molecules each peak represents two tin atoms while all other peaks correspond to one tin atom.

6.3 Results

Table 6.2 lists chemical shift and relative intensity of the peaks observed in the three experiments. Study of the first spectrum indicated that part of the low frequency range was not fully covered and so the window was adjusted for the next two spectra. With electron probe analysis indicating a bias of bromine over chlorine in Run 1 peak intensities in the NMR spectrum can be assigned on the assumption that the bromine rich anions are those to high field. (This assumption is confirmed by the results from Run 3 with its known bias of bromine). The most intense peak in both Runs 1 and 2, at -92.6ppm, is assigned to the two tins in the symmetric anion $\{Br_2ClSnCo(CO)_3SnBr_2Cl\}^-$ while the two peaks at -101 and -145ppm, being of similar intensity are assigned to Sn^1 and Sn^2 of $\{Br_2ClSn^1Co(CO)_3Sn^2Br_3\}^-$. Similar arguments regarding equivalent peak intensities for the two tins within one molecule lead to the assignments shown in Table 6.2.

The chemical shifts and relative intensities of the observed peaks in both of the first two runs indicates that the scrambling occurs readily

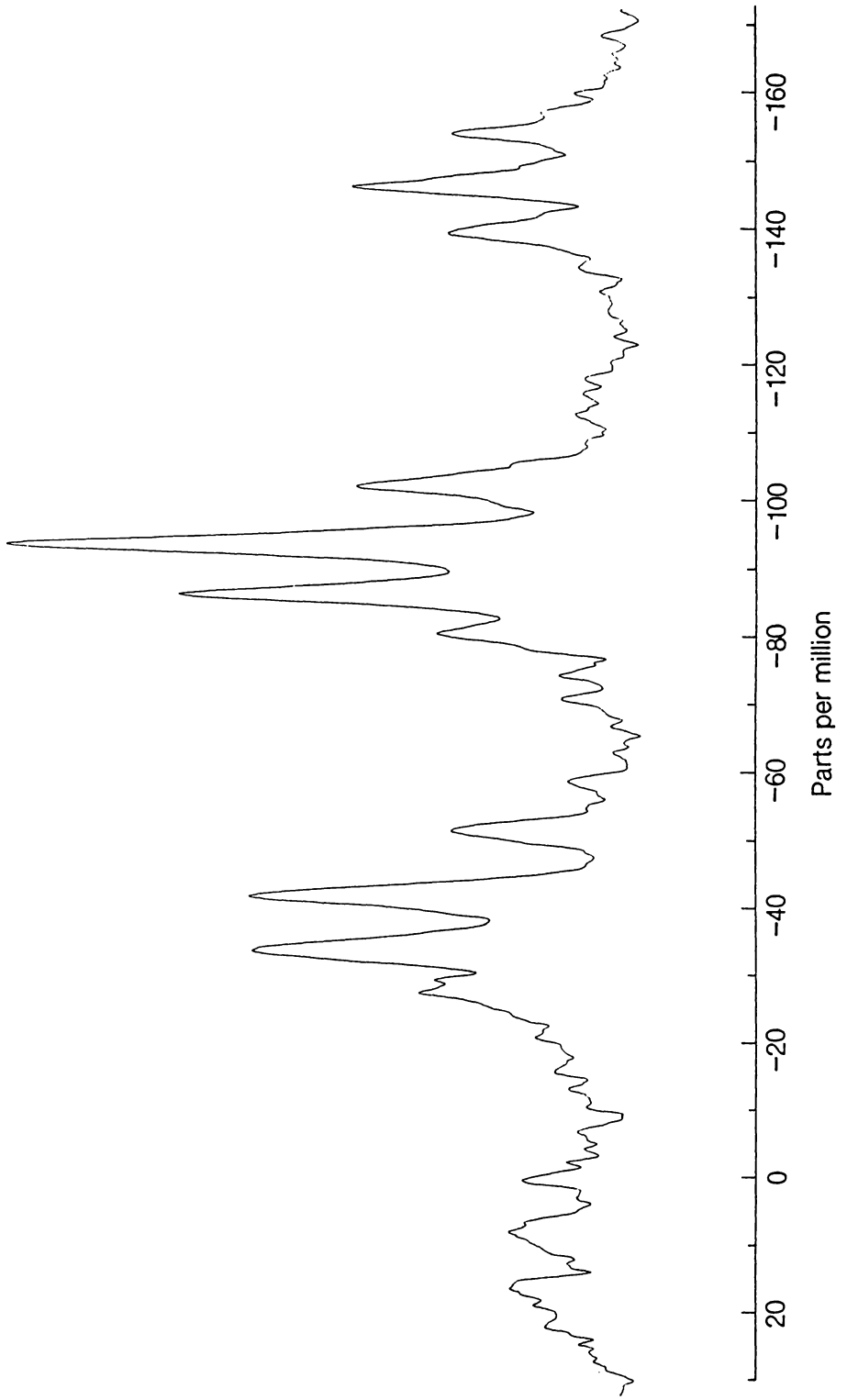

Fig. 6.3 The ^{119}Sn NMR spectrum of a CH_2Cl_2 solution of Et_4NSnBr_3 and $Cl_3SnCo(CO)_4$. 36,000 scans of 8K data points were collected over an 83,333Hz window.

Table 6.2 Chemical Shift and Relative Intensity of Peaks Observed in the ^{119}Sn Spectra of Cobalt-Tin Halide Anions.

Peak Position δ/ppm	Relative Intensity Run 1	Run 2	Run 3	Assignment[a]
-153	52	28	100	$\{Br_3\mathbf{Sn}Co(CO)_3\mathbf{Sn}Br_3\}^-$
-145	57	44	51	$\{Br_3\mathbf{Sn}Co(CO)_3SnBr_2Cl\}^-$
-138	36	29	n.o.	$\{Br_3\mathbf{Sn}Co(CO)_3SnBrCl_2\}^-$
-133	15	7	n.o.	$\{Br_3\mathbf{Sn}Co(CO)_3SnCl_3\}^-$
-101	64	44	51	$\{Br_2Cl\mathbf{Sn}Co(CO)_3SnBr_3\}^-$
-93	100	100	36	$\{Br_2Cl\mathbf{Sn}Co(CO)_3\mathbf{Sn}Br_2Cl\}^-$
-85	71	72	n.o.	$\{Br_2Cl\mathbf{Sn}Co(CO)_3SnBrCl_2\}^-$
-79	15	31	n.o.	$\{Br_2Cl\mathbf{Sn}Co(CO)_3SnCl_3\}^-$
-51	44	28	14	$\{BrCl_2\mathbf{Sn}Co(CO)_3SnBr_3\}^-$
-41	61	61	n.o.	$\{BrCl_2\mathbf{Sn}Co(CO)_3SnBr_2Cl\}^-$
-33	56	61	n.o.	$\{BrCl_2\mathbf{Sn}Co(CO)_3\mathbf{Sn}BrCl_2\}^-$
-28	22	34	n.o.	$\{BrCl_2\mathbf{Sn}Co(CO)_3SnCl_3\}^-$
1	n.o.	35	n.o.	$\{Cl_3\mathbf{Sn}Co(CO)_3SnBr_3\}^-$
10	15	37	n.o.	$\{Cl_3\mathbf{Sn}Co(CO)_3SnBr_2Cl\}^-$
17	(b)	37	n.o.	$\{Cl_3\mathbf{Sn}Co(CO)_3SnBrCl_2\}^-$
23	(b)	34	n.o.	$\{Cl_3\mathbf{Sn}Co(CO)_3\mathbf{Sn}Cl_3\}^-$

(a) The tin atom for which the peak is assigned is highlighted.

(b) Region not examined.

regardless of the method of formation of the compound. The better S/N ratio of the spectrum in Fig.6.3 has resulted in the confirmation of two further peaks in two of the previously observed families of multiplets, while the cluster of peaks in the 0-20ppm region of the spectrum are still not fully resolved even with the higher number of scans used in this second run. The third experiment, containing a 1:3 mixture of the two anions

$\{Cl_3SnCo(CO)_3SnCl_3\}^-$ and $\{Br_3SnCo(CO)_3SnBr_3\}^-$, confirms the high field position of the bromine rich species.

6.4 Discussion

This NMR study has confirmed the presence of halide exchange within the systems and has provided data on the relative proportion of each species within the mixture, information not available from any other data.

There are two effects when, say, one Br is replaced by a Cl. First, a chemical shift change averaging 51ppm per replacement is found in the substituted Sn resonance. Secondly, an approximate 7ppm shift per halogen replacement is found for the resonance of the tin atom at the opposite end of the molecule. This latter shift change is greatest, at 9ppm, when $SnBr_3$ is replaced by $SnBr_2Cl$. The change is less at each further stepwise exchange of Cl for Br in the remote group.

These shift changes compare with a change of 56ppm per chlorine/bromine replacement in the tin(II) halide ions and 122ppm per halogen exchange in the tin(IV) halides. Thus the size of the shift is close to that in the Sn(II) species, but the sign of the change is in the same direction as the tin(IV) halides.

Bonding to one or more transition elements leads to remarkably low shielding of the tin atom[7], with $MeSn[Co(CO)_4]_3$ having a $\delta(^{119}Sn)$ value of +483ppm, the highest so far known. For the compounds studied here Table 6.3 shows the approximate $\Delta\delta$ values when Br is replaced by $CoSnY_3$ in X_3Sn-Br.

The rather low shielding resulting from the bonding of a transition element is the opposite effect to that which might be expected from the attachment of an electropositive element to tin, and the expected electron withdrawal. $D\pi$-$d\pi$ overlap involving tin and the transition metal,

Table 6.3 $\Delta\delta$ Values Observed in the Series X_3Sn-Br vs. X_3Sn-$CoSnY_3$[a]

X_3	$\delta^{(119)}Sn$ (X_3Sn-Br)	$\delta^{(119)}Sn$ (X_3Sn-$CoSnY_3$)	$\Delta\delta$
Br_3	-638	-153	485
Br_2Cl	-508	-101	407
$BrCl_2$	-385	-51	334
Cl_3	-263	1	264

(a) The figures are calculated for the case where $Y_3 = Br_3$. There is a second order effect on the shifts resulting from changes in Y

leading to an effective reduction in ΔE has been proposed[7] as the cause of this large change in shielding in these Sn-T.M. species. A similar effect has also been noted in a new ^{207}Pb NMR study of some T.M.-organo-lead complexes[8].

This direction of change is of interest in the sense that the preparation of the anion results from the addition of $Sn^{(II)}Cl_3^-$ to $Cl_3SnCo(CO)_4$. It is a matter of long-standing debate whether X_3M'-M groups are to be formulated as $^-X_3M'^{(II)}$ Lewis bases or as $X_3M^{(IV)}$-M species. Overall the best description of the resultant molecule is one that consists of two tin atoms both in a +IV oxidation state leaving the cobalt atom in a -I oxidation state, as in $HCo(CO)_4$.

The study has not allowed the establishment of the mechanism of halogen exchange although the third experiment where the two anions were mixed indicate that the exchange can occur via an intermolecular pathway. Whether this involves a dissociation as a first step is unclear. Coddington and Taylor[4] found that they were unable to separate the individual peaks of the tin(II) halide ions until the sample was cooled to -60°C, a temperature well below that used in this study. It is clear that much work is still to be done on this system.

Chapter 6 References

1. R.G.Kidd and H.G.Spinney, *J. Am. Chem. Soc.*, **95**, *88*, 1973.
2. A.L.Wikins, P.J.Watkinson and K.M.Mackay, *J. Chem. Soc. Dalton Trans.*, *2365*, 1987.
3. J.J.Burke and P.C.Lauterbur, *J. Am. Chem. Soc.*, **83**, *326*, 1961.
4. J.Coddington and M.J.Taylor, *J. Chem. Soc. Dalton Trans.*, *2223*, 1989.
5. O.J.Curnow, M.Sc. Thesis, U. of Waikato, 1986.
6. M.Service, D. Phil. Thesis, U. of Waikato, 1988.
7. D.H.Harris, M.F.Lappert, J.S.Poland, and W.J.McFarlane, *J. Chem. Soc. Dalton Trans.*, *311*, 1975.
8. K.H.Pannell, J.M.Rozell, S.Cortez, and R.Kapoor, *Organometallics*, **9**, *1322*, 1990.

Appendix- Publications and Posters Resulting from this Work.

Publications

Preparations and Spectroscopic Properties of Some Germanes of the Types $Me_xGe_3H_{8-x}$, $Me_xGe(GeH_3)_{4-x}$, and $Me_xSi(GeH_3)_{4-x}$; S.P.Foster, Kin-Fai Leung, K.M.Mackay, and R.A.Thomson, *Aust. J. Chem.*, **39**, *1089,* 1986.

Germanium-73 Nuclear Magnetic Resonance: Esoteric Study or Useful Tool?; K.M.Mackay and R.A.Thomson; *Main Group Metal Chemistry*, **10**, *83*, 1987.

Suppression of Acoustic Ringing and Baseline Roll Effects in a Low-Frequency N.M.R. Nucleus - ^{73}Ge; A.L.Wilkins, R.A.Thomson and K.M.Mackay; *Main Group Metal Chemistry*, accepted 1990.

Characterisation by ^{119}Sn NMR and by Other Methods of the Series $[Cl_{3-x}Br_xSnCo(CO)_3SnBr_yCl_{3-y}]^-$ for x,y = 0 to 3; K.M. Mackay, B.K. Nicholson, M. Service, and R.A.Thomson, *Main Group Metal Chemistry*, accepted 1990.

Posters

Elucidation of the Structures of the Compounds $Me_xSi(GeH_3)_{4-x}$ Using ^{29}Si INEPT NMR. R.A.Thomson and K.M.Mackay, N.Z.I.C. Conference, Dunedin, 1986.

Use of Baseline Roll Suppression Techniques in ^{73}Ge NMR. R.A.Thomson, K.M.Mackay and A.L.Wilkins, NMR-88, Thredbo, 1988.